Scaled plane-wave Born cross sections for atoms and molecules

H. Tanaka

Department of Physics, Sophia University, Tokyo 102-8554, Japan

M. J. Brunger

School of Chemical and Physical Sciences, Flinders University, GPO Box 2100, Adelaide SA 5001, Australia and
Institute of Mathematical Sciences, University of Malaya, 5063 Kuala Lumpur, Malaysia

L. Campbell

School of Chemical and Physical Sciences, Flinders University, GPO Box 2100, Adelaide SA 5001, Australia

H. Kato

Department of Physics, Sophia University, Tokyo 102-8554, Japan

M. Hoshino

Department of Physics, Sophia University, Tokyo 102-8554, Japan

A. R. P. Rau

Department of Physics and Astronomy, Louisiana State University, Baton Rouge, Louisiana 70803, USA

(published 19 May 2016)

Integral cross sections for optically allowed electronic-state excitations of atoms and molecules by electron impact, by applying scaled plane-wave Born models, are reviewed. Over 40 years ago, Inokuti presented an influential review of charged-particle scattering, based on the theory pioneered by Bethe forty years earlier, which emphasized the importance of reliable cross-section data from low eV energies to high keV energies that are needed in many areas of radiation science with applications to astronomy, plasmas, and medicine. Yet, with a couple of possible exceptions, most computational methods in electron-atom scattering do not, in general, overlap each other's validity range in the region from threshold up to 300 eV and, in particular, in the intermediate region from 30 to 300 eV. This is even more so for electron-molecule scattering. In fact this entire energy range is of great importance and, to bridge the gap between the two regions of low and high energy, scaled plane-wave Born models were developed to provide reliable, comprehensive, and absolute integral cross sections, first for ionization by Kim and Rudd and then extended to optically allowed electronic-state excitation by Kim. These and other scaling models in a broad, general application to electron scattering from atoms and molecules, their theoretical basis, and their results for cross sections along with comparison to experimental measurements are reviewed. Where possible, these data are also compared to results from other computational approaches.

DOI: 10.1103/RevModPhys.88.025004

CONTENTS

I. INTRODUCTION

Phenomena involving electron collisions are of fundamental importance in atomic and molecular physics (Celotta and Huebner, 1979; Trajmar and Cartwright, 1984; Fano and Rau, 1986) and play an important role in other fields such as aeronomy, astrophysics, atmospheric physics (Campbell and Brunger, 2013), chemistry (Itikawa, 2003; Engmann *et al.*, 2013), plasma physics (Itikawa, 2007; White *et al.*, 2014a), and radiation science and medicine (Tanaka and Itikawa, 2011; Sanz *et al.*, 2012; Petrović *et al.*, 2014; White *et al.*, 2014b). A recent EU-FP7 e-infrastructure project devoted to building a common electronic infrastructure for the exchange and distribution of atomic and molecular data, the Virtual Atomic and Molecular Data Centre (VAMDC: http://sup-vamdc.vamdc.eu/), reflects this importance. In electron collisions with atomic systems (atoms and molecules), a wide variety of kinematic processes can occur: elastic and inelastic scattering, and reactions. Some reviews of a selection of the extensive, but still far from complete, measurements and calculations in electron-molecule scattering processes can be found in Brunger and Buckman (2002), Yoon *et al.* (2010), Anzai *et al.* (2012), and Flosadóttir *et al.* (2012).

After the discovery of the electron in 1897 (Thomson, 1897), the first inelastic electron collision experiments were performed by Lenard (1902). The Bohr model (Bohr, 1913a, 1915), which postulated quantized energy levels in atoms, was confirmed directly by studies of the inelastic scattering of electrons from Hg atoms in the electron swarm experiment of Franck and Hertz (1914) (Robson, White, and Hildebrandt, 2014). After the development of the quantum-mechanical scattering theory (Born, 1926), the well-known Bethe-Born approximation (Bethe, 1930; Massey and Mohr, 1931) was first applied to treat electron scattering at high incident energies. These early and significant efforts were reviewed by Mott and Massey (1965), Massey, Burhop, and Gilbody (1969), and Massey (1976).

There is a fascinating video interview of Bethe himself talking about the important paper of Born that included also the probability interpretation of quantum mechanics (http://www.webofstories.com/play/hans.bethe/12). Bethe extensively used the approximation introduced in that paper, having arrived independently at it. Now known as the Born approximation, Bethe comments in his own words about becoming aware of its prior introduction by Born, and that it was as if he had been "Moliere's Gentilhomme speaking prose" without being conscious of it. In his reminiscences about his paper, Bethe says he "considered it to be quite an important paper" and submitted it for his habilitation, also noting that he introduced a second step that has proved useful although it became "very clumsy and involved" (http://www.webofstories.com/play/hans.bethe/13) and was so criticized by Pauli.

After a hiatus that might be ascribed to World War II and a predominant shift in focus of the physics community to nuclear physics, there was renewed awareness in the early 1960s of electron scattering as a useful tool in elucidating the energy-absorbing properties of atoms and molecules. Specifically, since the latter half of the 1960s, Lassettre (1965, 1969) and Lassettre and Skerbele (1974) and the NBS [then National Bureau of Standards (U.S.), currently NIST, National Institute of Standards and Technology] (Vriens, Simpson, and Mielczarek, 1968; Huebner *et al.*, 1975; Kuyatt, Mielczarek, and Weiss, 1976) groups emphasized the need for the Bethe-Born (BB) approximation and pioneered its application. Those groups were strongly inspired by Fano and Cooper (1968). This was well reviewed theoretically by Inokuti (1971) who, along with Kim and their mentor Robert Platzman, strongly emphasized the need for consistent data in radiation science.

Since then, the field widely known as electron-impact spectroscopy has been clearly identified. Both the experimental and theoretical methods for studying collisions in electron-atomic systems have been extensively developed, not only in electron impact but also in combination with other techniques and fields (such as nuclear physics). Pertinent examples include (a) experimental techniques, including photon impact by laser and synchrotron radiation sources, ion-impact excitation, and coincidence techniques, etc., (b) the development of *ab initio* accurate scattering theory, such as the close-coupling (CC) and related methods (Bray *et al.*, 2002), the *R*-matrix method (Tennyson, 1996; Zatsarinny and Bartschat, 2013), complex Kohn and Schwinger multichannel variational methods (Takatsuka and McKoy, 1981), and others. Several excellent works dealing with these and later experimental and theoretical developments have been published by Celotta and Huebner (1979), Shimamura and Takayanagi (1984), Trajmar and Cartwright (1984), Fano and Rau (1986), and Huo and Gianturco (1995).

Along with their importance for providing a fundamental understanding of electron dynamics in atomic systems, electron-atom and electron-molecule collisional cross sections have become required input data for the design, modeling, and understanding of a wide variety of naturally occurring and laboratory-produced phenomena. Examples include planetary atmospheric entry plasmas (Bultel, Annaloro, and Morel, 2012), laboratory astrophysics (Savin *et al.*, 2012), the upper atomosphere of Titan (Lavvas *et al.*, 2011, 2015), plasma processes in cometary and planetary atmospheres (Campbell and Brunger, 2013), radiation effects and biomedical applications (Baccarelli *et al.*, 2011; Flosadóttir *et al.*, 2012; Engmann *et al.*, 2013), and low-temperature plasmas: applications in microelectronic device fabrication (Makabe and Petrovic, 2015).

Energy transfer from electrons is central to radiation penetration in matter, including chemical or biological matter, because regardless of the incident radiation, whether protons and heavier charged particles or x rays and gamma rays, the first steps of the interaction lead to energetic electrons, with these secondary electrons leading to further excitations and ionizations in matter (Hayashi and Udagawa, 2011; Tanaka and Itikawa, 2011; Sanz *et al.*, 2012; Petrović *et al.*, 2014; White *et al.*, 2014b). Of the about 10^5 ion pairs created by a 5 MeV alpha particle in water vapor before it stops, about half result from primary ionization by the alpha particle and the other half from the secondary electrons. The same proportion of one-half also applies to protons, while most of the energy of gamma rays is deposited through Compton electrons. Thus, a variety of electron-atom or molecule cross sections for excitation or valence and inner shell ionization are needed in radiation science.

For cross-section data to be applicable to any of those practical problems, they must fulfill the threefold requirement that the data be *correct*, *absolute*, and *comprehensive*. The word "absolute" means the cross sections should be available as numerical values in cm^2 or a_0^2, where a_0 is the Bohr radius (0.529 Å). The term "comprehensive" means that the data must cover a wide enough kinematic range of variables (energy and scattering angles of the incident, scattered, and, if applicable, ejected particles). However, unfortunately, our knowledge of cross sections is largely limited, with experimental and theoretical groups often disagreeing significantly even for familiar molecules (Trajmar and McConkey, 1994; Christophorou and Olthoff, 2001; Tanaka and Sueoka, 2001; Itikawa, 2003, 2007). Reliable theoretical predictions are particularly valuable for many of the interesting cross sections that are especially difficult to measure experimentally. Moreover, from the standpoint of using cross sections as input data in certain modeling applications (Sanz *et al.*, 2012; Campbell and Brunger, 2013; Petrović *et al.*, 2014; Robson, White, and Hildebrandt, 2014; White *et al.*, 2014a, 2014b), it is helpful to have an *analytical* expression (http://www.nist.gov/pml/data/ionization) for the cross section as a function of the collision energy. The merit of analytical expressions is of convenience and increased applicability when cross sections may be required in more complicated modeling situations.

Starting in the 1970s, it was especially the group of Inokuti, Kim, and their collaborators, working through a mix of theory, analytical extrapolations, and consistency checks of calculated or measured cross sections, that developed such a set of reliable data for radiation science. Nonetheless they were not alone in this endeavor. For example, there was historically a widely used formula proposed by Lotz (1968), for electron-atom ionization, and an analytical parametrization for the shape of atomic ionization cross sections put forward by Rost and Pattard (1997). This latter approach had the advantage of being not only applicable for electron-impact ionization, but could also be employed for positron-, proton-, and antiproton-impact ionization. However, perhaps the greatest rival to the work of Inokuti, Kim, and their collaborators, and which may be employed to calculate electron-impact ionization cross sections for atoms, ions, molecules, radicals, and clusters (Deutsch and Märk, 1987; Märk, 1992; Deutsch *et al.*, 1993, 1994, 1995, Deutsch, Becker, and Märk, 1995), is the so-called semiclassical Deutsch-Märk (DM) formalism. This approach has also been widely used within the community, and indeed an example of its efficacy is given in Sec. II.B for carbon difluoride. Our concentration on the scalings discussed by Kim and Inokuti is because they cover the range of energies from threshold to 300 eV mentioned in the abstract.

Collision phenomena are often divided into two classes, fast and slow, respectively, high and low energy, depending on a comparison of the incident electron velocity with the orbital velocity of the electrons in the target. The relatively simple first Born approximation gives, in general, quite reliable cross sections for low energy-loss processes at high incident energies, for example, above ~100 eV. The approximation applies with the incident electron acting only as an impulsive *perturbation* on the target system. Even if the interaction is itself not weak, the high speed of the incident particle and thereby the limited time of interaction restricts the momentum transferred to the atomic system. A description as an N-electron target plus one electron is natural, the electron remaining as a projectile distinct from the target and itself only slightly deflected. The first Born approximation thus neglects any change of the projectile to treat it as a plane wave and is sometimes referred to as plane-wave Born (PWB). Note that the projectile could be any other charged particle as well, a 1 keV electron being equivalent in velocity to a 2 MeV proton or a 8 MeV alpha particle.

Thus, fast collisions break naturally into two factors, the first a Rutherford cross section for elastic scattering of charged particles with a definite momentum transfer, and the second an inelastic "form factor" for the excitation of a particular state (including continuum states, that is, ionization) as a result of that momentum transfer. The first factor sets the magnitude and the dependence on incident electron energy of the cross section, the second form factor being a property of the N-electron atomic system alone. It is worth noting that the Rutherford factor does not involve the Planck constant $\hbar$ and is, therefore, part of the classical limit of quantum physics. Indeed, Bohr (1913a, 1913b, 1915) already derived some elements of stopping power before his quantum model of the hydrogen atom. He also employed a consistency check for the second factor in the form of a sum rule which states that

whatever the distribution of oscillator strength into the quantum states of the system through the new mechanics, the total integrated strength must equal the number of oscillators, namely, the number of electrons in the atom or molecule. It was independently discovered by others such as Thomas, Reiche, and Kuhn, and by Bethe in a more general form. This sum rule is also a key to the basic Heisenberg commutator that underlies quantum mechanics.

Bethe also speaks of his own effective use of a sum over cross sections multiplied by the energy change. This represents an effective average energy loss (http://www.webofstories.com/play/hans.bethe/22). Bethe, calling the Bohr work "a beautiful paper," elaborates on his own result differing very slightly, a feature that intrigued Bohr. As a result, Felix Bloch investigated and found the explanation that Bohr's classical formula works better for slow collisions, especially of a projectile with large charge, whereas Bethe's quantum formula applies to fast collisions of small charge (http://www.webofstories.com/play/hans.bethe/24).

Next a small momentum transfer is equivalent to a large impact parameter so that the target sees a pulse of broadband electromagnetic illumination as the incident electron goes by. In such glancing collisions, the dipole approximation dominates so that the energy-loss spectra in essence reduce to photoabsorption spectra. Cross sections for the secondary electrons produced, especially the slow ones, are often more difficult to obtain than photoionization spectra so that this theoretical connection is one of the important consistency checks for data on secondary electrons and their extrapolation to low energies. Normalization against total ionization cross sections requires knowledge of this low-energy region.

Turning to slow collisions, many sophisticated approaches have been carried out to study collision dynamics when the incoming slow electron couples strongly with the target and thereby becomes indistinguishable from the N orbital electrons, the whole now better treated as a $(N+1)$-electron system. As a result, optically forbidden valence and Rydberg transitions and short-lived *resonant* negative ion formation are all possible. Extensive comparisons between experimental data and computational results of Born and related approximations proved that these models do not produce reliable differential cross sections, and somewhat overestimate integral cross sections in the low- and intermediate-energy regions. These include the Born-Oppenheimer, Ochkur-Rudge, and first-order exchange approaches. A large number of those theoretical methods were reviewed by Lane (1980) and those details are not repeated here. However, in the somewhat ill-defined region between high and low energy, that is, at intermediate projectile energies from a few tens of electron volts up to 100 eV, there remain some unsolved issues. While convergent close coupling (CCC) (Bray *et al.*, 2002) and complex R-matrix (Zatsarinny and Bartschat, 2013) calculations build in all the relevant physics, they involve such large basis sets, complicated coupled equations, and integrations out to large distances that they are not easily applied to each specific atom or molecule for which data are needed. This has left the field open for further experimental and theoretical work (Anzai *et al.*, 2012; Brunger *et al.*, 2014) and it is this that is the subject of our review.

The binary-encounter-Bethe (BEB) theory developed by Kim and Rudd (1994) has been quite successful for computing electron-impact ionization cross sections for many atoms and molecules (http://www.nist.gov/pml/data/ionization). This method was extended to scale the plane-wave Born cross sections for electron-impact excitation of neutral atoms (Kim, 2001) and molecules (Kim, 2007), with the important restriction that the scaling is applicable only to integral cross sections (ICS) for electric dipole-allowed transitions. A selection of other scaling formulas for electron-molecule collision cross sections can be found in Green and Dutta (1967), Inokuti *et al.* (1994), Teulet, Sarrette, and Gomes (1999), Adamson *et al.* (2007), and Erwin and Kunc (2008). As described later, three intrinsic atomic properties—ionization energy, excitation energy, and the dipole optical oscillator strength (f)—are used in the so-called BE- and BEf-scaling approaches, which are all accessible from accurate target orbital wave functions, and hence in some sense are free of adjustable parameters. The scaling does not, however, describe resonances, which are often seen near excitation thresholds.

Our systematic comparison between the BEf-scaling results and corresponding experimental results also demonstrated that this conceptually simple approach has the capability to produce accurate ICS for the optically allowed electronic excitation cross sections in atoms (Hoshino *et al.*, 2009) and molecules (Anzai *et al.*, 2012), at intermediate energies in between the high- and low-energy regions.

We adopt two approaches to validate and use the scaling method:

(1) Since accurate values of the required atomic and molecular data are often available from other sources, Born cross sections calculated from simple wave functions serve as adequate starting points. Hereafter, we refer to this as the "computational approach."

(2) Along with the apparent generalized oscillator strength (GOS) introduced by Lassettre, Skerbele, and Dillon (1969), which applies at all incident energies and so is independent of the validity of the Born approximation, an integral first Born cross section based on measured values can be obtained by fitting to a semiempirical formula (Lassettre, 1965; Rau and Fano, 1967; Vriens, 1967; Vriens, Simpson, and Mielczarek, 1968), without recourse to the wave functions, and hereafter is referred to as the "experimental approach." In either case, based on the Born approximation, the scaling has proven very useful for producing reliable, comprehensive, and absolute integral cross sections for electric dipole-allowed transitions (Brunger, Thorn, Campbell, Kato *et al.*, 2008).

After comparing the similarities in shape and magnitude of the ionization cross sections and those for resonance excitation (the optically allowed transition) of the alkaline-earth elements, Chen and Gallagher (1976) noted that "these comparisons will help stimulate a search for a simple universal improvement on the Born and Bethe approximations for the intermediate-energy range." This article may serve this purpose by extending these approximations to more neutral atomic and molecular cases, leading one to realize that, while

its basis may still only be at the level of the Bethe-Born approximation, it is a useful set of approximations and scalings that go beyond the original Bethe theory.

The purpose of this article is to summarize the recent results of the theoretical and experimental scaling approaches for electron-impact excitation of atoms and molecules. Our emphasis will be on integral cross sections for optically allowed transitions in atoms and molecules, but in some cases differential cross sections will also be discussed as required. On this phenomenological approach to scaling, even while its physical content is not fully clarified, this paper may serve to show its wide application to many atoms and molecules. The low-energy region of less than a few tens of eV will not be discussed here except for comparisons between experiment and theory as presented in the figures.

It would be remiss of us not to mention the scaled Born dipole approximation (BDA) (Takayanagi and Itikawa, 1970) approach that was employed extensively by Ehrhardt's group [see Sohn *et al.* (1985) and references therein] to calculate vibrationally elastic and vibrational excitation cross sections, for polar molecules, at low electron-impact energies. In this case the scaling was effected by allowing the permanent dipole moment of the molecule in question to vary, until a best fit to the measured angular distributions, at many electron energies, was achieved. At that point reasonably reliable integral cross sections, for the processes in question and at each energy, could then be determined for use in modeling simulations. However, as this method no longer appears to be used by the scattering community and as the main thrust of this review is for ionization and discrete electronic-state excitation in atoms and molecules, by electrons with energies above the first ionization potential of the species in question, we do not discuss it further. Ours is not a theoretical review, but rather a guide to provide and assess reliable, absolute, and comprehensive cross sections as a bridge linking the low- and high-energy regimes.

An overview of the theoretical techniques is subdivided into the basic formulas and the scaling methods. Since the Bethe-Born approximation and the concept of the GOS were reviewed by Inokuti (1971), Celotta and Huebner (1979), and Hall and Read (1984), they will only be stated briefly along with results from earlier experimental studies by Lassettre (1965, 1969) and Lassettre and Skerbele (1974) in Sec. II.A. Section II.B summarizes the scaling methods initiated by Kim and Rudd (1994) and Kim (2007), while some germane experimental preliminaries are discussed for quantitative cross-section measurements in Sec. III. Section IV presents in some detail a procedure employed in the data analysis to obtain cross sections by fitting the experimental GOS data that were extracted from electron energy-loss spectra. A recent application of results for the rare gases and some typical small molecules is reviewed, and a discussion of such data is given in Sec. V. Section VI provides our concluding remarks.

II. AN OVERVIEW OF THE THEORETICAL BETHE-BORN AND SCALING METHODS

A. The basic formulas

Electron-impact spectroscopy provides information concerning a variety of energetically possible excitation processes (elastic scattering, excitation, ionization, dissociation, electron capture, etc.), and to various combinations of these elementary processes. The probability for those processes occurring is usually expressed in terms of quantities called cross sections. The total collision cross section (σ) includes the sum of the cross sections for all these processes, in addition to the elastic cross sections σ_0, that is,

$$\sigma = \sigma_0 + \sum_n \sigma_n + \int_0^{\varepsilon_{\max}} \sigma_\varepsilon d\varepsilon. \tag{1}$$

In Eq. (1), σ_n is the ICS for excitation of the nth state of the target atomic system and $\sigma_\varepsilon d\varepsilon$ is that for an ionizing collision in which the energy of the ejected electron lies between ε and $\varepsilon + d\varepsilon$, namely, excitation into a continuum state, with a continuous variable ε in place of the excitation energy E_n. Here an individual cross section such as σ_n is expressed in the following form:

$$\sigma_n = \int I_n(\theta) d\Omega = 2\pi \int_0^{\pi} I_n(\theta) \sin\theta d\theta, \tag{2}$$

where $I_n(\theta)d\Omega$, the differential cross section, with $d\Omega = 2\pi \sin\theta d\theta$, defines the angular distribution of the electrons that are scattered in exciting the target atomic system to the nth state. Note that azimuthal symmetry applies to atoms and for molecules when averaged over all orientations; otherwise, for aligned molecules, the differential cross section will also depend on the angle ϕ with integration over that variable in place of the 2π factor.

Returning to Eq. (1), we note that integration over ε yields the total cross section for ionization σ_i:

$$\sigma_i = \int_0^{\varepsilon_{\max}} \sigma_\varepsilon d\varepsilon. \tag{3}$$

These ionizing collisions give rise to a positive ion. If an electron is sufficiently energetic, there will be a finite chance that it will "knock out" more than one electron from the target system in an ionizing collision, leaving the target doubly, triply, or multiply ionized. Such direct ejection of several electrons will require extension of Eq. (1) with integrations over the energy distribution among the electrons.

The scattering amplitudes and the differential cross sections are formally represented in terms of the transition-matrix element T, that is, they are proportional to $|\langle\psi_f|T|\psi_i\rangle|^2$, where ψ_f and ψ_i are the final and initial wave functions for the $(N+1)$-electron system. Besides the many target electrons involved in electron-atom or electron-molecule scattering, theoretical calculations become more complicated in electron-molecule scattering due to the nonspherical nature of the molecular force fields experienced by the incident and scattered electrons. Nonetheless, some physically reasonable simplifications can be made in order to make the calculations more tractable and also assist in the interpretation of the measured energy-loss spectra. For instance, because the nuclei

are so much heavier than an electron, one might expect electron-impact excitation of nuclear motions (rotation, vibration, recoil) to be relatively unimportant at high impact energies. Thus, the molecular wave function is often assumed to be a product of the electronic, vibrational, and rotational parts, respectively, based on the Born-Oppenheimer (BO) adiabatic separation, so that the $(N+1)$-electron wave function can be factored as $\psi^e\psi^v\psi^r f_e$, where f_e is the scattered electron wave function. From the experimental side, even in simple diatomic molecules there can be significant overlap of vibrational sublevels of different electronic states, thus complicating the interpretation of the spectra. These are also difficult and time-consuming experiments, which might explain why relatively little work has been undertaken on electronic-state excitation in molecules.

For fast electrons as presented here, the Born approximation has been widely used to treat electron-impact excitation of atoms and molecules. Specifically, the first Born approximation, retaining the lowest order in a power-series expansion of the scattering T matrix with respect to the incident electron energy, is one where the exact wave function is replaced by a plane wave. Further simplifications can also follow. Since rotational levels, other than for H_2 (which has an unusually large rotational spacing), are not usually resolved in current electron-impact spectroscopy, the excitation cross section may be averaged over the initial rotational states and summed over the final states. Vibrational structure of an excited electronic state is, however, often observed in the electron energy-loss spectra as in the case of optical spectroscopy. This usually consists of a complicated overlapping of different vibrational modes corresponding to a particular electronic state or several neighboring states. In the energy range where the Born approximation is reliable, these relative vibrational intensities observed in the energy-loss spectrum are approximated by using the Franck-Condon (FC) factor that is well known in molecular spectroscopy (Lassettre *et al.*, 1968; Lassettre, 1969; Inokuti, 1971; Trajmar and Cartwright, 1984; Brunger and Buckman, 2002).

By combining these simplifications, the electronic excitation cross section is calculated at a fixed nuclear separation for a fixed molecular orientation and then averaged over all molecular orientations. In contrast to this, the elastic and ionization channels represent the major contributors to the total electron-scattering cross sections. Nonetheless, one must account for the largest electronic-state cross sections associated with the optically allowed transitions at intermediate impact energy and for small scattering angles. It is precisely these transitions that lead to the photon decays that play fundamental roles in low-temperature plasma diagnostics and remote sensing opportunities (Becker, Deutsch, and Inokuti, 2000; Campbell and Brunger, 2009; Campbell *et al.*, 2012; Buckman, Brunger, and Ratnavelu, 2013). Furthermore, since electron-exchange effects become progressively unimportant as the incident electron energy increases, the simple first Born approximation may be used, so that other Born-related methods to treat electron exchange are not included here in this discussion. Theoretical formulations of inelastic-scattering processes based on the Born approximation for rotational, vibrational, and electronic excitations were reviewed by Shimamura and Takayanagi (1984).

For simplicity, the following discussion briefly deals with electron-atom scattering for the basic formulas; generalization to molecules is then straightforward in principle. Excellent previous reviews are available for a theoretical guide (Inokuti, 1971; Shimamura and Takayanagi, 1984; Fano and Rau, 1986) on that point.

1. Some consequences of the Born approximation

For sufficiently fast electrons (but still nonrelativistic), the cross section for a collision that transfers a certain amount of energy and momentum consists of two factors. One factor, the Rutherford factor, concerns the kinematics of the scattered electron, and the other, the form factor, describes the excitation properties of the target. In a collision event in which an electron of mass m scatters from an atomic system (an atom or a molecule) in its ground electronic state and promotes a bound electron to an excited state n, with excitation energy E_n, the first Born approximation, neglecting exchange of the incident electron with one of the target electrons, gives for the differential cross section:

$$\frac{d\sigma_n}{d\Omega} = \frac{k'}{k}|f_n(\theta,\varphi)|^2 = a_0^2\frac{k'}{k}K^{-4}|\varepsilon_n(K)|^2, \tag{4a}$$

with

$$f_n(\theta,\phi) = -\frac{2me^2}{\hbar^2K^2}\int\cdots\int\psi_n\sum_{j=1}^{z}\exp(i\boldsymbol{K}\cdot\boldsymbol{r}_j)\psi_0 d\boldsymbol{r}_1\cdots d\boldsymbol{r}_z$$
$$= -\frac{2me^2}{\hbar^2K^2}\langle\psi_n|\sum_{j=1}^{z}\exp(i\boldsymbol{K}\cdot\boldsymbol{r}_j)|\psi_0\rangle, \tag{4b}$$

where the interaction potential is taken to be Coulombic and $\boldsymbol{K}$ is the momentum transfer vector $\boldsymbol{K}=\boldsymbol{k}-\boldsymbol{k}'$. The scalar magnitude of $\boldsymbol{K}$ can be related to the initial and the scattered electron momenta, $\boldsymbol{k}$ and $\boldsymbol{k}'$, and to the corresponding incident and final energies, T and $T'=T-E_n$, respectively, by conservation of energy and momentum:

$$(Ka_0)^2 = (ka_0)^2 + (k'a_0)^2 - 2kk'a_0^2\cos\theta \tag{5a}$$

$$= \frac{T}{\mathrm{Ry}} + \frac{T-E_n}{\mathrm{Ry}} - 2\frac{[T(T-E_n)]^{1/2}}{\mathrm{Ry}}\cos\theta, \tag{5b}$$

where T is the reduced kinetic energy, $T=mv^2/2$ with v the projectile speed, a_0 is the Bohr radius (0.529 Å), and Ry is the Rydberg energy (13.6 eV). The form factor or atomic matrix element $\varepsilon_n(K)$ and the scattering amplitude in Eq. (4) are defined later.

When the target is a diatomic molecule with a closed shell, the differential cross section is given for the initial a and final a' electronic $^1\Sigma$ states as

$$\frac{d\sigma_{a'v'}}{d\Omega} = \frac{k'}{k}\sum_{J',M'}|f(avJM,\boldsymbol{k}\to a'v'J'M',\boldsymbol{k}')|^2$$
$$= \frac{k'}{k}\left|\left(\frac{2me^2}{\hbar^2K^2}\right)\int\frac{d\hat{\boldsymbol{R}}}{4\pi}\iint\sum\nolimits_j \exp(i\boldsymbol{K}\cdot\boldsymbol{r}_j)\right.$$
$$\left.\times\chi^{v'}_{a'}(R)\phi^*_{a'}(\boldsymbol{r}_m,\boldsymbol{R})\chi^{v}_{a}(R)\phi_a(\boldsymbol{r}_m,\boldsymbol{R})dRd\boldsymbol{r}_m\right|^2, \quad (6a)$$

with v and v' the vibrational and J and J' the rotational quantum numbers, and the scattering amplitude is defined by

$$f(avJM,\boldsymbol{k}\to a'v'J'M',\boldsymbol{k}')$$
$$= -\frac{2me^2}{\hbar^2K^2}\iiint\sum_j \exp(i\boldsymbol{K}\cdot\boldsymbol{r}_j)\chi^{v',J'}_{a'}(\mathrm{R})Y^*_{J'M'}(\hat{\boldsymbol{R}})$$
$$\times\phi^*_{a'}(\boldsymbol{r}_m,\boldsymbol{R})\chi^{v,J}_{a}(R)Y_{J,M}(\hat{\boldsymbol{R}})\phi_a(\boldsymbol{r}_m,\boldsymbol{R})dRd\hat{\boldsymbol{R}}d\boldsymbol{r}_m. \quad (6b)$$

In Eqs. (6a) and (6b) the function ϕ_a represents the electronic state a for fixed internuclear distance $\boldsymbol{R}$, and $\boldsymbol{r}_m$ represents the electronic coordinate of electron m in the molecule, $\chi^{v,J}_a$ are the vibrational wave functions, and $Y_{J,M}(\hat{\boldsymbol{R}})$ the rotational wave function along the molecular axis $\hat{\boldsymbol{R}}$ (with dependence on the rotational quantum number due to the centrifugal potential, it is a spherical harmonic). When the rotational excitation is small, the dependence of the vibrational wave functions χ on the rotational excitation state is assumed to be negligibly small. The result is that the rotational quantum numbers appear only in the spherical harmonics. Here the absolute square of Eq. (6b) is summed over the final rotational state $J'M'$ in Eq. (6a) and further averaged over the initial rotational state.

As mentioned, Eq. (4a) includes two clearly identifiable parts: the first factor is determined completely by the experimental parameters of the projectile and is simply the Rutherford cross section for an electron scattered from a free and initially stationary electron. It is evaluated from the observable quantities k, k', and θ concerning the electron. Note that if quantum exchange between the incident and an atomic electron is included, as necessary at lower energies, it is replaced by the Mott cross section. The other quantity in Eq. (4a), $|\varepsilon_n(\boldsymbol{K})|$, is a form factor as occurs widely in physics and here is the absolute value of the transition-matrix element between the initial and final state functions ψ_0 and ψ_n of the target, respectively. It is given by

$$\varepsilon_n(\boldsymbol{K}) = \langle\psi_n|\sum_{j=1}^{N}\exp(i\boldsymbol{K}\cdot\boldsymbol{r}_j)|\psi_0\rangle, \quad (7)$$

where N is the total number of electrons in the target atomic system, and $\boldsymbol{r}_j$ is the position vector of the jth electron of the target. Referred to as the inelastic-scattering form factor (or collision strength), it is a property of the target as is evident from Eq. (7).

Remarks on the Born approximation and its validity were summarized by Inokuti (1971) and Fano and Rau (1986), and more conceptually illustrated by Inokuti (1981) and Inokuti *et al.* (1994). Therefore, we do not repeat those details here. However, in Fig. 1, we provide an updated version of the original figure of Inokuti (1981) that summarized the energy domains of validity of some of the important theoretical treatments. In the incident energy and angular momentum l plane, regions of validity of various methods are shown: first-order Born at higher, second-Born and other orders, and distorted-Born approximations at somewhat lower energies; close-coupling and R-matrix methods; the Wannier (1953) threshold region; and relativistic treatments at the highest energies.

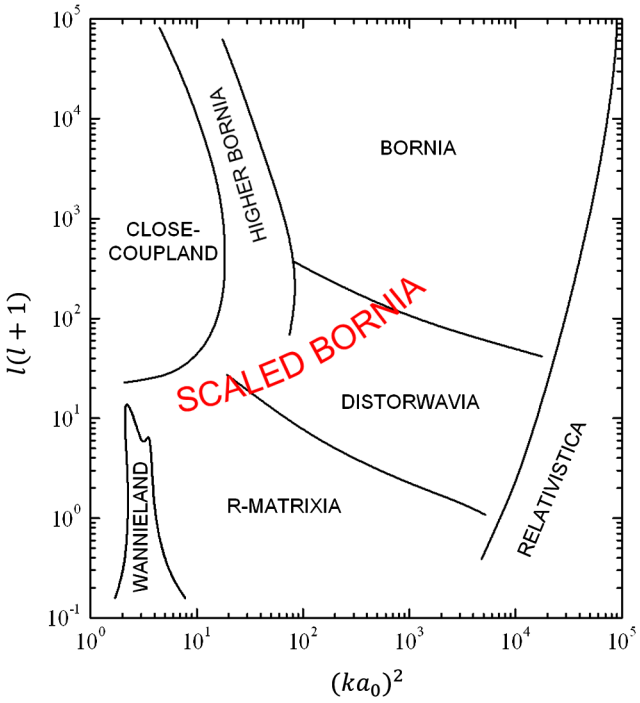

FIG. 1. Map showing the domains of applicability of different theoretical treatments for the process $e + A \to e' + A^*$. The horizontal axis represents the dimensionless energy $(ka_0)^2$ and the vertical axis the dimensionless angular momentum $\ell(\ell+1)$, both on logarithmic scales.

2. The generalized oscillator strength

In parallel with the theory for the absorption of electromagnetic radiation, Bethe introduced the concept of the GOS for an atom by using Eq. (4a),

$$f_n(K) = (E_n/\mathrm{Ry})(Ka_0)^{-2}|\varepsilon_n(\boldsymbol{K})|^2. \quad (8)$$

Analogously, the generalized oscillator strength for a molecule is defined by

$$F_{0\alpha}(K) = [(E_\alpha - E_0)/\mathrm{Ry}](Ka_0)^{-2}\langle|\varepsilon_{\alpha 0}(\boldsymbol{K})|^2\rangle_{av}, \quad (9a)$$

where

$$\varepsilon_{\alpha 0}(\boldsymbol{K}) = \iint\chi^{v'}_{a'}(R)\phi^*_{a'}(\boldsymbol{r}_m,\boldsymbol{R})\chi^{v}_{a}(R)\phi_a(\boldsymbol{r}_m,\boldsymbol{R})$$
$$\times\sum_j\exp(i\boldsymbol{K}\cdot\boldsymbol{r}_j)dRd\boldsymbol{r}_m, \quad (9b)$$

and E_0 and E_α are the internal energies of the molecule in the states $0(a, v)$ and $\alpha\,(a', v')$. Here the integrated cross section is obtained by integrating over the direction of the scattered electron $\boldsymbol{k}'$ in Eq. (6a),

$$\sigma(av \to a'v') = \frac{8\pi}{k^2}\left\langle \left| \int \chi_{a'}^{v'}(R)\phi_{a'}^{*}(\boldsymbol{r}_m, \boldsymbol{R})\chi_a^{v}(R)\phi_a(\boldsymbol{r}_m, \boldsymbol{R}) \times \sum_j \exp(i\boldsymbol{K}\cdot\boldsymbol{r}_j) dR d\boldsymbol{r}_m \right|^2 \right\rangle_{av}, \tag{9c}$$

where the symbol $\langle\rangle_{av}$ represents the averaging over the molecular orientations.

Here we emphasize again that our discussion will explicitly deal with an atom, which is generalized to molecules in principle by replacing $f_n(K)$ by $F_{0\alpha}\,(K)$ in the following equations. With Eq. (8) in Eq. (4a), we obtain an expression for the differential cross section:

$$\frac{d\sigma}{d\Omega} = 4{a_0}^2\frac{k'}{k}\left(\frac{1}{(Ka_0)^2}\right)\frac{f_n(K)}{E_n/\mathrm{Ry}} \tag{10a}$$

$$= \frac{4{a_0}^2}{T/\mathrm{Ry}}\frac{kk'}{K^2}\frac{f_n(K)}{E_n/\mathrm{Ry}}. \tag{10b}$$

Operationally, one can use Eqs. (10a) and (10b) to define an apparent GOS $f_n(K, T)$ that is based on the measured cross section and equals the Bethe GOS defined by Eqs. (7) and (8) when the Born approximation is valid. The apparent GOS (Lassettre, Skerbele, and Dillon, 1969) is thus defined as

$$f_n(K,T) = \frac{1}{4\pi a_0^2}\left(\frac{T}{\mathrm{Ry}}\right)\frac{K^2}{kk'}\frac{E_n}{\mathrm{Ry}}\frac{d\sigma}{d\Omega}, \tag{11a}$$

where

$$\frac{K^2}{kk'} = \gamma^2 + 4\sin^2\frac{\theta}{2}, \tag{11b}$$

with

$$\gamma^2 = \left(1 - \frac{E_n}{T}\right)^{-1/2}\left[1 - \left(1 - \frac{E_n}{T}\right)^{1/2}\right]^2. \tag{11c}$$

All quantities on the right-hand side of Eqs. (11) are experimentally measurable, and from the experimental point of view, Eq. (11) is essentially a definition. Equations (7) and (8) then represent theoretical analogs of this quantity and should equal Eqs. (11) only for sufficiently large incident electron energies where the Born approximation is valid. It is also important to note that when the Born approximation applies, the apparent GOS in Eq. (11a) is independent of T.

Although Eqs. (10a) and (10b) apply to excitations between discrete states, they are readily adapted for transitions to a continuum final state by replacing σ by $d\sigma/dE$ and $f_n\,(K)$ by $df\,(K, E)/dE$ as discussed by Inokuti (1971). For such cases, $df(K, E)/dE$ is the density of the generalized oscillator strength per unit range of E, and in practice is summed over all discrete and continuum states resulting in an energy transfer at the value E. A formula defining this density that includes Eq. (8) is

$$df(K,E)/dE = \sum_n (E_n/\mathrm{Ry})[|\varepsilon_n(K)|^2/(Ka_0)^2]\delta(E_n - E), \tag{12}$$

where $\delta(E_n - E)$ is a delta function of the energy transfer. This definition applies equally to discrete and continuous energy absorption.

The importance of the GOS formulation introduced by Bethe arises from the direct relation it bears to OOS, the optical (dipole) oscillator strength f_0 familiar from photoabsorption. This relation is closest in the limit of small momentum transfer $K \to 0$ a.u. (atomic units). A straightforward power series expansion of the operator in Eq. (7) gives

$$\varepsilon_n(K) = \sum_{m=1}^{\infty}\frac{(iKa_0)^m}{m!}\langle\psi_n|\sum_{j=1}^{N}\left(\frac{\boldsymbol{r}_j}{a_0}\cdot\hat{\boldsymbol{q}}\right)^m|\psi_0\rangle = \sum_{m=1}^{\infty}\frac{(iKa_0)^m}{m!}\varepsilon_{nm}, \tag{13}$$

where $\hat{\boldsymbol{q}}$ is a unit vector in the direction of $\boldsymbol{K}$, $e^{i\boldsymbol{K}\cdot\boldsymbol{r}_j} = 1 + i\boldsymbol{K}\cdot\boldsymbol{r} + (i^2/2!)(\boldsymbol{K}\cdot\boldsymbol{r})^2 +$ (higher order terms). Since the GOS is defined in terms of the square of the absolute value of $\varepsilon_n\,(K)$, only even powers of K occur in a final expression for $f_n\,(K)$. Using this power series expansion in Eq. (8), it is easy to show that only the dipole term survives at small momentum transfer. Consequently, in the limit as the momentum transfer K approaches zero, the GOS reduces to

$$\lim_{K\to 0} f_n(K) = \frac{E_n}{\mathrm{Ry}}|\varepsilon_n|^2 = f_0, \tag{14}$$

or to

$$\lim_{K\to 0}\frac{df}{dE} = \sum_n \frac{E_n}{\mathrm{Ry}}|\varepsilon_n|^2\delta(E_n - E) = \frac{df}{dE}. \tag{15}$$

The emergence of the optical, or dipole, oscillator strength in the limit of vanishing K is plausible since this corresponds to wavelengths large on the scale of atomic size, reducing the exponential in Eq. (13) to its first term, the dipole term with $m = 1$. Physically, as noted earlier, glancing collisions of low momentum transfer are equivalent to the atomic system experiencing a pulse of electromagnetic radiation. Higher expansion coefficients in Eq. (13) correspond to matrices of electronic multipole (electric quadrupole, octupole, etc.) transitions, all of which are optically forbidden.

Furthermore, the Bethe sum rule (Inokuti, 1971) gives

$$\sum_n f(K, E_n) + \int dE\frac{df(K,E)}{dE} = N, \tag{16}$$

where N is the number of electrons in the target and the sum over the energy loss of the discrete transitions and integration over the continuum is carried out at constant momentum transfer. Equation (16) is useful in principle for placing

relative intensity measurements on an absolute scale. This sum rule (Bethe and Salpeter, 1977), with various names such as Thomas, Reiche, and Kuhn attached to it (who derived it for the $K = 0$ optical limit), was already used by Bohr and Bethe in early investigations of the stopping power of radiation in matter and also as a guiding principle by Bohr and Heisenberg in the early days of the development of quantum mechanics. Whatever form the new mechanics took, broad conclusions of this kind on the total number of oscillators present in an N-electron system had to apply. Much like thermodynamics is a constraint on the underlying statistical mechanics, so also are such sum rules a constraint on the underlying mechanics. Mathematically, application of such rules by summing over an entire spectrum of discrete and continuum states is realized in what is called the closure of such a complete set of states.

It has also been noted (Inokuti, 1971) that the stopping power, or the closely related concept of a range of a charged particle in a medium, which is derived from the cross sections in Eqs. (4) and (10), has the velocity of the particle as the key variable. Bethe emphasizes the role this played, especially in the early years. In combination with the bending of such a charged particle in a magnetic field that depends on its momentum, it allowed determination of the mass of the particle (http://www.webofstories.com/play/hans.bethe/23).

Although this derivation assumes the same conditions implicit in Eqs. (4) (that is, within the Born approximation), it has been generally shown that the limiting value in Eqs. (14) and (15) is valid regardless of whether the Born approximation holds or not. Therefore, we refer to this as the Lassettre limit theorem (Lassettre, Skerbele, and Dillon, 1969), and it appears to be consistent with all available theoretical and experimental data. It is important to note the following two practical aspects: (a) because $K = 0$ a.u. cannot be achieved in a real electron collision experiment [see Inokuti (1971) for relevant plots and a discussion of the minimum and maximum values set by energy conservation and Eqs. (38)], the GOS can be determined only at finite values of K and its limiting optical value can be reached only by some extrapolation procedure, and (b) at low incident electron kinetic energies, the extrapolation may extend over a large region of K and can possibly lead to a large uncertainty in the limiting value obtained. However, due to its generality (Hall and Read, 1984), the limit theorem does provide a sound theoretical basis for comparing electron energy loss and optical spectra even at impact energies below those considered appropriate for using the Born approximation. This is especially important for the extraction of optical oscillator strength values from electron-impact measurements.

In terms of the generalized oscillator strength, the integral cross sections can also be obtained as

$$\sigma(0 \to n) = \frac{8\pi a_0^2}{T/\mathrm{Ry}} \int_{K_{\min}}^{K_{\max}} \frac{\mathrm{Ry}}{E_n - E_0} f_{0n}(K) \frac{dK}{K}, \tag{17}$$

where

$$d\Omega = \sin\theta d\theta d\varphi = \frac{d(K^2)}{2kk'} d\varphi, \tag{18}$$

with explicit values of $K_{\min}$ and $K_{\max}$ given in Eqs. (38). Ionization, however, involves excitation into the continuum and E_n is replaced by a continuous variable E.

Integrated cross sections per unit range of excitation energy E for transitions into the continuum from the ith orbital are given by

$$\frac{d\sigma_i}{dE} = \frac{8\pi a_0^2}{T/\mathrm{Ry}} \int_{K_{\min}}^{K_{\max}} \frac{df(K,E)/dE}{E/\mathrm{Ry}} \frac{dK}{K}. \tag{19a}$$

Integration of Eq. (19a) over the continuum energy E yields the so-called ionization cross section σ_i. According to Fano (1954), a convenient way of representing ionization cross sections at high energies is the simple asymptotic expression of Miller and Platzman (1957) (Inokuti, 1971; Fano and Rau, 1986),

$$\sigma_i = \frac{8\pi a_0^2}{T/\mathrm{Ry}} M_i^2 \ln(4c_i T_0/\mathrm{Ry}), \tag{19b}$$

where M_i^2 and c_i are constants,

$$M_i^2 = \int_{E_i}^{\infty} \frac{df}{dE} \frac{\mathrm{Ry}}{E} dE, \tag{19c}$$

and

$$\ln c_i = \ln[(Ka_0)^2(\mathrm{Ry}/E_i)^2], \tag{19d}$$

with E_i involving the binding energy B of the ith orbital in the subshell. Thus, a plot of $\sigma_i(T/\mathrm{Ry})$ vs $\ln(T/\mathrm{Ry})$ asymptotes to a straight line with slope dependent on the oscillator strength. For details and illustrative "Fano plots," see Inokuti (1971) and Fano and Rau (1986).

In terms of the generalized oscillator strength, the integrated Born cross sections for a molecule are given by

$$\sigma(0 \to \alpha) = \frac{8\pi a_0^2}{T/\mathrm{Ry}} \frac{\mathrm{Ry}}{E_\alpha - E_0} \int_{|k_0 - k_\alpha|}^{|k_0 + k_\alpha|} F_{0\alpha}(K) \frac{dK}{K}, \tag{20}$$

where in Eq. (17) f_{0n} has been simply replaced by $F_{0\alpha}$ for a molecule; see Eqs. (8) and (9a).

B. The scaling methods

As is well known, the Born approximation can be used at high incident energies ($E_0 \geq 1000$ eV) but, as the incident energy decreases, serious deviations set in at low and intermediate electron energies. Extensive comparisons between experimental and computational data show conclusively that the Born approximation and its related methods do not predict reliable differential cross sections, and that they generally overestimate the integral cross sections by a factor of 2–5 even in the case of an optically allowed transition, except at high incident electron energies. However, when there is a need to obtain rough estimates of cross sections, this approximation is still useful due to its simplicity in computation.

Second Born and other higher order approximations are extremely hard to implement, requiring sums over intermediate states that can be infinite in number. As a result, quantum scattering theory is still dependent for the most part on the Born approximation.

A theoretical model, free of adjustable fitting parameters, for calculating, without too much computational expense, electron-impact integral cross sections for atoms and molecules is needed, as noted earlier (Tanaka and Itikawa, 2011; Sanz *et al.*, 2012; Campbell and Brunger, 2013; Engmann *et al.*, 2013; Petrović *et al.*, 2014; White *et al.*, 2014a, 2014b), in a wide range of applications. These include modeling the plasmas used for plasma processing of semiconductors, designing mercury-free fluorescent lamps, assessing the efficiency of ion gauges, normalizing mass spectrometer output, understanding plasmas in magnetic fusion devices, and modeling radiation effects on materials (Graves *et al.*, 1996). With this in mind, Kim and Rudd (1994) and Kim (2001, 2007) developed several scaling methods: the BEB dipole, the scaled first-order plane-wave Born f scaling and BE scaling. These methods are described now in some detail.

1. Electron-impact ionization

Proper understanding of the role of ejected electrons is crucial because a large number of them, mostly slow electrons, are generated in the course of an energetic incident particle penetrating through matter (Sanz *et al.*, 2012). These electrons in turn interact with other species until the electrons are thermalized. Therefore, the basic formulation of the problem of electron-impact ionization cross sections has been extensively studied and been classified into three different approaches: (1) empirical and semiempirical rules and formulas, (2) classical and semiclassical collision theories, and (3) quantum-mechanical approximations. Review articles on them are well summarized by Märk (1984).

a. Binary-encounter dipole (BED) model

As described by Kim and Rudd (1994), there have been many attempts to combine the dipole contribution with either the Rutherford or Mott cross section (Mott, 1930) to derive the ionization cross section. The binary-encounter theory was also introduced into the Mott cross section, by assigning a velocity or momentum distribution to a target electron without a more complete description through a wave function (Burgess, 1964). But, they have had only limited success because they failed to find the correct ratio between "soft" and "hard" collisions (see later). As noted earlier, electron-atom collisions can be divided into soft or distant collisions with large impact parameters and hard or close collisions with small impact parameters.

The following is summarized from the original paper by Kim and Rudd (1994). Their starting point is the Rutherford cross section for an electron of kinetic energy T ejecting an electron of kinetic energy W,

$$\frac{d\sigma}{dW} = \frac{4\pi a_0^2}{W^2}\frac{\mathrm{Ry}}{T}.$$

As noted, this predates quantum physics and is the classical result for scattering of charged particles. The Born approximation also gives the same result and is valid at high energies. But, in extending to intermediate (or low) energies, quantum-mechanical exchange between the incident and ejected electrons has to be invoked, giving the Mott cross section that symmetrizes the amplitudes for W and $T-W$ before squaring,

$$\frac{d\sigma}{dW} = \frac{4\pi a_0^2 \mathrm{Ry}^2}{T}\left[\frac{1}{W^2} - \frac{1}{W(T-W)} + \frac{1}{(T-W)^2}\right].$$

Next, Kim and Rudd (1994) allowed for the fact that the ejected electron was bound with some binding energy B by replacing W by the energy transfer $E = W + B$ and T by $T + B$. With B providing a natural scale for energies, the above expression contains inverse powers of $[(W/B)+1]$ and $[(W/B)+(T/B)]$, leading to a more general series expansion of this form suggested to them by Inokuti:

$$\frac{d\sigma(W,T)}{dW} = \frac{S}{B}\sum_1^3 F_n(t)\left[\frac{1}{(\omega+1)^n} + \frac{1}{(t-\omega)^n}\right], \qquad (21)$$

where $S = 4\pi a_0^2 N(\mathrm{Ry}/B)^2$, $t = T/B$, $\omega = W/B$, $a_0 = 0.529$ Å, and $\mathrm{Ry} = 13.6$ eV. The number of electrons N has also been inserted as a multiplicative factor. The Mott cross section corresponds to the following choice of $F_n(t)$: $F_1 = -F_2/(t+1)$, $F_2 = 1/t$, $F_3 = 0$.

A theoretical justification for adding B to T is to observe that the K^{-2} factor in Eq. (4b), or its square K^{-4} in the basic Rutherford cross section of Coulomb scattering, arises from $\int e^{i\vec{K}\cdot\vec{r}}/r$, that is, the Fourier transform of $1/r$. Dillon and Inokuti (1981, 1985) argued that for the H atom, where the wave functions are analytically known, bound state wave functions in the matrix element also introduce an exponential factor involving the radial variable as $\exp(-r/na_0)$. This means a replacement of K by $(K + i/na_0)$ so the $|K|^2$ is similarly replaced by $[K^2 + (1/na_0)^2]$. Indeed, this led them to show that the exact expression for the H atom has such additions of the binding energy B to other energies such as T. The argument is actually more general because even in other atoms or molecules the large-r behavior of bound state radial wave functions involves such an exponential dropoff with the binding energy as a scale factor, making plausible these scalings introduced by Lassettre (1965, 1969), Lassettre, Skerbele, and Dillon (1969), Vriens (1969), Lassettre and Skerbele (1974), Kim and Rudd (1994), and Kim (2001). Similar arguments can be made for the general structure of the asymptotic behavior in K or E of the generalized oscillator strength (Rau and Fano, 1967).

A further variant called the binary encounter (each atomic electron seen as scattering from the incident electrons and acquiring all the momentum transfer) cross section for electron-impact ionization can also be characterized by the same form in Eq. (21). Instead of just B to characterize the bound electron, allowance is made for the momentum distribution in that bound orbital but without going to a complete wave function description. The orbital kinetic energy $U \equiv \langle \vec{p}^2 \rangle/2m$, with $\vec{p}$ the momentum of the electron in the

subshell, is invoked along with the binding energy B and the electron occupation number N to characterize the orbital. This idea was originally introduced by Burgess (1964) and Vriens (1966, 1969) to scale ionization cross sections, in which the orbital kinetic energy U was used in place of E in Eq. (21), and thus is referred to as Burgess-Vriens (BV) scaling. The binary-encounter cross section is reproduced by choosing $F_1 = -F_2/(t+1)$, $F_2 = 1/(t+u+1)$, and $F_3 = 4u/3(t+u+1)$, where $u = U/B$. According to the binary-encounter theory, the extra terms in the denominators of F_n, namely u and 1, represent the acceleration of the incident electron due to the nuclear attraction.

The $(t-\omega)^{-n}$ terms may be ignored in the asymptotic region $t \gg \omega$, that is, Eq. (21) becomes

$$\frac{d\sigma}{d\omega} = S\sum_{n=1}^{3} F_n f_n(\omega), \tag{22}$$

with

$$f_n(\omega) = \frac{1}{(\omega+1)^n} \qquad n = 1, 2. \tag{23}$$

The total cross section, upon integrating Eq. (22) over ω, does not however have the correct asymptotic behavior. Since the Bethe theory describes this correctly, with the dipole contribution dominant,

$$Q = \frac{2}{N}\int \frac{B}{B+W}\frac{df}{dW} \qquad \left(\equiv \frac{2B}{N}\int \frac{1}{\omega+1}\frac{df}{d\omega}d\omega\right), \tag{24}$$

Rudd and Kim corrected Eq. (23) with the choice

$$f_3(\omega) = \frac{1}{N(\omega+1)}\frac{df(\omega)}{d\omega}, \tag{25}$$

hence giving the name the binary-encounter dipole model.

In all, the BED model can be represented by $F_1 = -F_2/(t+1)$, $F_2 = 2 - (N_i/N)/(t+u+1)$, and $F_3 = \ln t/(t+u+1)$ in Eq. (22), where N is the number of bound electrons, and

$$N_i \equiv \int_0^\infty \frac{df}{d\omega}d\omega. \tag{26}$$

The upper limit of integration for N_i has been extended to ∞ in the anticipation that $f_3(\omega)$ diminishes rapidly enough (Dillon and Inokuti, 1985) as $\omega \to \infty$ to make it valid.

The BED model has a threshold behavior of the ionization cross section, when $t \to 1$, of $\sigma_i(1+\Delta t) = \text{const}\Delta t$, with $\Delta t \ll 1$. While this does not conform to the threshold behavior given by the Wannier theory (Wannier, 1953; Rau, 1971) that predicts $\sigma_i \propto (\Delta t)^{1.127}$ for nuclear charge $Z = 1$, the error made over the small threshold region (about 1–2 eV) by the linear behavior (Rudge, 1968) of the BED model is not very significant.

In practical applications of the BED model, values of B, U, N, and the differential oscillator strengths $df/d\omega$ are needed for each subshell of a given target. Of these, B and N are readily available from the literature or a commercially available quantum chemistry code such as GAUSSIAN (www.gaussian.com., Frisch *et al.*, 2010). The values of N_i and M_i^2 can be calculated from $df/d\omega$. The average kinetic energy U needed in the BED model is a theoretical construct that can easily be obtained from wave function codes such as GAUSSIAN. Good sources of differential oscillator strengths are in the book by Berkowitz (1979) and the review article by Gallagher *et al.* (1988), from which one can find the original papers. Rudd and Kim emphasized that they had used the experimental $df/d\omega$ when those were more reliable than the calculated ones, particularly near threshold. Note that although any form of theoretical $df/d\omega$ can be used, analytical fits are certainly more convenient to use than either numerical tables or graphs.

The important ingredient of the BED model is the differential dipole oscillator strength for ionization, which can be derived from either a theoretical or experimental photoionization cross section. The BED model constructs ionization cross sections subshell by subshell, and in principle can be used to construct ionization cross sections for any target atom or molecule as long as corresponding differential oscillator strengths for ionization are known. When high accuracy (10% or better) is not required, differential oscillator strengths calculated from Hartree-Fock or simpler wave functions are probably sufficient.

b. Binary-encounter-Bethe (BEB) dipole model

Kim and Rudd proposed a simpler version of the BED model, to be referred to as the BEB model, which may be used when the required differential oscillator strengths are not available. Combining the Mott cross section with the high-T behavior of the Bethe cross section, this BEB approach is known to be versatile and successfully provides total and partial ionization cross sections for atoms and molecules (Kim and Rudd, 1994, http://www.nist.gov/pml/data/ionization). To arrive at the BEB model, however, we must first introduce the Q-parametrized binary-encounter (BEQ) approach (http://www.nist.gov/pml/data/ionization).

In the BEQ model, for the integration to obtain N_i and M_i^2 in Eqs. (26) and (19c), respectively, a simple form of $df/d\omega$ is assumed. As observed from the simple shapes of $df/d\omega$ for H, He, and H_2, the differential oscillator strength is represented by inverse powers of $(\omega+1)$ as in Eqs. (23) and (25), in the form of a polynomial, starting from $(\omega+1)^{-2}$,

$$\frac{df}{d\omega} = \frac{b}{(\omega+1)^2} + \cdots, \tag{27}$$

where b is a constant. Combining Eq. (27) with Eqs. (19b)–(19d), and retaining only the first term, we have $M_i^2 = RN_i/2B$ and $Q = N_i/N$. Note E is replaced by $W+B$ in Eqs. (19b)–(19d).

Equation (27) is not, however, expected to hold for all subshells in targets with complicated shell structures. Then, one can reduce Eq. (25) to

$$f_3(\omega) = \frac{Q}{(\omega+1)^3}, \tag{28}$$

where $Q = N_i/N$ is substituted for $4u/3$. Finally, with $F_1 = -F_2/(t+1)$, $F_2 = 2 - Q/(t+u+1)$, and $F_3 = Q \times \ln t/(t+u+1)$, from Eq. (22), one has a convenient formula to estimate the total ionization cross section,

$$\sigma_{\mathrm{BEQ}} = \frac{S}{t+(u+1)/n}\left[\frac{Q\times\ln t}{2}\left(1-\frac{1}{t^2}\right) + (2-Q)\left(1-\frac{1}{t}-\frac{\ln t}{t+1}\right)\right], \tag{29}$$

where the constant n on the right-hand side is used for ion targets and for valence orbitals of large atoms, as discussed in more detail by Scott and Irikura (2005). This formula, distinguished in not having any fitting parameters, provides a simple analytical expression for the ionization cross section per atomic or molecular orbital.

This BEQ model is useful even without much knowledge of N_i, M_i^2, and $df/d\omega$, although at some cost to reliability. When df/dW is unknown, one can put $Q = 1$ in Eq. (29) as a further approximation and determine ionization cross sections of the correct order of magnitude even when nothing is known about differential or total dipole oscillator strengths. This final simplification leads us to the now well-known BEB model (Kim, Santos, and Parente, 2000). Rudd, Kim, and the NIST group provided extensive, reliable total ionization cross sections for many atoms and molecules (http://www.nist.gov/pml/data/ionization), validating this simple improvement on the Born and Bethe approximations for the intermediate-energy range.

c. Some examples of these scalings

Experimental data are available more for total ionization cross sections than for electronic excitations and largely verify the scaling given by the theoretical approach. Because ionization data are essential for plasma discharges, the BED and BEB scaling methods have been applied to many molecules relevant to plasma processing, and it has been shown that these approaches are useful for estimating unknown total ionization cross sections for hard-to-measure targets (http://www.nist.gov/pml/data/ionization). Scott and Irikura (2005) recommended an alternative, simpler procedure for molecules that contain heavier elements ($Z > 10$). Based on effective core potentials, it does not require any kinetic energy corrections.

The resulting ionization cross sections for small atoms, a variety of large and small molecules, and radicals, are 5% to 20% accurate from threshold to $T \sim 1$ keV. Just as important, all these cross sections are readily available to the public through the website (http://www.nist.gov/pml/data/ionization). We present a few representative data to illustrate the utility of this approach, and Sec. V considers many more atoms and molecules.

i. Atomic hydrogen (H). In Fig. 2, we depict the total ionization cross sections for electron scattering from atomic hydrogen. Shown in this figure are the measured cross sections from Shah, Elliott, and Gilbody (1987), a classical cross section from Gryziński (1965a, 1965b, 1965c), a distorted-wave Born result from Younger (1981), and the BEQ and BEB results. It is clear from this figure that both the BEQ and BEB cross sections, from threshold up to ~4 keV, are consistent with the measured results (Dillon and Inokuti, 1985) to within experimental errors. While not shown, the fully *ab initio* convergent close-coupling results (Bray *et al.*, 2012) also well reproduce the measured data and BEB and BEQ calculations.

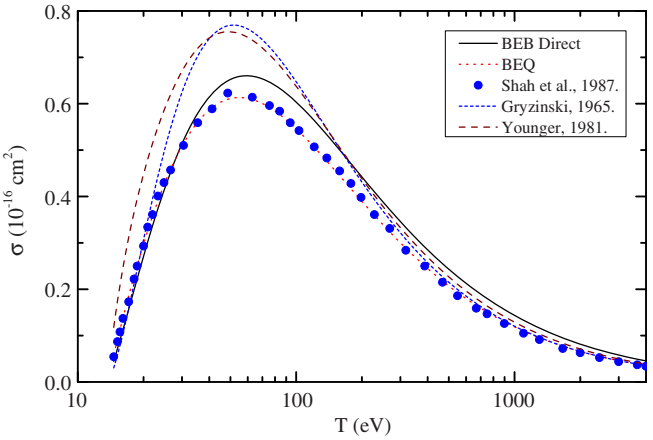

FIG. 2. Total cross section for ionization of H by electron impact. The abscissa is the incident electron energy T in eV. Circles, experimental data by Shah, Elliott, and Gilbody (1987); solid line, BEB cross section; short-dashed line, BEQ cross section; medium-dashed line, Gryzinski's classical cross section (Gryziński, 1965a, 1965b, 1965c); long-dashed line, distorted-wave Born cross section with electron-exchange correction by Younger (1981).

ii. Helium (He). If anything, the level of accord between the BEQ and BEB results and the measured ionization cross sections from Montague, Harrison, and Smith (1984) and Shah *et al.* (1988) for electron-He scattering is even more impressive than that for H. This is seen in Fig. 3. Note that the distorted-wave Born calculation (Younger, 1981) again fails to reproduce the data at intermediate energies and, although not shown, the convergent close-coupling computational result (Bray *et al.*, 2012) also does an excellent job in reproducing the measurements.

iii. Atomic oxygen (O). The example of the ionization of O by electron impact is one for which direct experimental measurement is a challenge. This is because discharges are often required to produce O from the molecular oxygen precursor, and the dissociation process is rarely 100% effective, leading to a mixture of O_2, O, and excited O (O^*). Both O and O^* play important roles in the atmospheric chemistry of our planet and that of Jupiter's moon Europa (Campbell *et al.*, 2012), and as a consequence a knowledge of these cross sections is important. In Fig. 4, we show experimental measurements from Brook, Harrison, and Smith (1978), Zipf (1985), and Thompson, Shah, and Gilbody (1995), compared to the BEB results for direct ionization from the ground state of O, ionization from O^*, and the sum of these ionization cross

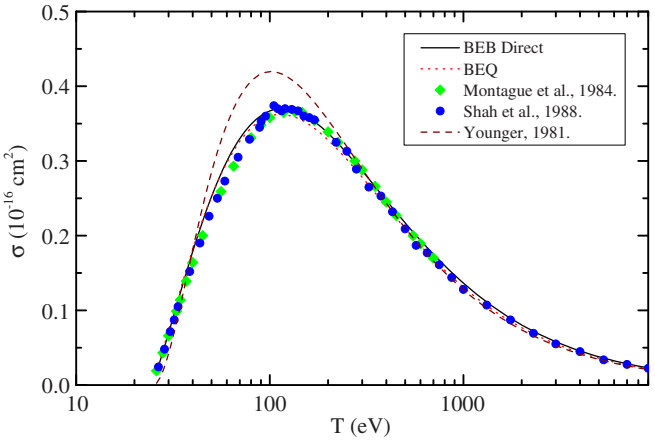

FIG. 3. Total cross section for ionization of He by electron impact. Filled circles, experimental data by Shah *et al.* (1988); filled diamonds, data by Montague, Harrison, and Smith (1984); solid line, BEB cross section (with the $t + u + 1$ denominator for a neutral target); medium-dashed line, Younger's distorted-wave Born cross section (Younger, 1981); short-dashed line, BEQ cross section.

sections to give the total ionization cross section for $e^- + O$ (Thompson, Shah, and Gilbody, 1995). As can be observed from Fig. 4, this total BEB ionization cross section is in good agreement with the measured data, to within the stated errors on those data. This suggests that even when reliable experimental data are unavailable, the BEB approach might be used to calculate the unknown ionization cross sections with some confidence.

iv. Carbon tetrafluoride (CF_4). Before its deleterious effects on the environment, as indicated by its large global warming

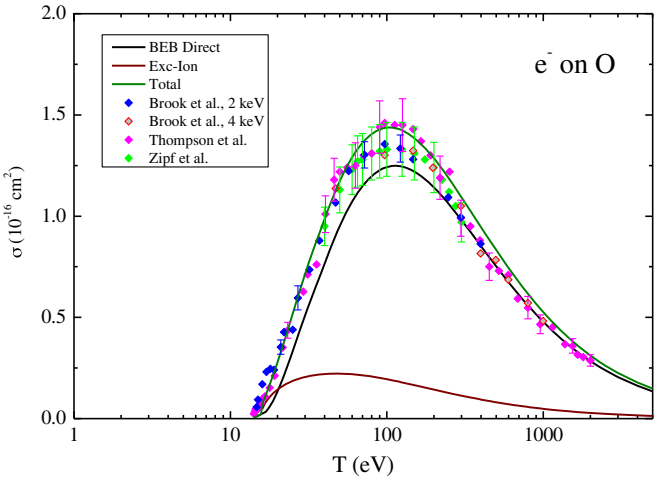

FIG. 4. Total cross section for ionization of atomic oxygen by electron impact. Shown are the BEB result for direct ionization from its ground state, ionization from excited electronic states of O within a BEB approach, and their sum to give the total BEB ionization cross section. Also shown are experimental results, at the incident electron energies indicated in the legend, from Brook, Harrison, and Smith (1978), Zipf (1985), and Thompson, Shah, and Gilbody (1995). See also the legend. The BEB results are taken from Kim and Desclaux (2002).

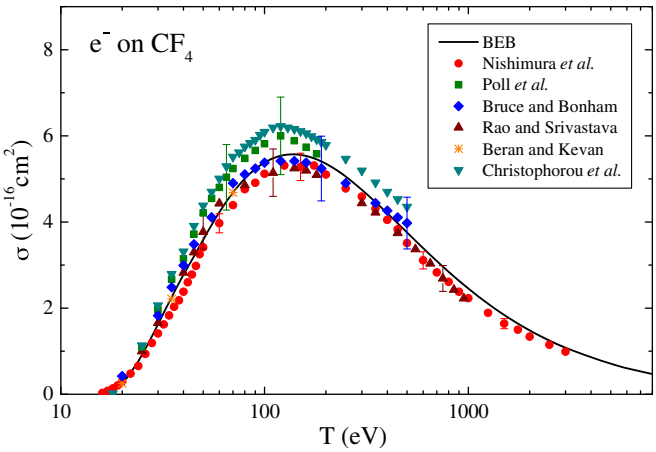

FIG. 5. Total ionization cross sections for electron scattering from CF_4. See the legend and the text for further details.

potential, were appreciated, CF_4 was a popular feedstock gas in low-temperature plasma etch reactors. Therefore a knowledge of its ionization cross sections was important in trying to model the behavior of those plasmas. In Fig. 5, we compare the BEB ionization cross sections (Nishimura *et al.*, 1999) against a selection of the measured data from Beran and Kevan (1969), Poll *et al.* (1992), Bruce and Bonham (1993), Rao and Srivastava (1997), and Nishimura *et al.* (1999) and a recommended set of data from Christophorou, Olthoff, and Rao (1996). We again find that to within the error bars of the experimental results BEB scaling provides a good description for the total ionization cross section of this system.

v. Carbon difluoride (CF_2). It is well known (Nikitović *et al.*, 2009) that in a plasma with CF_4 as the feedstock gas, radicals such as CF, CF_2, and CF_3 will also be formed. As an example of one of these species, we now look at the total ionization cross sections for electron scattering from CF_2. In Fig. 6, we show results from the BEB approach, a modified BED approach that allows for shielding of the long-range dipole potential in the collision (siBED) (Huo, Tarnovsky, and Becker, 2002), a result using the DM model (Deutsch *et al.*, 2000), and experimental data from Huo, Tarnovsky, and Becker (2002). In this case we find that it is the siBED approach that best reproduces the measured data, although the BEB scaling result is far from being hopeless. Further work by Becker and colleagues (Huo, Tarnovsky, and Becker, 2002) suggested that for radicals the modified siBED scaling method might give the most accurate data. In addition to the CF_2 ionization cross sections being important to modeling the behavior of plasma reactors in which it is a constituent, they also played a crucial role in allowing Maddern and colleagues (Maddern, Hargreaves, Bolorizadeh *et al.*, 2008; Francis-Staite *et al.*, 2009) to set the absolute scale of their CF_2 elastic differential and consequently integral cross-section data. Since, in the modeling of any plasma reactor, cross sections for all relevant scattering processes over a wide energy range are required, this was a crucial result.

vi. Carbon tetrachloride (CCl_4). We conclude our examples on the efficacy of the ionization scaling approaches in electron scattering by looking at the results for a molecule (CCl_4)

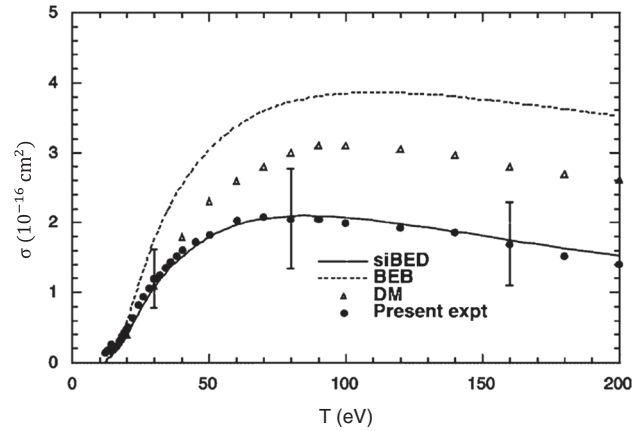

FIG. 6. Total single ionization cross section of CF_2 calculated using the siBED model and the experimental data. Also presented are theoretical cross sections calculated using the BEB model of Kim and Rudd (1994) and the DM model (Deutsch *et al.*, 2000). "Present expt" refers to data from Huo, Tarnovsky, and Becker (2002).

which contains an atom (Cl) with $Z > 10$. In this case see Scott and Irikura (2005) for full details, with a summary of the results given in Fig. 7. Here we find that when the standard BEB approach is modified to allow for the effective core potential, good agreement is found with most of the available experimental data (Hudson *et al.*, 2001; Lindsay *et al.*, 2004; Martinez *et al.*, 2004) to within the uncertainty on those data. While we have given an example only for the case of a chlorine atom in a molecule, the NIST website (http://www.nist.gov/pml/data/ionization) shows that this modified BEB scaling method is equally effective for other species that include an atom with $Z > 10$.

While we have thus far concentrated on the nonrelativistic BEB cross sections for electron-impact ionization, the method has also been extended to deal with relativistic incident

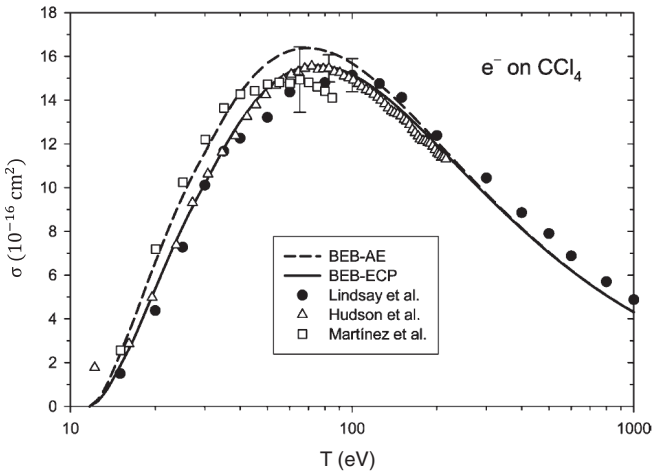

FIG. 7. Total ionization cross section for CCl_4. Theoretical values are indicated by the solid (effective core-potential) and dashed (all-electron) curves. Experimental values are indicated by the symbols. See Scott and Irikura (2005) and text for further details.

electron energies (Kim, Santos, and Parente, 2000). However, a thorough discussion of that extension is excluded here as it is outside the scope of this review. In Sec. II.B.2, the BEB model for ionization of atoms and molecules is extended to the case of dipole-allowed transitions in the electron-impact excitation of neutral atoms and molecules. Furthermore, the performance of this new scaling method for estimating unknown discrete electronic-state data that might not be accessible experimentally is demonstrated. Limitations on this method of Kim (Suzuki *et al.*, 2011) are also noted where appropriate.

2. Electron-impact discrete excitation

After the success of the BEB theory for describing ionization cross sections for atoms and molecules, Kim extended it to scale the first-order PWB cross sections for electron-impact excitation of neutral atoms (Kim, 2001) and molecules (Kim, 2007), provided that the scaling is applicable only to integral cross sections for electric dipole-allowed transitions. It is not applicable to the differential cross sections. As in the case of ionization, three atomic properties—the ionization energy, excitation energy, and dipole f value—are used in the new scalings called BE and BEf scalings. These quantities are accessible from accurate wave functions and hence are free of adjustable parameters. The new scaling approaches do not, however, allow for the resonances often seen near excitation thresholds, nor do they fare well in systems where interchannel coupling between the target electronic states is strong, with an example of this being Rydberg-valence mixing in molecular oxygen (O_2) (Suzuki *et al.*, 2011).

a. The BE-scaling model

Once again, as the starting point, the first-order PWB cross section is used in the scaling because (a) the plane wave is the correct wave function at infinity for an electron colliding with a neutral atom or molecule, and (b) it is the simplest, first-order perturbation result that uses the target wave function explicitly. For brevity, the asymptotic Born cross section derived from Eq. (19b) is rewritten as

$$\sigma_{\mathrm{PWB}} = \frac{8\pi a_0^2 \mathrm{Ry}}{T} M_\alpha^2 \ln\left(\frac{4c_\alpha T}{\mathrm{Ry}}\right) \equiv \frac{8\pi a_0^2 \mathrm{Ry}}{T} F_{\mathrm{PWB}}(T), \quad (30)$$

where $F_{\mathrm{PWB}}(T)$ is the collision strength.

From the analogy with the scaling for the ionization cross sections, Kim replaced T in the denominator of Eq. (30) by $T + B + E$, where E is the excitation energy. That is, the BE scaling is given by

$$\sigma_{\mathrm{BE}}(T) = \frac{T}{T + B + E} \sigma_{\mathrm{Born}}(T). \quad (31)$$

As before, this BE scaling corrects the well-known deficiency of the Born approximation at low T, without losing its validity at high T. The additional constant of $B + E$ accounts in a simple but effective manner for the electron exchange, distortion, and polarization effects that are absent in the first-order PWB approximation. These scaled PWB cross

sections for integral cross sections of dipole-allowed transitions have been quite successfully applied to describe electron-impact excitation of neutral atoms and molecules as will be seen.

b. f scaling

The f scaling is introduced to take advantage of the availability of reliable f values from other sources. The f-scaled Born cross section σ_f is given by

$$\sigma_f(T) = \frac{f_{\text{accur}}}{f_{\text{Born}}}\sigma_{\text{Born}}(T), \tag{32}$$

where T is again the incident electron energy, f_{accur} is an accurate dipole f value from an accurate wave function or experiment, and f_{Born} is the dipole f value from the same wave function used to calculate the unscaled Born cross section σ_{Born}. The f-scaling process has the effect of replacing (normalizing) the wave function used for σ_{Born} with an accurate wave function. Experimental f values are discussed in Sec. IV.

c. BEf *scaling*

If we now combine these two models, the BEf-scaled Born cross section $\sigma_{\text{BE}f}$ is given by

$$\sigma_{\text{BE}f}(T) = \frac{f_{\text{accur}}T}{f_{\text{Born}}(T+B+E)}\sigma_{\text{Born}}(T). \tag{33}$$

If an unscaled σ_{Born} is obtained from poor quality wave functions while an accurate f value is known, then both f scaling and BE scaling can be applied to obtain a BEf-scaled Born cross section $\sigma_{\text{BE}f}$. These three models to scale plane-wave Born cross sections have been shown to produce atomic excitation cross sections comparable in accuracy to those obtained by more sophisticated collision theories. In addition, Kim demonstrated that these models could also be successfully applied to molecular systems and indeed our scaled Born integral cross sections have been found to be in excellent agreement, from near threshold to 200 eV, with those derived from experiments for integral cross sections for electric dipole-allowed transitions in some molecules (Brunger, Thorn, Campbell, Kato *et al.*, 2008). In particular, we note the comparisons for the scaling results with experiment for the atoms He (Hoshino *et al.*, 2010) and Ne (Hoshino, Murai, Kato, Itikawa *et al.*, 2013; Hoshino, Murai, Kato, Brunger *et al.*, 2013) and for molecules H_2 (Kato *et al.*, 2008), CO (Kato *et al.*, 2007; Kawahara *et al.*, 2008a), O_2 (Suzuki *et al.*, 2011), CO_2 (Kawahara *et al.*, 2008b), N_2O (Kawahara *et al.*, 2009), OCS (Limão-Vieira *et al.*, 2015), H_2O (Thorn *et al.*, 2007b), BF_3 (Duflot *et al.*, 2014), and C_6H_6 (Kato *et al.*, 2011) in Sec. V. Note that, in comparing with results from the experimental approach, the BE scaling itself, without using the f scaling, has also proved reliable in many cases.

III. EXPERIMENTAL RESULTS

A. Experimental preliminaries

Over the last 40 or so years, there has been a convergence in ideas on how to make accurate and reliable absolute cross-section measurements for electron scattering from atoms and molecules. To reach this level of consensus has seen extensive contributions from many different groups. These include, and this is by no means an exhaustive list, the seminal contribution of Read's group at the University of Manchester in practical electron-optics design criteria [see, e.g., Harting and Read (1976) and Imhof and Read (1977)], the methodology and theory behind the relative flow technique for absolute elastic scattering differential cross-section measurements from the JPL group of Trajmar and colleagues [see, e.g., Csanak *et al.* (1984), Trajmar and Register (1984), Nickel *et al.* (1989), and Trajmar and McConkey (1994)], and the approaches to inelastic cross-section measurements pioneered by Ehrhardt's group [see, e.g., Gote and Ehrhardt (1995)], Linder's group [see, e.g., Rohr and Linder (1976)], and the JPL group [see, e.g., Nickel *et al.* (1989)]. All of those and other earlier experimental contributions, including from the group at Fribourg [see, e.g., Allan (1995)], Flinders University [see, e.g., Brunger and Teubner (1990)], Argonne National Laboratory [see, e.g., Tanaka and Heubner (1976) and Spence *et al.* (1984)], Sophia University [see, e.g., Wakiya (1978) and Tanaka *et al.* (1982)], the Australian National University [see, e.g., Brunger, Buckman, and Newman (1990) and Brunger *et al.* (1991)], and CSU at Fullerton [see, e.g., Khakoo and Segura (1994) are adequately summarized in the review of Brunger and Buckman (2002) and so they are not repeated again here. Subsequent to that review, there have been several important developments in experimental measurement techniques. These include the analyzer transmission calibration approach from Allan (2005), the use of an orifice as an atomic or molecular beam forming device, in particular, for application with the relative flow technique for elastic scattering from Khakoo *et al.* (2010), and references therein, the extension of the relative flow technique to pulsed supersonic target-molecule expansions, to enable radicals to be studied, by Maddern and colleagues (Hargreaves *et al.*, 2007; Maddern, Hargreaves, Francis-Staite *et al.*, 2008), the development of an electron-trap (pulsed) source by the Madrid group (Fuss *et al.*, 2013), and the evolution of the experimental approaches at Sophia University which we shortly discuss in some detail.

The experimental technique employed in generating the data used for comparison with the scaling results discussed earlier in this review can be found in Kim (2001, 2007), specifically, in regard to the total ionization measurements. Here we describe as a representative example measurement techniques for absolute cross sections at Sophia University for excitation of discrete electronic states in molecules. Other, currently active, groups employ somewhat similar spectrometers and experimental procedures (Kanik, Nickel, and Trajmar, 1992; Brunger and Buckman, 2002; Allan, 2005; Khakoo *et al.*, 2008). For a quantitative measurement of the cross sections, characterizing the analyzer transmission function for the range of scattered electron energies associated

with the excitation of electronic states in atoms and molecules is, in particular, an important issue.

One note of caution is in order here. In this review, measurements of differential cross sections (DCSs) by electron impact will be needed to evaluate the efficacy of the scaled Born integral cross sections for the intermediate-energy region down to ~20–30 eV. However, in the so-called experimental approach, DCSs for only some very forward angles at the higher incident electron energies of 100 to 300 eV are sufficient to scale the integral Born cross section $\sigma_{\mathrm{Born}}(T)$. This is one of the expected advantages in employing the experimental approach when using BEf scaling. In the description that follows, we outline the measurement techniques for the specific case of e-Ne scattering but they are equally applicable to other species we discuss later in Sec. V. There were in fact two crossed-beam configurations used for the electron energy-loss spectroscopy of Ne, which we denote as "setup 1" and "setup 2."

Setup 1: For incident energies below 50 eV, the experimental apparatus and method were described in detail earlier (Tanaka *et al.*, 1988; 1998) and only some specific features of the neon work are briefly highlighted here. The spectrometer consists of an electron-scattering spectrometer, gas flow system, computer-driven voltages, and counting electronics for detecting and storing the scattered electron signal. The scattering spectrometer, as shown in Fig. 8, is of conventional crossed-beam geometry with an electron gun, single hemispherical energy selector and analyzer, cylindrical lens systems, and a channeltron for the detection of the scattered electrons.

Setup 2: Above 100 eV, we effectively have setup 1 but with the addition of double tandem hemispheres in the analyzer system (Hoshino, Murai, Kato, Itikawa *et al.*, 2013) and a real aperture placed between the analyzer hemispheres to eliminate the unwanted part of the electron beam due to any background scattering or primary electron beam interference. Indeed, this spectrometer was used for all the measurements between 100 and 300 eV, and thus was crucial in determining the experimental approach BEf-scaled ICS.

The nozzle (a simple tube of diameter 0.3 mm and length 5 mm), through which target gas effuses to produce a well-defined beam of the target gas, was kept at 50 °C above room temperature in order to prevent accumulation of any surface charges. Variations in the electron beam intensity as different gases are cycled through the chamber are reduced by enclosing the electron-beam generating system and the analyzer in separate casings, and pumping them differentially. No effects of the target gases on either of the spectrometers were observed. A combination of a 2-mm-thick μ-metal shield with Helmholtz coils around the top and bottom flanges of the vacuum vessel reduced the Earth's magnetic field to less than a few mG. The angular resolution amounts to about ±2° below 50 eV and ±1° above 100 eV, with the true zero-scattering angle being determined by noting the symmetry of the measured elastic scattering and/or the inelastic intensities [He 2^1P [21.218 eV] (Trajmar *et al.*, 1992; Hoshino *et al.*, 2010) and/or Ne $3s'[1/2]_1$ [16.848 eV] (Hoshino, Murai, Kato, Brunger *et al.*, 2013) as obtained in the neon study (Hoshino *et al.*, 2010; Hoshino, Murai, Kato, Itikawa *et al.*, 2013)]. When assembling the spectrometer, the geometrical alignment for mounting both the selector and the analyzer relative to the nozzle center was checked as precisely as possible by employing a laser beam.

Typically, the spectrometer in setup 1 was operated at fixed incident electron energies between 20 and 50 eV and over the scattered electron angular range from −20° to 130°. At higher incident energies, with the double tandem hemispheres in the analyzer (setup 2) system, the scattering angles usually covered were limited to 2°–12.6° for 100 eV, 1.6°–15.6° for 200 eV, and 0.53°–5.48° for 300 eV. The overall energy resolution, at Faraday-cup currents of 3–7 nA, was about 28 meV (full width at half maximum of the observed elastic peaks), sufficient to separate the four peaks in neon under consideration as shown in Fig. 9. By fitting to a Gaussian

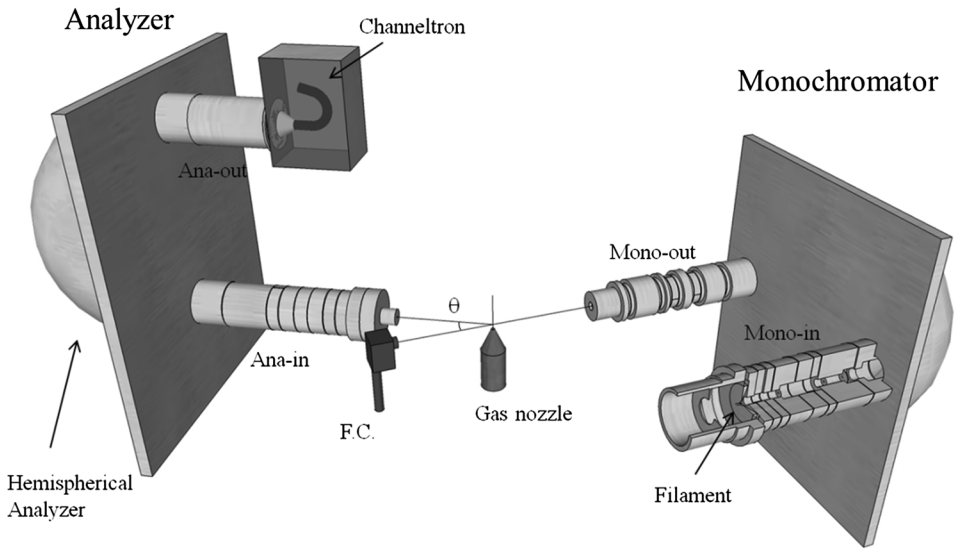

FIG. 8. The configuration of a typical crossed-beam apparatus, such as was used at Sophia University, for making the DCS measurements.

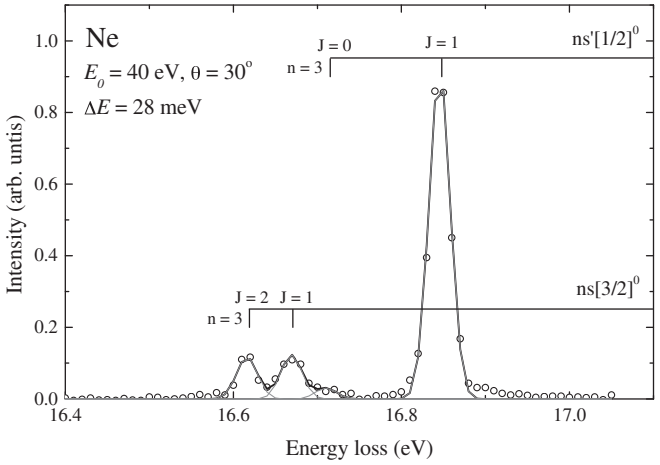

FIG. 9. Typical energy-loss spectrum in neon (Hoshino, Murai, Kato, Itikawa *et al.*, 2013). The incident beam energy was 40 eV and the scattered electron angle was 30°.

profile, the relative contributions of the $3s[3/2]_1(^3P_0)$ and $3s'[1/2]_1(^1P_1)$ states were determined. The impact energy was invariably calibrated against the 19.366 eV resonance of He (Brunt, King, and Read, 1977).

B. Transmission function

For the incident energies of interest ($E_0 = 20$, 25, 30, 50, 100, 200, and 300 eV), and energy losses $\Delta E = 15.5$–17.5 eV in neon, their ratio lies in the range $0.05 < \Delta E/E_0 < 0.88$. It is important to establish the transmission of the analyzer over this entire range. At Sophia University, the spectrometer employed a crossed-beam method with either single and/or double tandem hemispherical energy selectors and a pass energy of 1.5–2 eV with virtual entrance and exit apertures. Cylindrical lenses are used throughout to transport the electron beam. Three possible approaches could be adopted to calibrate the analyzer transmission as described.

(1) All lens voltages have been calculated with a computer program that traces the electrons through the electric fields of the lenses and minimizes the sum of the squared deviations from user-specified aims such as the image position, magnification, and beam angle. [CPO, Ltd., computer code CPO (charged particle optics program) (http://www.electronoptics.com)]. This is achieved by automatically adjusting up to three of the lens voltages at any given time. Other voltages are set such that the maximum angle (beam angle plus pencil angle) is less than 5.5° over the full range of residual energies down to 0.5 eV. After calculating a set of variable voltages for the analyzer for the residual energies of interest ($\Delta E_r = E_0 - \Delta E$), we fit a cubic spline through the data and use the result to drive the lens voltages under computer control. Such voltage sets have been calculated for all impact energies from 20 to 300 eV and for all the residual energy ranges of interest.

(2) The second procedure is a more direct way to characterize the analyzer response. At each T or E_0 of interest, both the energy selector and analyzer are optimized initially by the calculated set of voltages and then refined using He and the elastic scattering process at a scattering angle of 30°. By readjusting the incident electron energy from a residual energy of 0 eV to a residual energy range of interest, while monitoring the current carefully at the Faraday cup (placed at 10 mm from the collision center with 2-mm acceptance diameter), the elastic scattering intensities from He were measured by the analyzer under the same conditions as those for the initial optimization at T (or E_0). The measured intensity is scaled to a constant initial electron current as well as being normalized to the absolute He cross section. A constant factor over all residual energies implies an ideal response of the analyzer, which is achieved above $E_0 = 30$ eV to within a few % and, conversely, a strongly nonuniform response showed up as a consistent pattern in all plots of the scaling factor as a function of residual energies below $E_0 = 25$ eV as expected. Figure 10 shows one example of the variations in the transmission function of the analyzer, over a relevant residual energy range, for the impact energy range of 20–50 eV. Note that, below $E_0 = 30$ eV, over the range from 0 eV to some residual energy, the collision volume is assumed to be constant whereas the current intensity only varies like the electron current monitored in the Faraday cup.

(3) The third way to estimate the transmission factor is to make a comparison with the energy dependence of other measured cross sections for inelastic scattering. For determining the response function of the analyzer, a reliable and absolute inelastic cross section is essential; furthermore, the energy-loss region should preferably be close to that of Ne for the $3s'[1/2]_1$ state at 16.848 eV. In the Sophia University experiment, the excitation of the 2^1P state in He was employed, as the only benchmark cross-section data available, to gauge the analyzer response although its energy loss is larger than for Ne $3s'[1/2]_1$. Absolute scales were thus placed in terms of the measured intensity of the 2^1P to the elastic intensity ratio at 30° for each E_0 of 25, 30, and 50 eV. Consequently, ratios of those measured cross sections to the benchmark data correspond to the analyzer transmission at 21.2 eV as shown in Fig. 10, which are seen to be consistent with those estimated above in method 2. As a consequence, it was found that determining the analyzer transmission response is crucial below 25 eV but not above 50 eV.

Not all experimentalists seem to have been equally careful in calibrating the transmission response of their spectrometers. This contributes to some of the uncertainties and variations in the existing measured cross sections at low-impact energy. Therefore, in terms of assessing the validity of a BEf-scaling result, we have carefully checked the absolute scale of those previous data.

C. Normalization and integration of the cross sections

The observed counts of the scattered electrons from Ne, although it could equally well be any of the species we

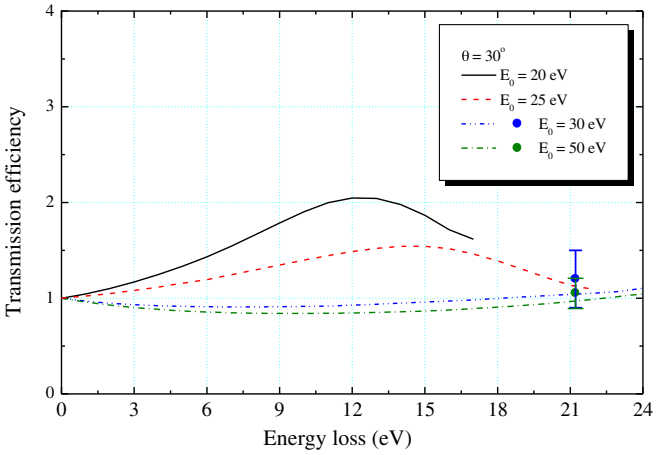

FIG. 10. Typical results in He for calibrating the analyzer transmission response at the scattered electron angle of 30° (Hoshino, Murai, Kato, Brunger *et al.*, 2013). Results using method 2 at $T = 20$ (solid line), 25 (dashed line), 30 (dash-dot-dotted line), and 50 eV (dash-dotted line), and method 3 at $T = 30$ (top circle, blue) and 50 eV (bottom circle, green) are shown.

considered in Sec. V, were converted into absolute cross sections by sequential remeasurement of the known DCSs of He (Boesten and Tanaka, 1992) in conjunction with the relative flow method (Srivastava, Chutjian, and Trajmar, 1975; Nickel *et al.*, 1989). The calibration requires constant Knudsen numbers for equal Ne and He densities in the collision volume, for which the values of the relevant hard sphere diameters for He (2.18 Å) and Ne (2.60 Å) (Lide, 2007) were used. Under the framework of Lassettre's theorem (Lassettre, 1965, 1969; Lassettre, Skerbele, and Dillon, 1969; Lassettre and Skerbele, 1974), the normalized $\mathrm{DCS}_{\mathrm{expt}}$ were next integrated to obtain the integral cross section by using an apparent (or experimental) generalized oscillator strength ($\mathrm{GOS}_{\mathrm{expt}}$ or G_{expt}) as per the fitting procedures described in Sec. IV. Normally, this procedure is applied at high impact energies but, throughout this study, this approach has been extended to low-impact energies to ensure the integrity of the ICS determination over the entire relevant impact energy range.

The errors associated with the data stem from (1) normalization with the reference elastic He DCS (∼10%), (2) and/or normalization with the reference inelastic feature He 2^1P DCS (∼12%), (3) the uncertainty in the transmission response of the analyzer (10%), and (4) statistical (5%) and other uncertainties (for example, in the deconvolution process if it is needed) in the evaluation of the inelastic peak heights (15%). In the case of neon, these latter uncertainties are quite small for the strongest feature (i.e., the $3s'[1/2]_1$ ($^1P_1$) state) but are the dominant errors for the weak and composite features of the $3s[3/2]_1$ ($^3P_0$) state. The sum of all the contributing errors [that is, $\tilde{X} = (\sum_i X_i^2)^{1/2}$] has been calculated as the total error of ∼22% in the DCSs. In addition to these errors, further uncertainties arise in the extrapolation of the DCSs to the 0° and 180° scattering angles for determining the integral excitation cross section. Although corresponding integral cross sections were derived analytically by applying a generalized oscillator strength analysis as described in Sec. IV, an uncertainty of ∼26% on the ICS necessarily arises due to the unknown behavior of the DCSs at small and large scattering angles. Thus a least-squares fit of the experimental GOS would typically add an additional 4% error to the ICS from the value quoted earlier for the respective DCSs.

For consistency, the most practical and reliable method of generating absolute electron-impact excitation cross sections for a given target is to normalize its measured relative excitation cross sections to those for its elastic scattering cross section, which in turn can be accurately determined by normalization to elastic scattering from He. To determine the BE scaling and/or BEf-scaling curve, on the other hand, it is sufficient to measure the DCSs at high-energy impact, above at least 100 eV, and for small scattering angles. Hence, with a good measurement, one can undertake the BE scaling and/or BEf scaling where only the cross section for the elastic scattering in He, as the benchmark, is required to be known.

IV. FITTING PROCEDURES OF THE GOS

To perform the scaling of the Born cross section, we start with the theorem of the limiting oscillator strength (Lassettre, 1965, 1969; Lassettre, Skerbele, and Dillon, 1969; Lassettre and Skerbele, 1974) which makes possible the utilization of electrons as pseudophotons, thus determining optical absorption and ionization cross sections from electron-impact data. That is, as per Eq. (14), the generalized oscillator strength $f_n(K)$ obtained from electron collision measurements approaches the optical f_0 value at small K. Further, as discussed earlier in Sec. II.A.2, within the first Born approximation, it was demonstrated that as the generalized oscillator strength can be expanded in a series of even powers of K, with f_0 as the first term, the limiting value of $f_n(K)$ as K goes to zero is f_0. In addition, Lassettre, Skerbele, and Dillon (1969) proved a more general theorem which applies at all incident energies T and is independent of the validity of the first Born approximation. In this case, f_n is the apparent generalized oscillator strength as defined in Eq. (11a).

In practice, one measures electron-impact cross sections as a function of the scattering angle at high impact energies and converts them into generalized oscillator strengths (or apparent generalized oscillator strengths) as a function of the momentum transfer squared. An extrapolation of these quantities to zero momentum transfer then yields the optical f value. It must be noted, however, that the extrapolation method considers the following points that equally affect the inverse procedure of normalizing electron-impact data to optical f_0 values. Namely, (1) the optical limit is approached most closely at $\theta = 0°$, but in practice it is not possible to measure at this angle since the detector must accept a finite range of angles and there is also necessarily a finite range of angles in the incident electron beam (Lassettre, Skerbele, and Dillon, 1969). (2) The low-angle DCSs, being important in the limit of zero momentum transfer, suffer from experimental uncertainties. Nevertheless, this procedure has proven to be very useful and in some instances it is the only procedure available for normalization of the inelastic electron-scattering data.

Along these lines, extensive experimental effort has been made to generate optical f_0 values. For example, we highlight the following:

(a) Lassettre and co-workers (Lassettre, 1965, 1969; Lassettre, Skerbele, and Dillon, 1969; Lassettre and Skerbele, 1974) determined many such generalized oscillator strengths of valence, Rydberg, and continuum levels of many simple molecules by using this type of extrapolation to deduce f_0. Their DCS measurements were usually carried out at impact energies from 300 to 700 eV. The overall error was estimated to be typically less than 10%, made up of the experimental and extrapolation uncertainties.

(b) The NBS (presently NIST) group (Celotta and Huebner, 1979) provided useful results for optical oscillator strengths by the zero-scattering electron energy-loss technique at $T = 100$ eV. The finite analyzer acceptance solid angle was corrected through oscillator strengths derived from zero-angle energy-loss spectra and the incident electron beam was also highly collimated in this work. The relative oscillator strength determined from the (relative) energy-loss intensity distribution was normalized to a selected optically measured value at one point in the smooth continuous spectrum. Alternatively, a gas mixture was used for the normalization in which the sample gas is precisely mixed with a reference gas such as He that has many well-known optical oscillator strengths. These data agreed to within 10%.

(c) Brion and co-workers (Brion, 1975; Tan *et al.*, 1978) conducted systematic measurements of optical oscillator strengths at an incident energy of $T = 2.5$ keV, with coincidence techniques applied to obtain quantitative photoionization, photofragmentation, and photofluorescence cross sections. Normalization of the experimental data to the absolute scale was achieved by the oscillator strength sum rule. The uncertainty on the absolute oscillator strength scale is claimed to lie within $\pm 5\%$. Moreover, from the dependence of $f(K)$ on K, one can discriminate between optically allowed and forbidden transitions. More details are given in Inokuti (1971). Thus, the electron energy-loss technique still has the advantage of providing an easier and usually more accurate calibration of the absorption spectrum over very wide energy ranges, even today with synchrotron radiation sources in widespread use.

Based on these characteristics of f_n, the discrete excitation scaling has been carried out for atoms and molecules as follows. In the theoretical approach, an unscaled Born cross section corresponds to the theoretical data in the form of dimensionless GOS, tabulated as a function of the momentum transfer squared. In the experimental approach, one can use the experimental data reported in the previous articles at various angles and energies (preferably at small angles and high impact energies) to plot the apparent $f_n(K)$ values as a function of K^2, and then extrapolate the resulting curve to zero momentum transfer. Alternatively, one can carry out one's own experiment at very high impact energy and low scattering angles and assume that the results correspond to the optical limit.

As the scaling methods described previously are valid only for integral cross sections, it is convenient to present a GOS in an analytical form. Vriens (1967) proposed the following formula to represent a GOS for a dipole-allowed excitation:

$$f(x) = \frac{1}{(1+x)^6}\left[\sum_{m=0}^{\infty} \frac{a_m x^m}{(1+x)^m}\right], \tag{34}$$

where

$$x = Q/\alpha^2 \tag{35}$$

and

$$\alpha = \sqrt{B/\mathrm{Ry}} + \sqrt{(B-E)/\mathrm{Ry}}. \tag{36}$$

In Eq. (34), a_m are the fitting coefficients and α is identified from the analytic properties of the GOS, while the binding energy B of an electron in a many-electron molecule can be defined only in the context of a simple independent particle model. As a fitting parameter along with the a_m, the simple form α^2 in Eq. (35) was found to illustrate a GOS calculated from multiconfiguration wave functions. To fit a theoretical GOS, the OOS [f_0 in Eq. (14)] should be the one obtained with the same wave functions as those used to calculate the GOS. A GOS for a dipole-allowed excitation usually peaks at the optical limit, that is, $K = 0$. Sometimes, however, a theoretical GOS has a second peak at a larger K value due to radial nodes in the wave functions. For more details on this latter point, see the review of Inokuti (1971).

The same analytical formula can also be used to fit and extrapolate experimental DCSs to the forward and backward angles not observed in the experiment, and then to integrate that DCS. Here even f_0 should be treated as a fitting parameter. The so-called "experimental" GOS can be obtained by substituting the values of the measured DCSs into Eq. (11a). At low T, experimental GOS often have secondary peaks, as seen later. The secondary peaks here have a very different origin than those seen in the theoretical GOS: the former come from interactions not represented in the Born approximation—such as interference between the direct and exchange scattering amplitudes—while the latter, as noted previously, come from the radial nodes in the wave functions.

The secondary peaks in the experimental GOS at low T cannot be well fitted by directly including extra terms in Eq. (34). Instead, the following function with two fitting parameters b and c, in addition to the leading fraction in Eq. (34), was found to well represent the experimental GOS at low T:

$$g(x) = bx \exp\,(-cx). \tag{37}$$

For He 2^1P, the unscaled GOS curve was drawn from the measured DCS at high impact energies of 100 to 300 eV. The unscaled GOS was verified by the Lassettre limit theorem to compare with the optical limit at $K = 0$ a.u. An example of

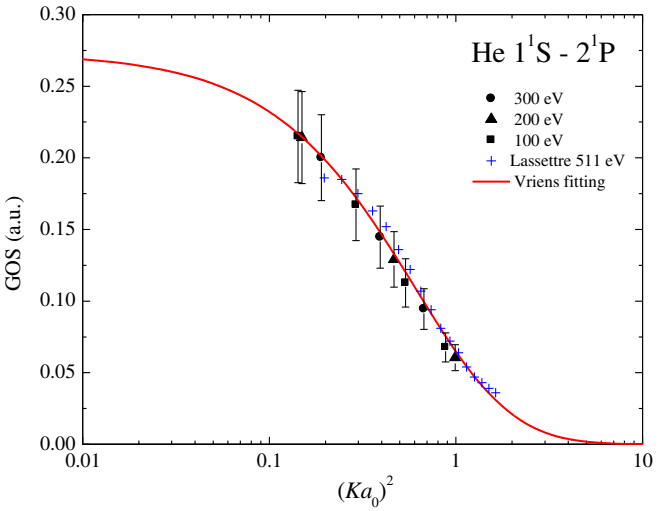

FIG. 11. Example GOS vs K^2 plot, in this case for electron-impact excitation of the 2^1P electronic state in He. From Hoshino *et al.*, 2009.

the GOS versus K^2 fits, specifically for the He 2^1P state, can be found in Fig. 11. As can be seen from this figure, the fit to the data by a modified Vriens parametrization [Eqs. (34) and (37)] was very good.

Integral cross sections are now obtained by integrating the GOS over the limits corresponding to $\theta = 0°$ and $\theta = 180°$ in Eqs. (17) and (19a) with

$$K_{\min} = 2\frac{T}{\mathrm{Ry}}\left[1 - \frac{E}{2T} - \sqrt{1 - \frac{E}{T}}\right],$$
$$K_{\max} = 2\frac{T}{\mathrm{Ry}}\left[1 - \frac{E}{2T} + \sqrt{1 - \frac{E}{T}}\right]. \quad (38)$$

In the case of experimental integral cross sections, Eqs. (17), (19a), and (38) remain valid, although it is the analytical form of $f_{\mathrm{exp}}(K)$ that is explicitly used in Eqs. (17) and (19a), with the result now being the $\sigma_{\mathrm{exp}}(T)$ of interest. This experimental approach has been applied for atoms and molecules at Sophia University and also on a more limited scale at Flinders University.

V. APPLICATIONS: EXAMPLES AND DISCUSSION

Systematic comparisons between the scaling and experimental results were performed to investigate the validity of this simple scaling approach to produce optically allowed electronic excitation cross sections for atoms (Inokuti *et al.*, 1994; Kim, 2001) and molecules (Brunger, Thorn, Campbell, Kato *et al.*, 2008a; Anzai *et al.*, 2012). In the experimental approach, we applied the scaling to the largest cross sections associated with the optically allowed transitions at intermediate impact energies (and small scattering angles). The values of these cross sections increase gradually with increasing impact energy, from threshold to about 10 times the threshold energy, and then slowly decrease in magnitude at high energy. The angular distributions are typically forward peaked, more so with increasing impact energy. On the other hand, integral cross sections for the optically forbidden transitions, like a spin-forbidden transition, rise steeply in magnitude near threshold, reach their peak value within a few electron volts of their threshold energy, and then decrease sharply with increasing impact energy. See illustrative examples of this behavior in Inokuti (1971). The DCSs associated with these forbidden transitions are in many cases nearly isotropic. The latter observation may result in a deviation from the scaling ICS, when a forbidden transition overlaps with an allowed one due to the finite energy resolution of the spectrometer, as in the case of CO (Kato *et al.*, 2007; Kawahara *et al.*, 2008a).

In accordance with the progress in applying the BEf-scaling approach, this section is divided into a discussion of results for atoms and molecules. Only fundamental, well-established, physical and chemical constants are required, such as given by Kim (2001, 2007), http://physics.nist.gov/PhysRefData/ASD/levels_form.html, Ogawa and Ogawa (1975), Pantos, Philis, and Bolovinos (1978), Lewis *et al.* (1988), Hagenow *et al.* (1989), Chan, Cooper, and Brion (1993a, 1993b, 1993c, 1994), Berkowitz (2002), Hoshino, Murai, Kato, Itikawa *et al.*, 2013, and Limão-Vieira *et al.* (2015) and shown in Table 1 in the Supplemental Material [370], in conjunction with the scattering data, to employ the approaches described earlier.

A. Atoms

Employing the Born cross sections calculated from simple wave functions, Kim (2001) demonstrated that the BE and f scalings produced excitation cross sections comparable in accuracy to those obtained by more sophisticated theories such as the CCC method (Bray *et al.*, 2002) and the R-matrix method (Zatsarinny and Bartschat, 2013). As noted previously, he used the plane-wave Born approximation as the starting point because (a) the plane wave is the correct wave function at infinity for an electron colliding with a neutral atom, and (b) it is the simplest collision theory that uses wave functions explicitly. The explicit presentation of target wave functions enables one to use relativistic wave functions for heavy atoms and to distinguish the final state of the target. Along our so-called theoretical approach, Kim further showed that the scaled cross sections were in excellent agreement with available theoretical and experimental data for excitations in H, He, Li, Be, Na, Mg, K, Ca, Rb, Sr, Cs, Ba, Hg, and Tl. Since then, following the so-called experimental approach, the scaling method has been performed for a subset of the available excitation processes in He, Ne, Ar, Kr, and Xe, although we note that at this time only data for He (Hoshino *et al.*, 2010) and Ne (Hoshino, Murai, Kato, Itikawa *et al.*, 2013; Hoshino, Murai, Kato, Brunger *et al.*, 2013) have been published. Those results verified the possibility that rapid and reliable estimations of excitation cross sections can be achieved with the scaling method for many other neutral atoms. The validity of that assertion was fully discussed in the original papers, but some representative examples are briefly summarized for H, He, Ne, Li, Be, and Hg next.

The scaling method does not account for the resonances often observed near excitation thresholds, electron exchange with target electrons, distortion of the plane waves in the vicinity of the target atom, and the polarization of the target

due to the incident electron. Furthermore, the proposed scaling approaches apply only to the integrated excitation cross sections, not to their angular distributions, because the scaling does not alter the shape of the angular distribution as described by the unscaled Born cross sections.

1. Hydrogen and helium

Electron scattering from atomic hydrogen and helium are of fundamental theoretical interest. But, for the H atom, experimental investigation of electron scattering is something of a challenge as it requires preparing the atomic beam source from molecular hydrogen. The first measurements were performed in the late 1950s by microwave techniques to dissociate molecular hydrogen. Because of this experimental difficulty and also problems related to normalization, the measured data have not yet settled down for the electronic excitations of H. As stated by Kim (2001), under those circumstances, the scaling can demonstrate its validity, as shown in Fig. 12, by its excellent agreement with the well-established CCC method (Bray and Stelbovics, 1992). For reference, the BE-scaled ICS curve is added in Fig. 12, which is derived from the DCS data of Williams (1981) using the experimental scaling approach.

Another typical example, in this case for excitation of its 2^1P state, is shown for He in Fig. 13 (Hoshino *et al.*, 2010). Helium has served for many years as a prototype for investigating the fundamentals of electron correlation, both theoretically and experimentally, and Hoshino *et al.* (2009) quite recently studied in depth excitation of the $n = 2$ electronic-state manifold in He at the differential cross-section level. Many of the available data are in good agreement with one another and with sophisticated theories like the CCC approach. Thus, at least for the $n = 2$ states, helium can be considered to be a *benchmarked* system, for both the inelastic and elastic scattering cross sections. Note that in the relative flow method developed by Srivastava and colleagues (Srivastava, Chutjian, and Trajmar, 1975; Nickel *et al.*, 1989), the He elastic scattering cross section (Boesten and Tanaka, 1992) is referred to as the normalization standard. As a consequence, the data shown in Fig. 13 are particularly strong evidence in support of the utility of the scaling methods. As pointed out by Kim, the scaled cross section is somewhat lower in magnitude around the maximum of the ICS and that discrepancy is still an open question. However, even if accidental, the agreement is remarkably good near threshold. As an analytical form for the cross section, the scaling method is useful here for modeling and simulation in practical applications.

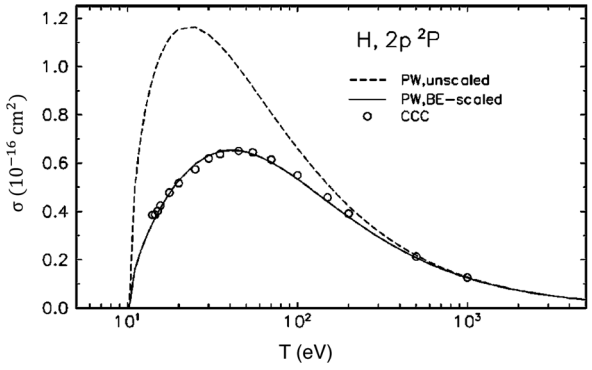

FIG. 12. Comparison of the $1s$-$2p$ excitation cross sections of H. Solid curve, plane-wave Born cross section with BE scaling; dashed curve, unscaled plane-wave Born cross section; open circles, CCC cross section. From Bray and Stelbovics, 1992.

2. Neon

Electron scattering from neon is important in simulation studies in the lighting and laser industries (Puech and Mizzi, 1991; Gray, Latimer, and Spoor, 1996), plasma processing (Malyshev, Donnelly, and Samukawa, 1998; Moshkalyov *et al.*, 1999; Dodt *et al.*, 2010), and for the interpretation of astrophysical data (Hauschildt *et al.*, 1995; Kanik, Ajello, and James, 1996). Therefore, it is not surprising that there have been some quite significant experimental (Register *et al.*, 1984; Suzuki *et al.*, 1994; Khakoo *et al.*, 2002; Allan, Zatsarinny, and Bartschat, 2006; Allan *et al.*, 2009; Hoshino, Murai, Kato, Itikawa *et al.*, 2013; Hoshino, Murai, Kato, Brunger *et al.*, 2013) and theoretical (Machado, Leal, and Csanak, 1982; Zeman *et al.*, 1997; Ballance and Griffin, 2004; Zatsarinny and Bartschat, 2004, 2012a, 2012b; Pflüger *et al.*, 2013) studies of its scattering behavior. The most recent study of the excitation of the $3s[3/2]_1$ and $3s'[1/2]_1$ electronic states in Ne was undertaken by Hoshino, Murai, Kato, Itikawa *et al.* (2013) and Hoshino, Murai, Kato, Brunger *et al.*, 2013, with an example of a typical energy-loss spectrum from that work being found in Fig. 9. Using the experimental methods detailed earlier in Sec. III, they determined absolute DCSs that were subsequently converted into generalized oscillator strengths as a function of the momentum transfer squared (K^2). Those results are plotted in Fig. 14, along with corresponding relevant data from Register *et al.* (1984), Suzuki *et al.* (1994), Khakoo *et al.* (2002), and Cheng *et al.* (2005), and a relativistic distorted-wave calculation from Vos *et al.* (2011).

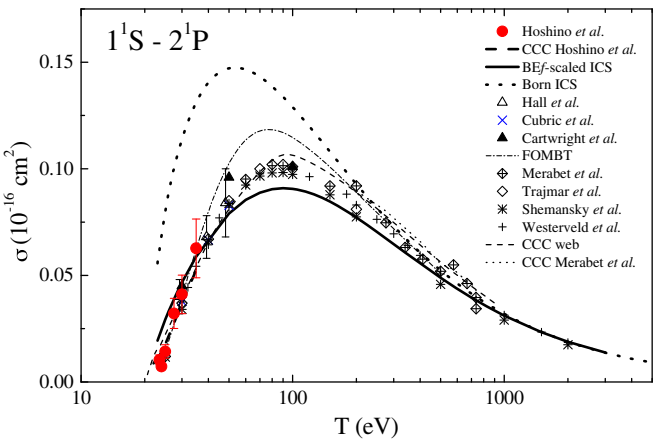

FIG. 13. Electron-impact excitation of the 2^1P electronic state in helium. The BEf-scaled result is shown as the solid line. See also the legend for further details and references (Hall *et al.*, 1973; Trajmar, 1973; Westerveld, Heideman, and van Eck, 1979; Shemansky *et al.*, 1985; Cartwright *et al.*, 1992; Cubric *et al.*, 1999; Merabet *et al.*, 2001; Hoshino *et al.*, 2010; http://www.nist.gov/pml/data/ionization).

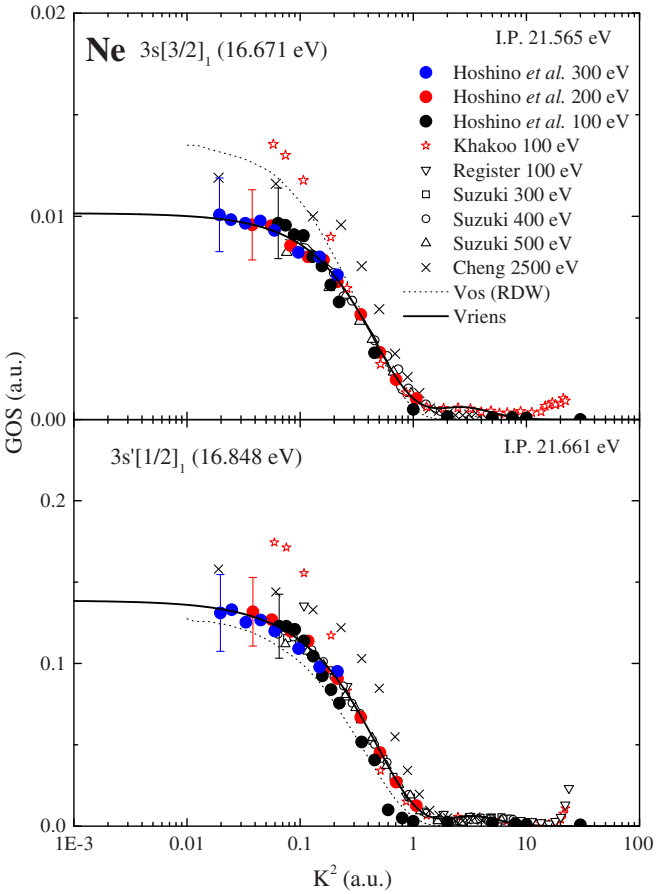

FIG. 14. GOS vs K^2 for excitation of the $3s[3/2]_1$ and $3s'[1/2]_1$ states in neon. Data from Hoshino, Murai, Kato, Brunger *et al.* (2013) and see also the legend. Fits to the GOS data using the formalism of Vriens (1967) (—) and the result of a relativistic distorted-wave calculation from Vos *et al.* (2011) are also plotted.

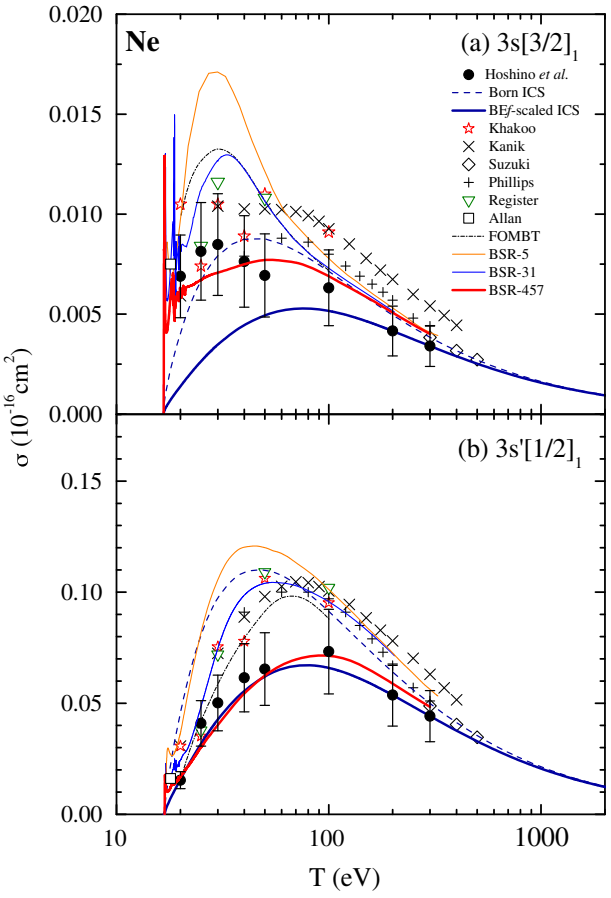

FIG. 15. ICSs from Hoshino, Murai, Kato, Itikawa *et al.*, 2013, both experimental and BEf-scaling calculations, compared to previous results. See the legend and text for further details.

Applying now the formulation of Vriens (1967), as described earlier in Sec. IV, Hoshino, Murai, Kato, Brunger *et al.*, 2013 were able to determine OOS for both states [see Eq. (14)], with their derived values being in good agreement with many earlier independent results as summarized in Table 2 in the Supplemental Material [370]. These experimental and theoretical OOSs are from Wiese, Smith, and Glennon (1966), Gruzdev and Loginov (1973), Natali, Kuyatt, and Mielczarek (1973), Albat and Gruen (1974), Aleksandrov *et al.* (1983), Tsurubuchi, Watanabe, and Arikawa (1990), Chan, Cooper, Guo, and Brion (1992), Hibbert, Ledourneuf, and Mohan (1993), Ligtenberg *et al.* (1994), Suzuki *et al.* (1994), Curtis *et al.* (1995), Gibson and Risley (1995), Zhong *et al.* (1997), Avgoustoglou and Beck (1998), and Hoshino, Murai, Kato, Brunger *et al.* (2013). Note the ICSs (Hoshino, Murai, Kato, Itikawa *et al.*, 2013) were corrected for $E_0 \geq 100$ eV in Fig. 15 (Hoshino, Murai, Kato, Itikawa *et al.*, 2015), although those corrections were minor.

Using fits such as those in Fig. 14, in conjunction with Eqs. (17) and (38), Hoshino, Murai, Kato, Itikawa *et al.* (2013) were able to derive ICSs for both Ne states. Those ICS data, in conjunction with their relevant BEf-scaling results and other experimental (Register *et al.*, 1984; Phillips, Anderson, and Lin, 1985; Suzuki *et al.*, 1994; Kanik, Ajello, and James, 1996; Khakoo *et al.*, 2002; Allan, Zatsarinny, and Bartschat, 2006; Allan *et al.*, 2009) and theoretical results (Machado, Leal, and Csanak, 1982; Zatsarinny and Bartschat, 2012b), are plotted in Fig. 15. For the strong dipole-allowed transition to the $3s'[1/2]_1$ state, excellent agreement was found between the measured ICSs of Hoshino, Murai, Kato, Itikawa *et al.* (2013), their BEf-scaling result, and the B-spline R-matrix result (Zatsarinny and Bartschat, 2012b) over the common energy ranges. Indeed, for this state, only near threshold where the R-matrix calculation shows some resonance structure is there any major discrepancy between the BEf-scaling and R-matrix results. For the $3s[3/2]_1$ state, however, while agreement between the measured data of Hoshino, Murai, Kato, Itikawa *et al.* (2013) and the B-spline R-matrix computation is excellent over their common energy range, their agreement with the BEf-scaling result is satisfactory only for $E_0 \geq 100$ eV. This behavior can be interpreted as follows. In strict LS-coupling terms, the $3s[3/2]_1$ state is in fact optically forbidden. However, due to configuration mixing, the wave function requires both a singlet and a triplet coefficient for a proper description. Therefore, at high energies where the singlet coefficient dominates, the BEf-scaling result agrees well with the measured data for the $3s[3/2]_1$ state. But, at lower energies,

where the triplet coefficient becomes more important as exchange scattering begins to contribute, we find that the BEf-scaling result, which as noted previously does not account for electron exchange, necessarily underestimates the magnitude of the experimental ICS.

The top pane in Fig. 15 also indicates important near-threshold resonance structure in the $3s[3/2]_1$ cross section, which also cannot be accounted for within the plane-wave Born scaling framework we consider here. Hence, in this case, the utility of the BEf-scaling results is limited to the higher energy regime although this is still useful for the modeling and simulation communities. Finally, we note that Hoshino, Murai, Kato, Itikawa *et al.* (2013) recently detected a minor error in their ICS for both states and for $E_0 \geq 100$ eV. The correct ICS are plotted here in Fig. 15, with full details being found in the errata of Hoshino, Murai, Kato, Brunger *et al.* (2015) and Hoshino, Murai, Kato, Itikawa *et al.* (2015).

3. Alkali and alkaline-earth elements

There is an extensive series of electron-impact optical emission measurements on the alkali metals from Gallagher and co-workers. All of those studies largely concentrate on the main dipole-allowed transitions, an appropriate filter being used to select the required wavelengths for the emission in question. Corrections to the raw data for cascade contributions and for the polarization of the emitted radiation were attempted for each atom, with the normalization of the corrected photon signal, as a function of energy, being achieved through the use of a high-energy Born calculation. Typical errors on the so determined ICS were usually better than 10%. As just one example, although the conclusions from it also hold for the main dipole-allowed transitions in sodium, potassium, rubidium, and cesium, let us consider the results for the $2s$-$2p$ excitation in lithium. In Fig. 16, we compare the unscaled plane-wave Born cross sections and BEf-scaled ICS with the experimental $2s$-$2p$ results of Leep and Gallagher (1976) and a CCC calculation result from Schweinzer *et al.* (1999). It is clear that the BEf-scaling method gives cross sections that are in excellent agreement with the measurements across all the common energy range. Indeed, for Li, the scaling method results are quite probably in better accord with the experimental results than those from the more sophisticated CCC approach. The utility of using the scaling method for this system is thus evident.

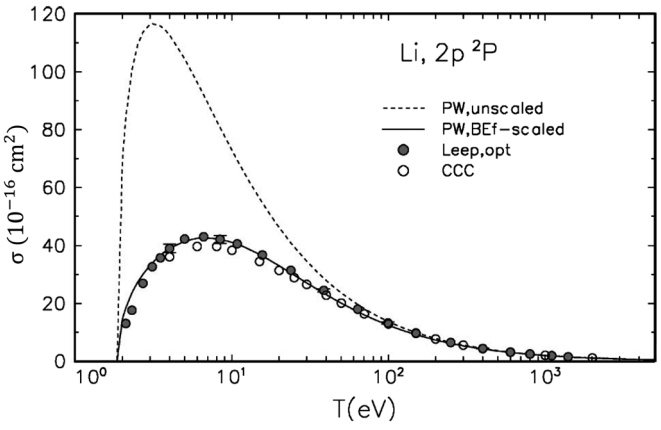

FIG. 16. Comparison of the $2s$-$2p$ excitation cross sections of Li. Dashed curve: unscaled plane-wave Born σ_{PWB}; solid curve: BE- and f-scaled σ_{PWB}; solid dots: experimental data for optical emission from Leep and Gallagher (1976); and circles: CCC theory of Schweinzer *et al.* (1999).

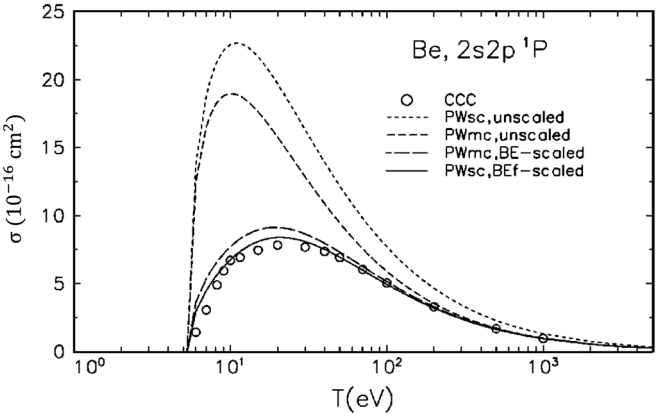

FIG. 17. Comparison of the $2s^2$-$2s2p^1P$ excitation cross sections of Be. Circles: CCC cross section (Fursa and Bray, 1997); short-dashed curve: unscaled plane-wave Born cross section from uncorrelated wave functions; medium-dashed curve: unscaled plane-wave Born cross section from multiconfiguration wave functions; long-dashed curve: BE-scaled plane-wave Born cross section from multiconfiguration wave functions; solid curve: BE- and f-scaled plane-wave Born cross sections from uncorrelated wave functions.

Beryllium is the first member of the group IIA alkaline-earth elements with its scaled Born cross sections for the excitation of the 2^1P level having been calculated by Kim (2001) with both Dirac-Fock and multiconfiguration wave functions. Those ICSs are plotted in Fig. 17 and compared with independent CCC calculations from Fursa and Bray (1997). While no experimental data exist for the excitation of the $2s2p^1P$ state in Be, we note the good agreement between Born scaling results and various measurements in magnesium (Mg: 3^1P state) (Leep and Gallagher, 1976), calcium (Ca: 4^1P state) (Ehlers and Gallagher, 1973), strontium (Sr: 5^1P state) (Chen, Leep, and Gallagher, 1976), and barium (Ba: 6^1P state) (Chen and Gallagher, 1976). This, and the excellent agreement seen in Fig. 17 between the BEf-scaling results and the CCC results, gives us confidence in the validity of applying the scaling approach to the group IIA elements, at least for the main dipole-allowed ($E1$) transitions in modeling studies. Further details for all the group IIA elements are well summarized by Kim (2001). Note that Be has assumed some importance recently as one of the materials for use in the International Thermonuclear Experimental Reactor (ITER) project. Modeling of its performance under the anticipated operational conditions is thus crucial, with reliable electron cross sections being a part of the extensive data base that is needed for such modeling.

4. Heavy elements

Ever since the seminal experiment of Franck and Hertz (1914), members of both the electron-scattering and gaseous

electronics communities have been very interested in understanding the fundamental physics that underpins the phenomena they observed (Robson, White, and Hildebrandt, 2014). Thus, integral cross sections for the main electron-scattering excitation processes in mercury, including the $6s^2$-$6s6p\,^1P$ optically allowed transition, have been of topical interest for quite some time and as a consequence Kim (2001) provided scaled Born cross-section results for that main dipole transition. Those results are plotted in Fig. 18, along with corresponding experimental data from Peitzmann and Kessler (1990) and Panajotović *et al.* (1993), and a relativistic distorted-wave theory (RDW) result from Srivastava *et al.* (1993). It is clear from Fig. 18 that both the RDW and unscaled Born cross sections overestimate, quite significantly, the magnitude of the $6\,^1P$ integral cross section, whereas both the BE- and BEf-scaled results are in much better accord with the measured data (Peitzmann and Kessler, 1990; Panajotović *et al.*, 1993). Indeed the results from Peitzmann and Kessler (1990), at 15, 60, and 100 eV, are in excellent agreement with those from the BEf-scaled ICSs, while the data of Panajotović *et al.* (1993) lie typically between the BE- and BEf-scaled calculations. However, the absolute scale of the Panajotović *et al.* cross sections was set using the optical oscillator strength from Lurio (1965) whose value is about 10% higher than more recent OOS results for this transition on the NIST website (http://www.nist.gov/pml/data/ionization). If the results from Panajotović *et al.* were scaled down by ∼10% to account for this observation, then good agreement across the common energy range would now be found with the BEf-scaled cross sections. This illustrates the usefulness of the Born scaling method even for heavy elements, where a relativistic description of the target might be anticipated as being required.

B. Molecules

Along with the apparent (or experimental) GOS introduced by Lassettre, Skerbele, and Dillon (1969), which applies at all incident energies and is independent of the validity of the Born approximation, the integral first Born cross section based on the measured differential cross section (see Sec. IV) can be obtained by the fitting of a semiempirical formula (Lassettre, 1965, 1969; Vriens, 1967; Lassettre, Skerbele, and Dillon, 1969; Lassettre and Skerbele, 1974) to the derived GOS as a function of K^2. This is important for electron-molecule scattering cases because unscaled Born cross sections are seldom readily available for molecules.

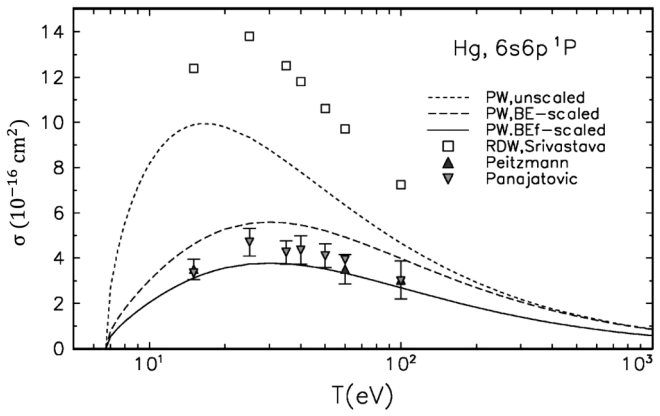

FIG. 18. Comparison of the $6s^2$-$6s6p\,^1P$ excitation cross sections of Hg. Short-dashed curve: unscaled plane-wave σ_{PWB}; medium-dashed curve: BE-scaled σ_{PWB}; solid curve: BE- and f-scaled σ_{PWB}; squares: relativistic distorted-wave Born theory of Srivastava *et al.* (1993); upright triangles: experimental data for direct excitation from Peitzmann and Kessler (1990); and inverted triangles: data for direct excitation from Panajotović *et al.* (1993).

As mentioned previously, in electron-molecule scattering *ab initio* theoretical calculations are complicated because of the nonspherical, multicentered composite target with its associated internal degrees of freedom of motion: rotation, vibration, and dissociation. The analysis is further complicated due to the often significant overlap of the vibrational progressions of the different electronic states, as shown in Figs. 19(a) and 20(a), for even simple diatomic molecules such as H_2 and CO. Calculation and analysis of the spectra thus becomes much more complicated than in atoms.

However, for inelastic electron-molecule collisions at high energy, the integrated cross section in Eq. (9c) is simplified by introducing the following two approximations to give

$$\sigma(a, v \to a', v') = \frac{8\pi}{k^2}\left|\int dR\chi_{a'}^{v'}\chi_a^v\right|^2 \int_{k-k'}^{k+k'} \frac{dK}{K^3 a_0^2}\langle|\epsilon_{a,a'}(\overline{R}, \boldsymbol{K})|^2\rangle_{av}, \tag{39}$$

where (1) we assumed that the vibrational spacing is considerably less than both the electronic excitation energy in question and the incident energy T, and (2) based on the Franck-Condon principle, the integral over the electronic coordinates is assumed to be independent of R, that is, an appropriate constant $\overline{R}$ (such as the equilibrium bond length) is substituted for R in Eqs. (6a) and (6b). Here each vibrational component of a given electronic state is characterized by the Franck-Condon factor. Note that although Eq. (39) is derived under quite restrictive assumptions (Lassettre *et al.*, 1968; Inokuti, 1971), experimental evidence suggests that the Franck-Condon factor approach is valid. The relative intensities for vibrational peaks belonging to the same electronic transition are found to be remarkably independent of the scattering angle and the incident electron energy down to around 20–30 eV for a number of molecular transitions with excitation energies as high as about 10 eV. This situation in which the first Born approximation is clearly inappropriate suggests application of a sudden approximation to the nuclear motion.

Thus, also assuming that k' depends only slightly on v', the vibrational wave functions are factorized in the integrated cross section as

$$\epsilon_{a,a'}(\overline{R}, \boldsymbol{K}) = \int d\boldsymbol{r}_m \phi_{a'}^*(\boldsymbol{r}_m, \overline{R})\phi_0(\boldsymbol{r}_m, \overline{R}). \tag{40}$$

Consequently, the electronic excitation cross section is calculated at the equilibrium distance ($R_e = \overline{R}$) in the initial state and then averaged over all molecular orientations. Furthermore, if the excited states in the Franck-Condon region are repulsive, a continuous energy band emerges over a

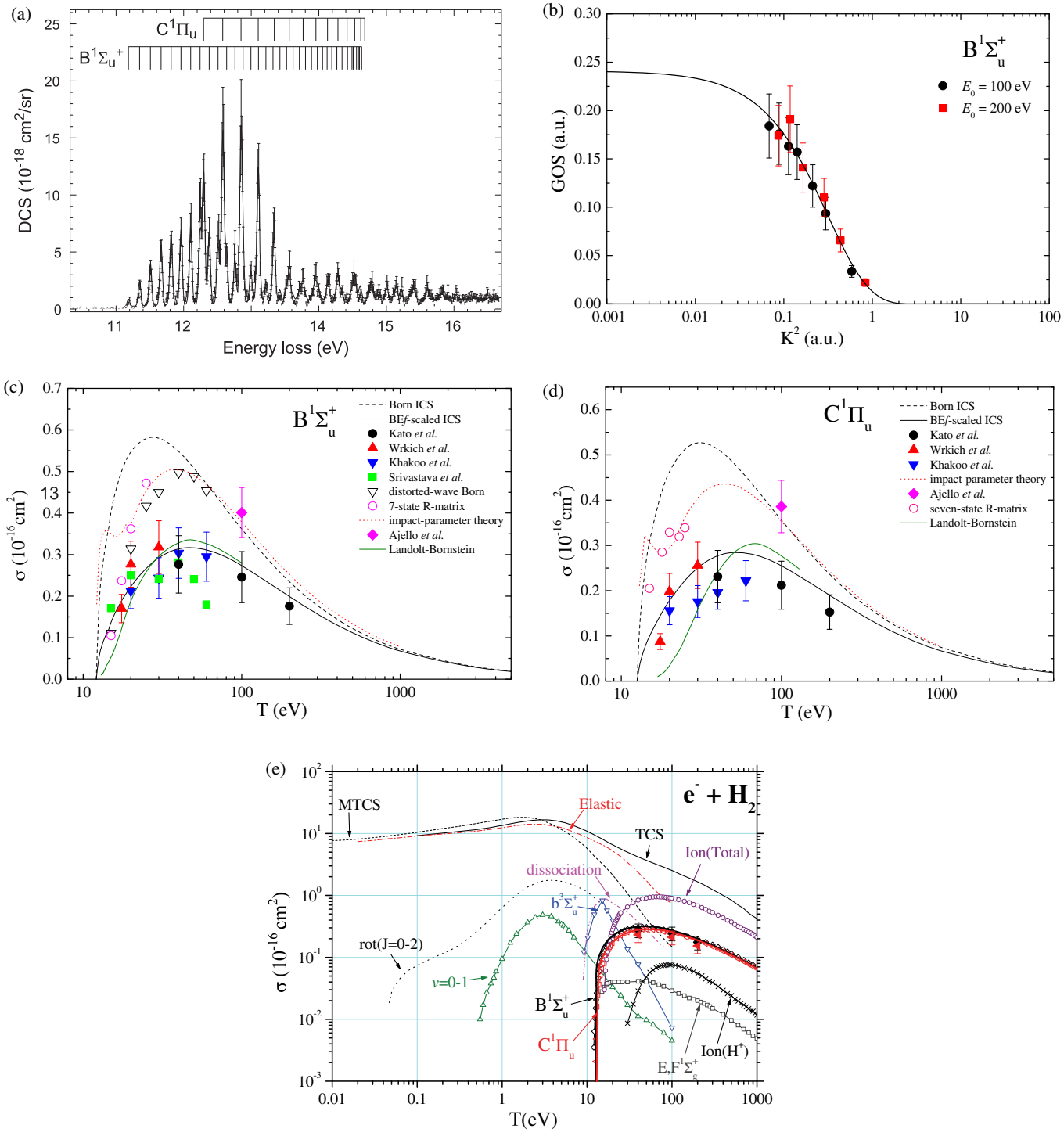

FIG. 19. Electron impact on H_2: (a) Typical electron energy-loss spectrum and its associated spectral deconvolution (Kato *et al.*, 2008) for 40 eV, at 10°. Also plotted are the relevant vibrational sublevels of the respective $B^1\Sigma_u^+$ and $C^1\Pi_u$ electronic states. (b) GOS as a function of K^2 for the $B^1\Sigma_u^+$ electronic state for two different impact kinetic energies, illustrating the procedure for determining the OOS in the limit of small K and the form of the GOS from which the integrated cross section can be determined. (c) ICSs for the $B^1\Sigma_u^+$ electronic state. (d) ICSs for the $C^1\Pi_u$ electronic state. (c) and (d) See the legend and the text for details. (e) Recommended cross-section data from Itikawa and colleagues (Yoon *et al.*, 2008), updated to include recent ICS (Kato *et al.*, 2008) and with corresponding BEf-scaling results (Anzai *et al.*, 2012).

portion of the energy-loss spectrum, the so-called dissociation continuum. An example of this in molecular oxygen, for the Schumann-Runge continuum (Suzuki *et al.*, 2011), can be seen in Fig. 21(a). Because of the high density of available excited states in polyatomic molecules, dissociative continua frequently overlap discrete states and tend to mask their presence. When the discrete and continuum states are coupled, discrete lines may be broadened by the nonradiative decay

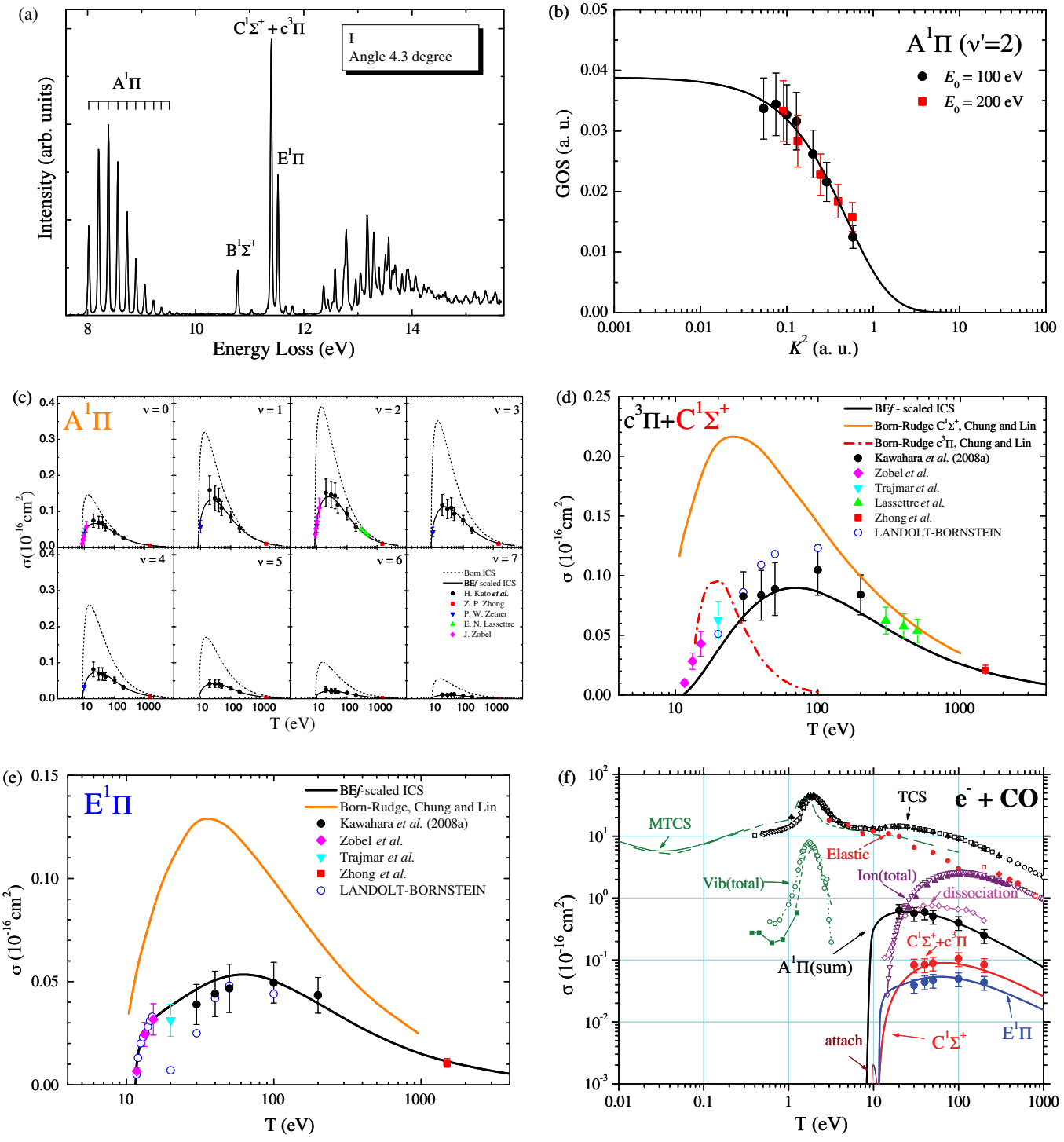

FIG. 20. Electron impact on CO: (a) Typical electron energy-loss (ΔE) spectrum, $\Delta E \sim 7.5$–15.5 eV, for electronic-state excitation. The incident energy is 100 eV and the scattered electron angle is 4.3°. (b) GOS vs K^2 for the $A^1\Pi$ ($\nu' = 2$) electronic state. A Vriens-type fit (Vriens, 1967) to the measured data at 100 and 200 eV is shown. From Kato *et al.*, 2009. (c) ICSs for the vibrational sublevels of the $A^1\Pi$ electronic state. (d) ICSs for the $C^1\Sigma^+ + c^3\Pi$ electronic states. (e) ICSs for the $E^1\Pi$ electronic state. (c)–(e) See the legend and the text for details. (f) Recommended cross-section data set from Zecca, Karwasz, and Brusa (1996), updated to include the recent ICS (Kato *et al.*, 2007; Kawahara *et al.*, 2008a) and with corresponding BEf-scaling results (Anzai *et al.*, 2012).

channel, with an effect called predissociation. Several Rydberg states are also observed as a series of peaks in the energy-loss spectra. However, when Rydberg and valence states strongly couple, expected vibrational sublevels may be suppressed in the energy-loss spectra. This effect is known to be strongly dependent on the kinematical conditions under investigation (Lewis *et al.*, 2001). Moreover, disagreement between the scaling results and the measured ICS data may be caused by contributions from optically forbidden transitions near the electronic excitation threshold.

Because these complications in the data analysis are inevitable for molecules, note that the present scaling method has some inherent performance limitations in addition to those caused by the instrumental energy resolution. Even so, however, as shown later, the scaling model is a promising approach to provide reliable cross sections for optically allowed excitations in molecules. This, when coupled with its efficacy for describing ionization, as established earlier, makes the scaling model a potentially useful tool in describing phenomena for which electron-driven processes are important.

The first demonstration to validate scaling methods for molecules was carried out for H_2 by Kim just before his tragic death (Kim, 2007). There were several reasons for this initial choice: H_2 is the simplest molecule, playing the same role among molecules as does the hydrogen atom among atoms, and considerable data are available to test the scaling models for the excitation of ground-state H_2 to the lowest two dipole-allowed excited electronic states $B^1\Sigma_u^+$ and $C^1\Pi_u$ (Kim, 2007). However, Kim found that the energy dependence and magnitude of the available integrated excitation cross sections differed between the existing theories and experiments (Kim, 2007). Consequently, more reliable experimental data were required to assess the scaling models. A subsequent paper (Kato *et al.*, 2008) showed that the scaled Born integral cross sections in H_2 were in good agreement with experiment, from near threshold to 200 eV (and from some of the earlier results) for integral cross sections for those electric dipole-allowed transitions.

The scaling model was extended to CO (Kato *et al.*, 2007; Kawahara *et al.*, 2008a), O_2 (Suzuki *et al.*, 2011), N_2, NO, CO_2 (Kawahara *et al.*, 2008b), OCS (Limão-Vieira *et al.*, 2015), BF_3 (Duflot *et al.*, 2014), H_2O (Thorn *et al.*, 2007b), N_2O (Kawahara *et al.*, 2009), and C_6H_6 (Kato *et al.*, 2011), some of which are summarized later. In addition, as they now represent benchmark electronic-state cross sections, these integral cross sections, for some of the dipole-allowed excitations in these molecules, are added into the original cross-section sets taken from the data reviews for H_2 (Yoon *et al.*, 2008), O_2 (Itikawa, 2009), CO_2 (Itikawa, 2002), H_2O (Itikawa and Mason, 2005), CO (Zecca, Karwasz, and Brusa, 1996), and N_2O (Karwasz, Brusa, and Zecca, 2001). The review of Itikawa and Mason (2005) for H_2O is now generally regarded as being out of date, with a more complete and benchmarked compilation being found in de Urquijo *et al.* (2014). Similarly, a recent compilation for CO (Itikawa, 2015) supercedes the earlier review of Zecca and colleagues.

1. H_2

Electron energy-loss (ΔE) spectroscopy (EELS) measurements were made for various incident energies (E_0) in the range 40 to 200 eV, and for scattered electron angles θ from 3.5° to 130° (Kato *et al.*, 2008). A typical energy-loss spectrum is plotted for the $B^1\Sigma_u^+$ and $C^1\Pi_u$ excitation states in Fig. 19(a) over the energy-loss range from ~10.5 to 16.7 eV, at $E_0 = 40$ eV and $\theta = 10°$.

The complication here in the data analysis is that there are many overlapping vibrational sublevels of the respective H_2 electronic states in this energy-loss range. As a consequence, the various $B^1\Sigma_u^+$ and $C^1\Pi_u$ contributions to the energy-loss spectra had to be spectrally deconvolved very carefully. To achieve this, Kato *et al.* (2008) adapted the approach outlined in detail by Campbell *et al.* (1997), modified here to incorporate the relevant energies and Franck-Condon factors from Wrkich *et al.* (2002) and from the International Atomic Energy Agency (IAEA) website (http://www-amdis.iaea.org/data/INDC-457/).

Using energy-loss spectra such as in Fig. 19(a), obtained by employing the experimental techniques and normalization procedure outlined earlier in Sec. III, as well as a spectral deconvolution of the overlapping vibrational features, Kato *et al.* (2008) were able to determine manifold differential cross sections as a function of the scattered electron angle for both the $B^1\Sigma_u^+$ and $C^1\Pi_u$ states. Those DCSs as a function of θ were then, using Eqs. (10b) and (5a), transformed to generalized oscillator strengths as a function of K^2 whereupon a Vriens-type analysis (see Sec. IV) was performed. A typical result from that approach, for data taken at 100 and 200 eV and for the $B^1\Sigma_u^+$ electronic state, is illustrated in Fig. 19(b).

Here we find that a single function represents the data well at both 100 and 200 eV, and from Eq. (14) the limiting value at $K^2 \to 0$ a.u. is the optical oscillator strength for that transition. Results of the OOS determined by Kato *et al.* (2008) for both the $B^1\Sigma_u^+$ and $C^1\Pi_u$ electronic states are summarized in Table 3 in the Supplemental Material [370], along with a selection of previous experimental work from Geiger and Schmoranzer (1969), Fabian and Lewis (1974), Berkowitz (1979), Chan, Cooper, and Brion (1992), and Zhong *et al.* (1998), and theoretical work from Allison and Dalgarno (1970), Arrighini, Biondi, and Guidotti (1980), Liu and Hagstrom (1993), and Borges and Bielschowsky (1999). While the OOSs, to within their stated error of 20%, of Kato *et al.* (2008) were consistent with most of the other results in Table 3, their values for both the $B^1\Sigma_u^+$ and $C^1\Pi_u$ states were a little bit lower (systematically) than those other data. This might be an indication that 100 and 200 eV are a little low in energy if your main aim is to determine OOS. However, this observation in no way affects the use of the apparent GOS in order to determine the ICS for those states at each energy.

Employing the derived apparent GOS in Eq. (20) and using Eqs. (38), Kato *et al.* (2008) determined relevant ICS at each energy they studied, for both the $B^1\Sigma_u^+$ and $C^1\Pi_u$ electronic states with those results being plotted in Figs. 19(c) and 19(d), respectively. Also plotted in these figures are corresponding results from Srivastava and Jensen (1977), Ajello *et al.* (1984), Khakoo and Trajmar (1986), and Wrkich *et al.* (2002), a distorted-wave Born calculation (Fliflet and McKoy, 1980), both unscaled and scaled plane-wave Born calculations (Kim, 2007), an R-matrix calculation (Branchett, Tennyson, and Morgan, 1990), and a data compilation from Landolt-Bornstein (Brunger, Buckman, and Elford, 2003). Both Figs. 19(c) and 19(d) demonstrate the efficacy of the BEf-scaling results (Kim, 2007) to describe the ICSs for each of the $B^1\Sigma_u^+$ and $C^1\Pi_u$ electronic states. Note that Ajello *et al.* (1984) measured the intensity of light emitted from the states in question, after the H_2 molecule was excited by electron impact. This method has the disadvantage of possible cascade contamination from higher states (Kim, 2007).

The updated cross-section data set of H_2 from Itikawa and colleagues (Yoon *et al.*, 2008) is shown in Fig. 19(e), along with integrated cross sections for the H_2 $^1\Sigma_u^+$ and $^1\Pi_u$ electronic excitation states assessed against BEf-scaling computation for a wide energy range from threshold to 1000 eV. Within the paradigm of the BEf-scaling method, the calculated cross sections track reasonably well the experimental results over the entire common energy range and are also mostly consistent with the previously recommended data.

2. CO

Electron energy-loss spectra were measured (Kato *et al.*, 2007, 2009; Kawahara *et al.*, 2008a) at various incident energies in the range 20 to 200 eV for scattered electron angles from 3.5° to 130°. A typical energy-loss spectrum is plotted for the $A^1\Pi$, $C^1\Sigma^+ + c^3\Pi$, and $E^1\Pi$ states in Fig. 20(a). The $A^1\Pi$ state consists of the vibrationally resolved ($\nu' = 0$–8) sublevels, while the optically forbidden $c^3\Pi$ electronic state is almost degenerate in energy with the $C^1\Sigma^+$ state. As there was no possibility, with the current energy resolution, of uniquely resolving those c and C states, no attempt by Kawahara *et al.* (2008a) and Kato *et al.* (2009) was made to do so. Note that the $A^1\Pi$ electronic state represents an excellent choice to test the BEf-scaling approach, because it is a strong optically allowed transition from the ground state and because it is isolated from the other excited electronic states in the spectrum of CO [see Fig. 20(a)].

Using the techniques and procedures described previously in Secs. III and IV, Kato *et al.* (2007) and Kawahara *et al.* (2008a) determined absolute DCSs for each of the vibrational sublevels of the $A^1\Pi$ electronic state and for the $C^1\Sigma^+ + c^3\Pi$, and $E^1\Pi$ electronic states. The 100 and 200 eV data were then converted into apparent GOS as a function of K^2 and a Vriens-type fit (Vriens, 1967) performed in each case. Note that at these higher energies the $c^3\Pi$ contribution will be very small and can be effectively ignored. An example of this process for the $\nu' = 2$ sublevel of the $A^1\Pi$ electronic state can be found in Fig. 20(b). Taking the limit as $K^2 \to 0$ a.u., OOSs for each vibrational sublevel of the $A^1\Pi$ state and for the $C^1\Sigma^+$ and $E^1\Pi$ states were subsequently determined. Those data are summarized in Table 4 in the Supplemental Material [370] and compared with other relevant experimental determinations from Lassettre and Skerbele (1971), Chan, Cooper, and Brion (1993a), Zhong *et al.* (1997), and Eidelsberg *et al.* (1999), and theory from Kirby and Cooper (1989) and Chantranupong *et al.* (1992). Typically the OOSs from Kato *et al.* (2007) and Kawahara *et al.* (2008a) were found to be in good agreement with those from Chan, Cooper, and Brion (1993a) and Zhong *et al.* (1997). This demonstrates the elegance, power, and usefulness of the limit theorem in Eq. (14). However, the theoretical OOS values from Chantranupong *et al.* do not agree with those from the experiments due to their vibrational wave functions for higher ν' being inaccurate.

The updated integral cross-section data sets of CO are shown in Figs. 20(c)–20(e), with the ICS for the $A^1\Pi$, $C^1\Sigma^+ + c^3\Pi$, and $E^1\Pi$ electronic excitation states from Kato *et al.* (2007) and Kawahara *et al.* (2008a) benchmarked against a corresponding BEf-scaling computation for a wide energy range from threshold to 1000 eV. Here the theoretical ICSs are determined from the work of Chantranupong *et al.* (1992). Also shown in Figs. 20(c)–20(e) are other experimental results from Lassettre and Skerbele (1971), Trajmar, Williams, and Cartwright (1971), Zobel *et al.* (1996), Zhong *et al.* (1997), and Zetner, Kanik, and Trajmar (1998), and a Landölt-Bornstein compilation (Brunger, Buckman, and Elford, 2003). A Born-Rudge calculation result from Chung and Lin (1974) is also plotted where possible. For the $A^1\Pi$ state in Fig. 20(c), excellent agreement was found between the experimental and BEf-scaled ICS for each vibrational sublevel. For the $C^1\Sigma^+ + c^3\Pi$ states in Fig. 20(d), at the higher (>30 eV) energies, the $C^1\Sigma^+$ BEf-scaling calculation is in good agreement with the experimental data and most of the other experimental data at least to within the stated uncertainties on those ICS (Kawahara *et al.*, 2008a). At lower (<30 eV) energies, however, the available ICS tend to be somewhat higher in magnitude than the BEf-scaling result. This discrepancy is due to the contribution from the $c^3\Pi$ state that cannot be experimentally resolved. For the $E^1\Pi$ state, there is again excellent agreement between the experimental data and the BEf-scaled result. This can be clearly seen in Fig. 20(e).

Finally, in Fig. 20(f) we update the recommended data compilation for CO of Zecca, Karwasz, and Brusa (1996) to incorporate both the measured ICS of Kawahara *et al.* (2008a) and their BEf-scaling results. Only the manifold $A^1\Pi$ integral cross section has been plotted here. A plot such as Fig. 20(f) is illustrative in showing that the contribution of the excited electronic states in CO to the total cross section is really quite small. Nonetheless, it is the emissions from precisely those excited states that, for just one example, provide important remote sensing opportunities for studying planetary atmospheres (Campbell and Brunger, 2013). Itikawa (2015) recently compiled a recommended data compilation for electron-CO scattering. This database incorporates all the results from Kawahara *et al.* (2008a), including their BEf-scaling computations.

3. O_2

EELS were measured at various incident energies in the range 15 to 200 eV for scattered electrons ranging from 2° to 130°. A typical energy-loss spectrum from Suzuki *et al.* (2011) is plotted for the $B^3\Sigma_u^-$ [the Schumann-Runge (SR) continuum], $E^3\Sigma_u^-(v' = 0)$ [longest band (LB)], and $E^3\Sigma_u^-(v' = 1)$ [second band (SB)] electronic excitation states in Fig. 21(a), over the energy-loss range from 4.9 to 14.4 eV and at $E_0 = 100$ eV and $\theta = 5.1°$. The electronic-state spectroscopy of O_2 is actually quite complicated (Cartwright, 2005), as indicated in Fig. 21(b), and it is well known that the SR continuum, LB, and SB states in O_2 suffer from the effects of extensive Rydberg-valence interactions in varying degrees (Lefebvre-Brion and Field, 1986). In particular, it is generally considered (Lewis *et al.*, 2001) that these Rydberg-valence perturbations lead to an anomalous (non-Franck-Condon) behavior in the vibrational intensity distribution of the $E^3\Sigma_u^-$ state. This is seen in Fig. 21(c) where an avoided level crossing is apparent. Hence, the LB and SB transitions actually arise as excitations from the ground

molecular state of O_2 to the lowest two members of the vibrational progression in the excited $E^3\Sigma_u^-$ electronic state.

Despite the complicated valence electronic structure of O_2, Suzuki *et al.* (2011) were able to measure cross sections for the SR, LB, and SB states. Those data are plotted in Figs. 21(d)–21(f), respectively, where they are compared to corresponding experimental ICSs from Lassettre, Silverman, and Krasnow (1964), Trajmar, Williams, and Kuppermann (1972), Wakiya (1978), Newell, Khakoo, and Smith (1980), Shyn, Sweeney, and Grafe (1994), and Shyn, Sweeney, Grafe, and Sharp (1994). For the case of the SR continuum, ICSs derived from electron-transport (swarm) data by Hake and Phelps (1967) are also plotted. Plane-wave Born ICSs and BE*f*-scaled ICSs were additionally determined by Suzuki *et al.* (2011), with those results also being shown in Figs. 21(d)–21(f). For the SR continuum, Suzuki *et al.* (2011) used the experimental GOS of Xu *et al.* (2010) to determine the unscaled Born ICS and the accurate OOS from Chan, Cooper, and Brion (1993b) to then effect the BE*f*-scaling method; for the LB and SB states the unscaled Born ICSs were found using the theory results from Li *et al.* (1992), while the required accurate OOSs were taken from Ogawa and Ogawa (1975) and Lewis *et al.* (1988), respectively.

Finally, but only for the SR continuum, in Fig. 21(d) some theoretical impact parameter ICSs (Garrett *et al.*, 1985; Laricchiuta, Celiberto, and Capitelli, 2000) and a Born-Ochkur level ICS (Chung and Lin, 1980) are given. The following points are worth noting: (1) For the SR-continuum transition, the absolute values of the Suzuki *et al.* (2011) experimental ICS were largely consistent with the higher (>100 eV) energy experimental data and the calculations available. Their data in the other lower (<100 eV) energy range were also appropriate for the trend of the earlier measured cross sections over the entire energy range, although this agreement was more marginal with the previous results from other groups (Suzuki *et al.*, 2011) that showed more scatter. The experimental SR-continuum ICSs of Suzuki *et al.*

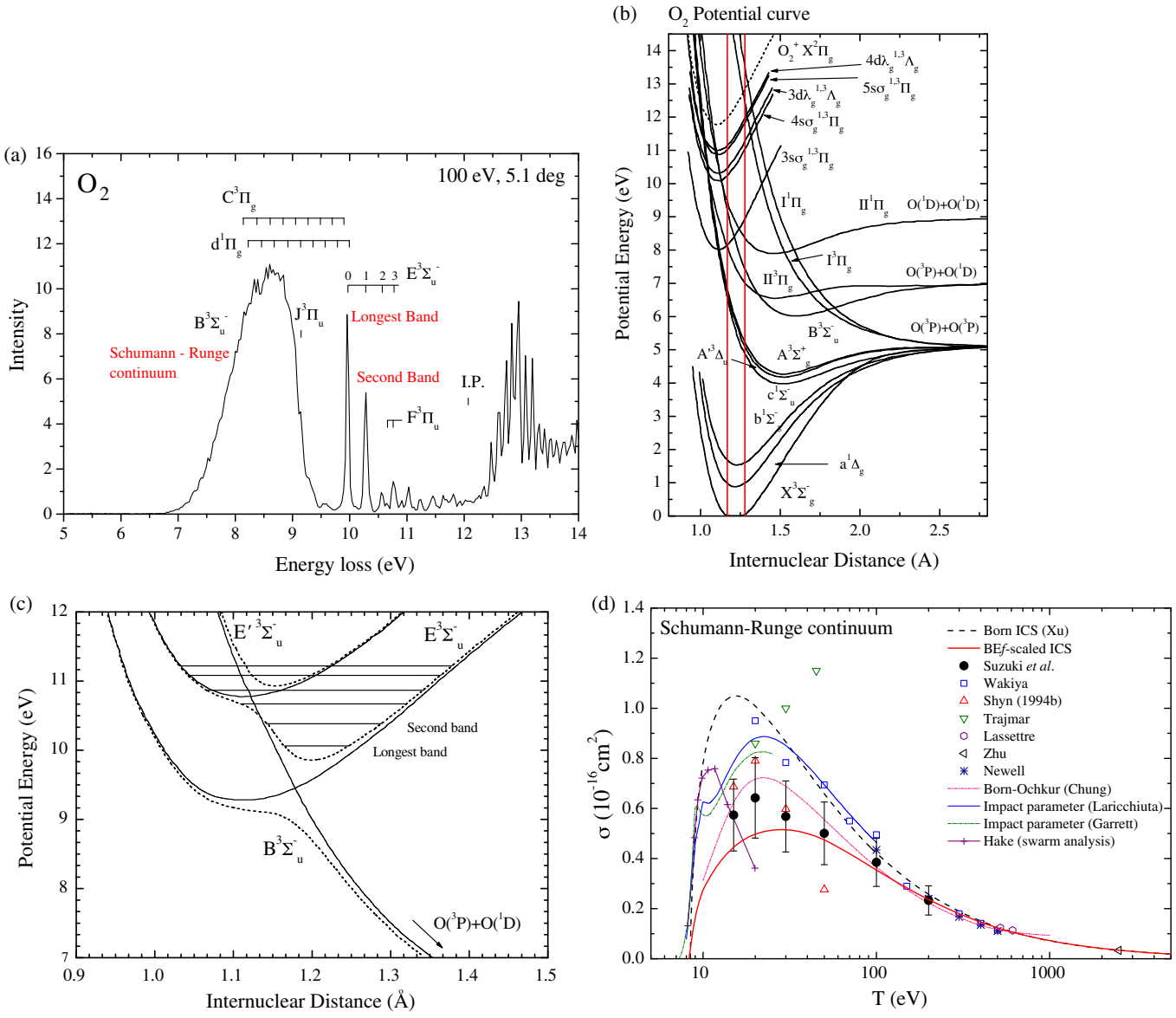

FIG. 21. *Continued.*

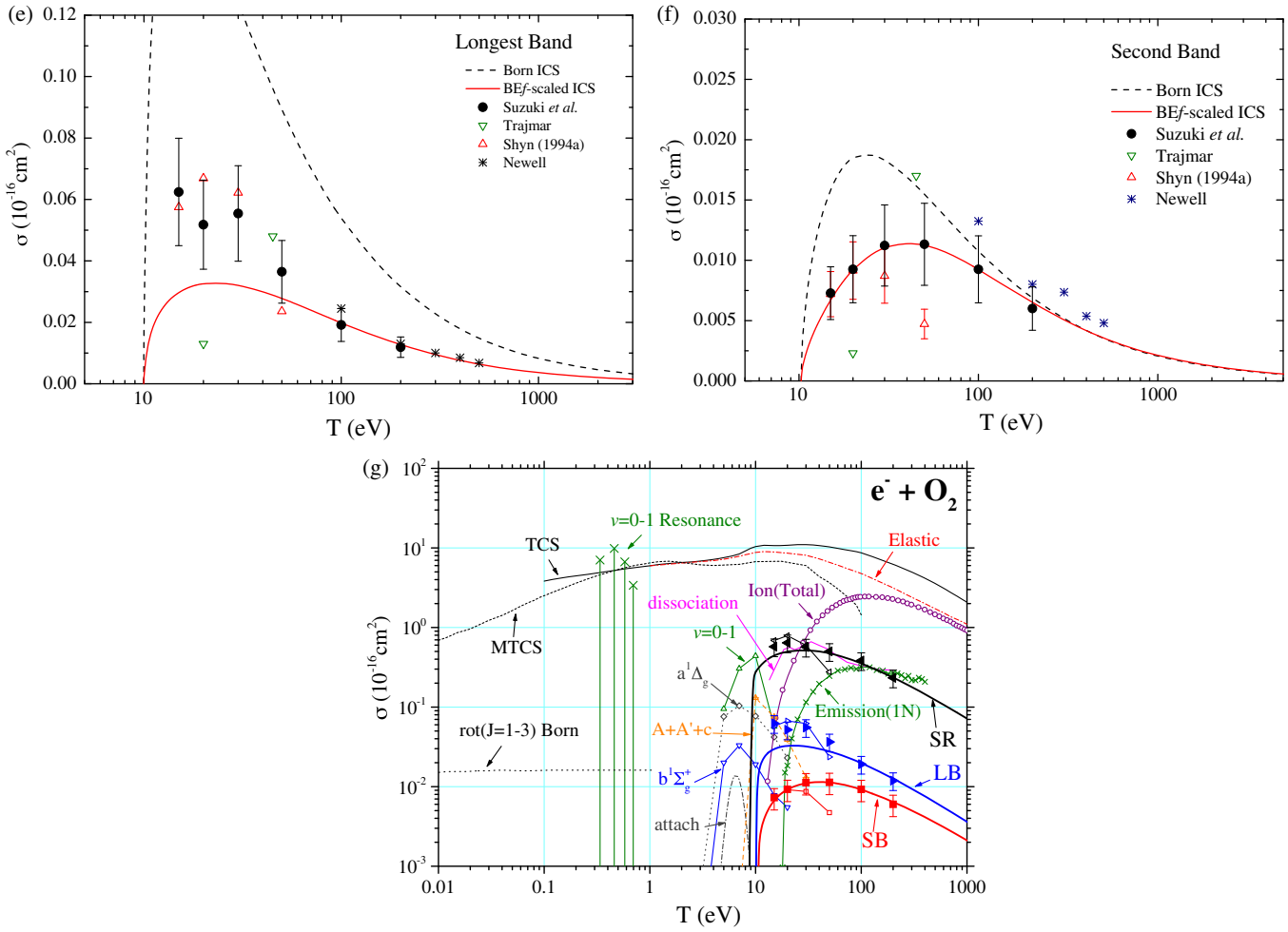

FIG. 21. Electron impact on O_2: (a) Typical electron energy-loss spectrum, $\Delta E \sim 4.9$–14.4 eV, for electronic-state excitation. The incident electron energy was 100 eV and the scattered electron angle was 5.1°. From Suzuki *et al.*, 2011. (b) Potential energy (eV) as a function of internuclear distance (Å) for the electronic states of O_2 and O_2^-. From Cartwright, 2005. (c) The effect of the Rydberg-valence interactions leading to avoided level crossings. From Lewis *et al.*, 2001. (d) ICSs for excitation of the Schumann-Runge continuum. (e) ICSs for excitation of the longest band. (f) ICSs for excitation of the second band. (d)–(f) See the legend and the text for details. (g) Recommended cross-section data set from Itikawa (2009), updated to include the recent ICSs from Suzuki *et al.* (2011) and their corresponding BE*f*-scaling results.

were systematically higher in magnitude than their corresponding BE*f*-scaling results, for energies less than about 100 eV, suggesting contamination from the accidentally degenerate or near-degenerate states of $C^3\Pi_g$ and $d^1\Pi_g$ classification. (2) For the LB, there is significantly less measured data and no other theory against which we can compare the recent Suzuki *et al.* (2011) results. The breakdown in the applicability of the BE*f*-scaling method emerged here due to the well-known (Lewis *et al.*, 2001) strong Rydberg-valence perturbations that affect the $E^3\Sigma_u^-$ ($v' = 0$) state in O_2. Thus any use of the BE*f*-scaling ICSs for systems with strong interchannel coupling should be undertaken with caution. (3) For the SB, through the assessment of Suzuki *et al.* (2011) by applying the BE*f*-scaling method, a more reliable ICS can now be provided.

The original recommended cross-section database for O_2 from Itikawa (2009) can now be updated to use the measured and/or BE*f*-scaled O_2 ICSs from Suzuki *et al.* (2011). This is illustrated in Fig. 21(g). Further updates of that recommended set, to incorporate ICSs for the $\nu' = 0 \rightarrow 2$, 3, and 4 ground-state vibrational excitation processes, using data from Noble *et al.* (1996), should probably also be contemplated.

4. CO_2

We now shift our focus away from diatomic species to consider a series of triatomic molecules, namely, CO_2, N_2O, OCS, and H_2O. The first of these molecules that we consider is CO_2, which was identified (Morrison and Greene, 1978) as being an important constituent in the atmospheres of Venus and Mars in terms of electron energy transfer processes. It is also well known to play a significant role in global warming on planet Earth. EELS spectra were measured by Kawahara *et al.* (2008b) at various incident energies in the range 30 to 200 eV, and for scattered electron angles from 3.5° to 130°. A typical energy-loss spectrum is plotted, that includes the $^1\Sigma_u^+$ and $^1\Pi_u$ excitation states, in Fig. 22(a), over the energy-loss range from ~6 to 14 eV and at $E_0 = 100$ eV and $\theta = 15°$.

From EELS such as in Fig. 22(a), absolute DCSs for both the $^1\Sigma_u{}^+$ and $^1\Pi_u$ electronic states were derived following the methods outlined earlier in Sec. III. Those cross sections were then transformed, using Eqs. (5a) and (10b), to GOSs as a function of K^2. Subsequently, on the 100 and 200 eV data of Kawahara *et al.* (2008b), a Vriens analysis (see Sec. IV) was performed with the results from this process being given in Fig. 22(b). Also shown in Fig. 22(b) are corresponding results, although from experiments for which the incident electron energies were 300 and 500 eV, from Klump and Lassettre (1978). To within the uncertainties on both sets of data, we see that they are largely consistent. Using the limit theorem,

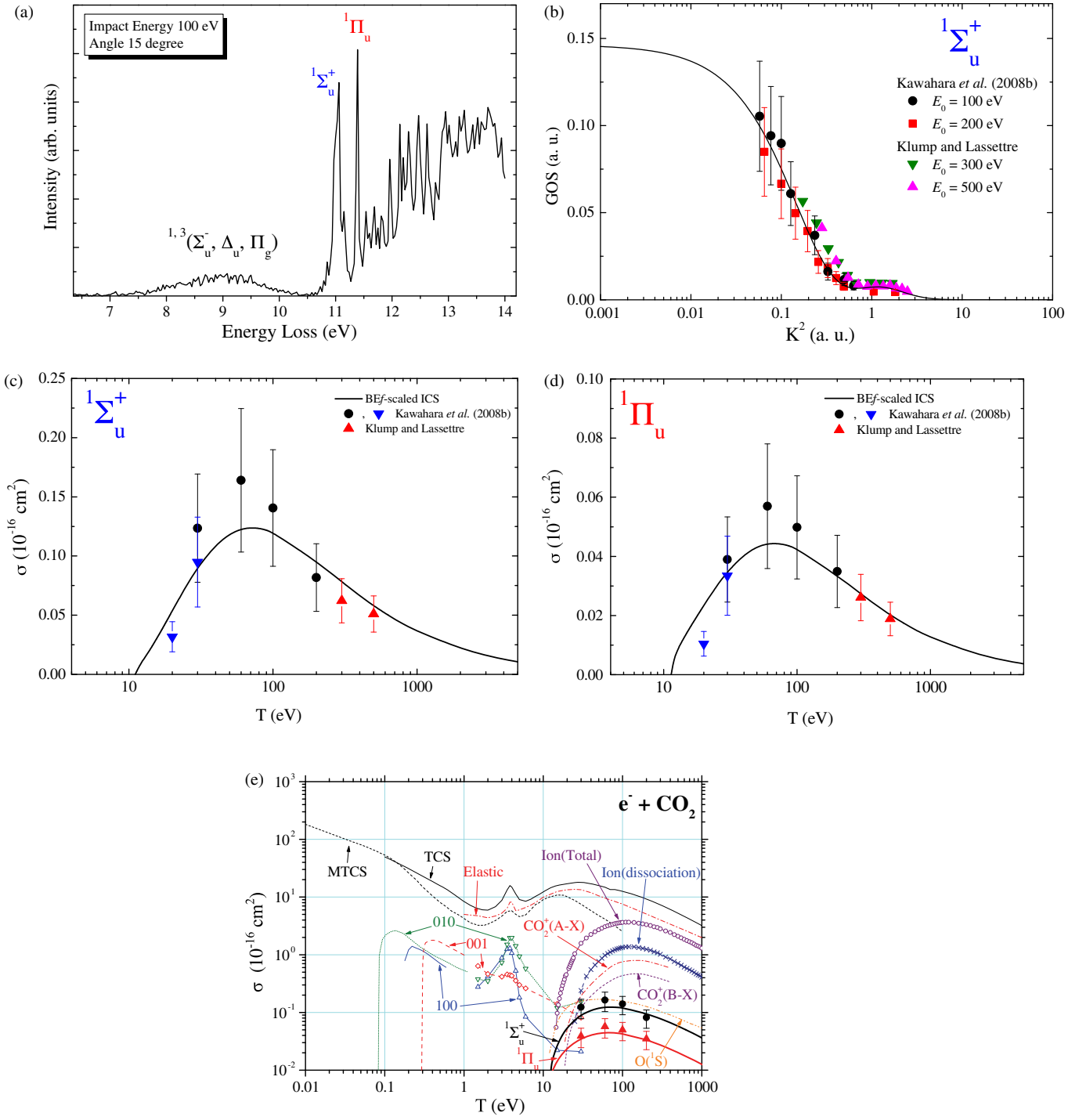

FIG. 22. Electron impact on CO_2. (a) Typical electron energy-loss spectrum, $\Delta E \sim 6.0$–14 eV, for electronic-state excitation. The incident energy is 100 eV and the scattered electron angle is 15°. (b) GOS vs K^2 for the $^1\Sigma_u{}^+$ electronic state. A Vriens-type fit (Vriens, 1967) to the available experimental data (Klump and Lassettre, 1978; Kawahara *et al.*, 2008b) is also shown. (c) ICSs for excitation of the $^1\Sigma_u{}^+$ electronic state. (d) ICSs for the excitation of the $^1\Pi_u$ electronic state. (b)–(d) See the legends and the text for details. (e) Recommended cross-section data from Itikawa (2002), updated to include recent ICSs from Kawahara *et al.* (2008b) and corresponding BEf-scaling results.

Eq. (14), Kawahara *et al.* (2009) determined OOSs for both the $^1\Sigma_u^+$ and $^1\Pi_u$ electronic states. Those data are presented in Table 5 in the Supplemental Material [370], where they are compared to other experimental results from Inn, Watanabe, and Zelikoff (1953), Klump and Lassettre (1978), and Chan, Cooper, and Brion (1993c), and with theoretical results from McCurdy and McKoy (1974), Padial *et al.* (1981), and Buenker *et al.* (2000). While the measured results, for both electronic states in question, of Chan, Cooper, and Brion (1993c) and Kawahara *et al.* (2008b) are in good accord, none of the available theories reproduce them very well. This indicates an inadequacy in the target basis description of the $^1\Sigma_u^+$ and $^1\Pi_u$ states in all of those calculations (McCurdy and McKoy, 1974; Padial *et al.*, 1981; Buenker *et al.*, 2000).

Employing the derived apparent GOS for each state in Eq. (20) and using Eqs. (38), Kawahara *et al.* (2008b) determined relevant ICS with those results for the $^1\Sigma_u^+$ state being plotted in Fig. 22(c) and for the $^1\Pi_u$ state in Fig. 22(d). Note that here the new results in Kawahara *et al.* incorporated data from measurements independently made at Sophia University and Flinders University, and that at the common energy of 30 eV the agreement between them was excellent. Also plotted in Figs. 22(c) and 22(d) are ICSs from Klump and Lassettre (1978) and BEf-scaling results that were originally determined from the work of Buenker *et al.* (2000), BE scaling, and then corrected using the OOSs from Chan, Cooper, and Brion (1993c), in each case, to effect the f-scaling procedure. It is clear from Figs. 22(c) and 22(d) that, over the common energy range, the BEf-scaling ICSs were found to be in good agreement with the measured data. Thus, once again, the efficacy of the BEf-scaling method has been demonstrated here for the first time for a triatomic molecule.

The updated cross-section data set of CO_2 from Itikawa (2002) is shown in Fig. 22(e), with the ICS from Kawahara *et al.* (2008b) for the $^1\Sigma_u^+$ and $^1\Pi_u$ electronic excitation states being assessed against their own BEf-scaling computation for a wide energy range from threshold to 1000 eV. The interesting thing about Fig. 22(e) is that for CO_2 there appears to be a database that covers many of the relevant scattering processes and an extended energy range. The data are absolute and if also correct, the threefold requirement we outlined earlier for a database to be useful in modeling and simulation applications would appear to be met here.

5. N_2O

EELS spectra were measured by Kawahara *et al.* (2009) at various incident energies in the range 15 to 200 eV, and for scattered electron angles from 2° to 130°. A typical energy-loss spectrum is plotted that includes the $C^1\Pi$ and $D^1\Sigma^+$ electronic excitation states of interest in Fig. 23(a) over the energy-loss range from 4 to 13 eV and at $E_0 = 100$ eV and $\theta = 4.3°$. Note that, as indicated in this figure, some $d^3\Pi$ contribution to the $C^1\Pi$ dipole-allowed excitation and some $2^3\Pi$ contribution to the $D^1\Sigma^+$ dipole-allowed excitation may be important here. N_2O is isoelectronic with CO_2, both molecules are linear triatomics and both species have very similar dipole polarizabilities (Kawahara *et al.*, 2009). However, while CO_2 is nonpolar, we find that N_2O has a weak permanent dipole moment of ~0.16 D (Jalink, Parker, and Stolte, 1987) and, more importantly, CO_2 has a C_{2v} point group symmetry while that for N_2O is $C_{\infty v}$. Therefore we would, at best, expect to find only a qualitative similarity in the valence electronic structures of CO_2 and N_2O and this is indeed what we observe when we compare Fig. 22(a) for CO_2 with Fig. 23(a) for N_2O.

Following the now established process, Kawahara *et al.* (2009) transformed their measured DCSs for the $C^1\Pi$ and $D^1\Sigma^+$ electronic states into apparent generalized oscillator strengths as a function of K^2. From those, estimates for the ICS of both of these states could then be obtained at each energy studied. If we consider the GOS vs K^2 result of Kawahara *et al.* (2009) for their highest energy measured (200 eV), where any triplet contribution would be effectively zero or small enough to be ignored, and considering only for the $D^1\Sigma^+$ electronic state here, we find the result given in Fig. 23(b). Also plotted in Fig. 23(b) are corresponding 2.5 keV results from Zhu, Sun, and Xu (2007), 1 keV results from Boechat-Roberty *et al.* (2000), and a Vriens-type fit (Vriens, 1967) to all three sets of the experimental results. A good fit to the measurements is observed, leading to (using the limit theorem) an estimate of the OOS as tabulated in Table 6 in the Supplemental Material [370].

This same approach for the $C^1\Pi$ electronic state was also followed by Kawahara *et al.* (2009), and that value for the OOS is also listed in Table 6 in the Supplemental Material [370]. The results from Kawahara *et al.* (2009) are compared with earlier measurements from Zelikoff, Watanabe, and Inn (1953), Rabalais *et al.* (1971), Huebner *et al.* (1975), Lee and Suto (1984), and Chan, Cooper, and Brion (1994), as well as a theory result from Chutjian and Segal (1972) in that table. Good agreement is generally found between the measured data, except for the OOS from Zelikoff, Watanabe, and Inn (1953), for both states.

While the main focus of this review is on examining the validity of the scaling approaches we introduced, we continue to highlight the OOS results, in our consideration of dipole-allowed discrete excitations, for the following two reasons. First, for the experimentalists, the determination of the OOS and its comparison to independent results provides a self-consistency check for their measurement techniques and analysis. Second, for the theoreticians, an accurate OOS gives a strong benchmark for the quality of the target basis set description being used for the species in question. A good description of the wave function will lead to a theoretical OOS in good agreement with an accurate experimental OOS. However, if that agreement is not found, then this is an indication that the target wave function is inaccurate. Of course if the target description is inaccurate, scattering cross sections computed with that wave function will also likely be inaccurate.

Shown in Fig. 23(c) are the ICSs for electron-impact excitation of the $C^1\Pi$ electronic state from Kawahara *et al.* (2009). Also plotted is a BEf-scaled ICS that employed the theoretical work of Peyerimhoff and Buenker (1968) to compute the unscaled Born cross section and the accurate OOS from Chan, Cooper, and Brion (1994) and an experimental result from Zhu, Sun, and Xu (2007). For energies greater than about 40 eV, excellent agreement is found

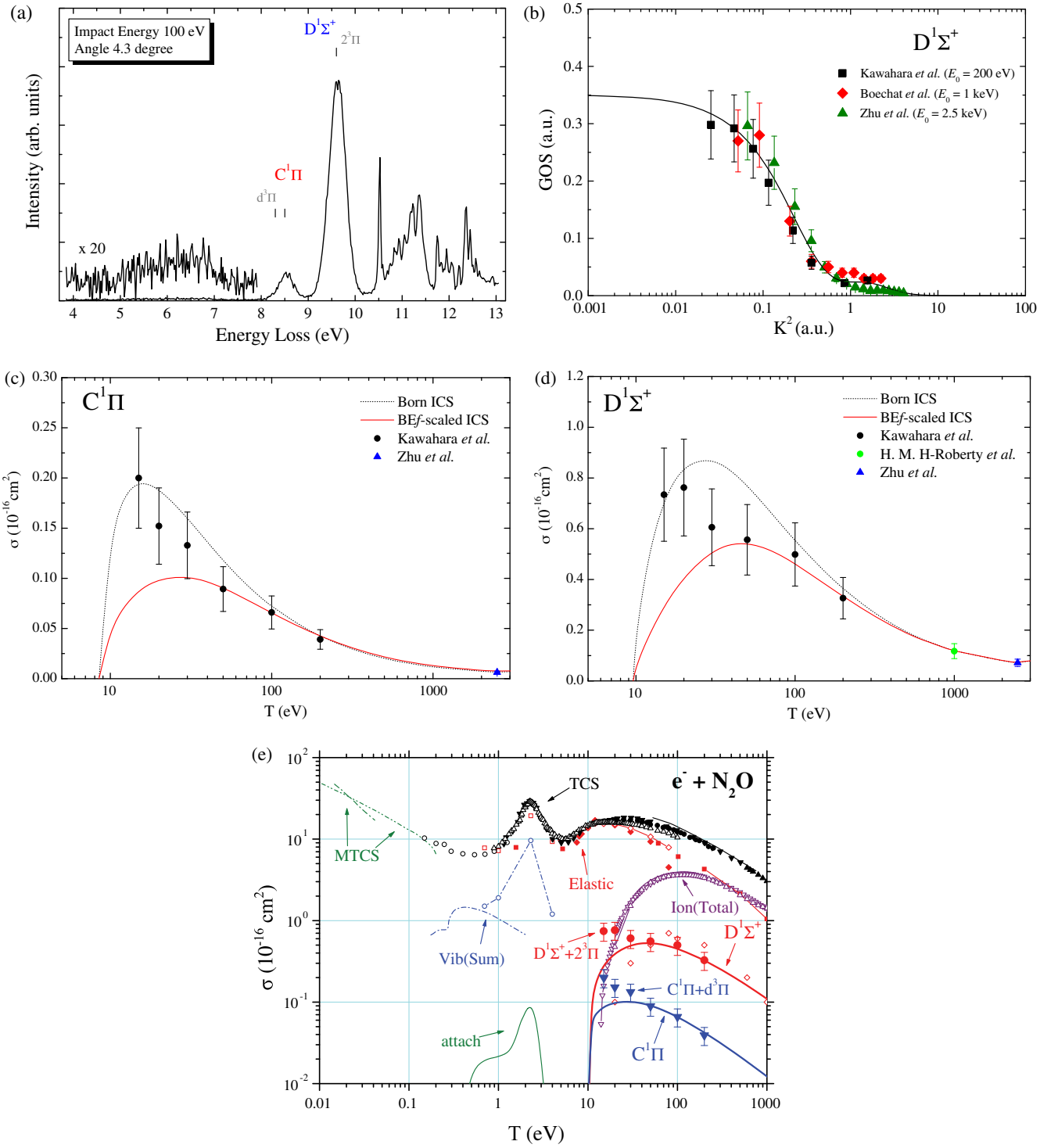

FIG. 23. Electron impact on N_2O. (a) Typical electron energy-loss spectrum $\Delta E \sim 4$–13 eV for electronic-state excitation. The incident electron energy is 100 eV and the scattered electron angle is 4.3°. (b) GOS vs K^2 for the $D^1\Sigma^+$ electronic state. A Vriens-type fit (Vriens, 1967) to the available experimental data (Kawahara *et al.*, 2009) is also shown. (c) ICSs for excitation of the $C^1\Pi$ electronic state. (d) Similar to (c) but for the $D^1\Sigma^+$ electronic state. (b)–(d) See the legends and the text for details. (e) Recommended cross-section data set from Zecca and colleagues (Karwasz, Brusa, and Zecca, 2001), updated to include recent ICSs (Kawahara *et al.*, 2009) and corresponding BEf-scaling results.

between the BEf-scaled ICS and all the measured data. For energies <40 eV, however, the experimental ICS is larger in magnitude than that predicted by the BEf-scaled result. This observation we believe is likely to be explained by the $d^3\Pi$ state contribution [the $d^3\Pi$ state strongly overlaps the $C^1\Pi$ state in the EELS of Fig. 23(a)] to the measured $C^1\Pi$ signal at those lower energies. A similar story is also found in Fig. 23(d) for the $D^1\Sigma^+$ electronic state, although in this case it is the $2^3\Pi$ electronic state that contributes to the $D^1\Sigma^+$ intensity. The results in Figs. 23(c) and 23(d) raise an

intriguing possibility. On the basis of the level of accord we saw earlier for other molecules, if we accept the validity of the BEf-scaled results for the $C^1\Pi$ and $D^1\Sigma^+$ electronic states here then we could subtract in each case their ICSs from the measured cross sections (Kawahara *et al.*, 2009) with the result being estimates for the $d^3\Pi$ and $2^3\Pi$ ICSs, respectively. As it is unlikely those triplet cross sections will be measured directly, this perhaps allows an expansion of the N_2O database beyond what is currently available.

The updated cross-section data set of Zecca and colleagues (Karwasz, Brusa, and Zecca, 2001) for N_2O is shown in Fig. 23(e), with the ICS of Kawahara *et al.* (2009) for the $C^1\Pi$ and $D^1\Sigma^+$ electronic excitation states assessed against their own BEf-scaling computation for a wide energy range from threshold to 1000 eV. It is clear from Fig. 23(e) that the recommended data set from Karwasz, Brusa, and Zecca (2001) is far from complete, suggesting that more work needs to be undertaken in N_2O before the threefold requirement is met.

Electronic-state spectroscopy of another linear triatomic molecule, namely, carbonyl sulphide (COS), has recently been investigated using high resolution vacuum ultraviolet photoabsorption spectroscopy and electron energy-loss spectroscopy in the energy-loss range of 4.0 to 10.8 eV. The absolute optical oscillator strengths derived from the photoabsorption cross section are determined for the $^1\Sigma^+$ and $^1\Pi$ transitions, which agreed well with the corresponding f_0 values derived by applying a generalized oscillator strength analysis. ICSs predicted by the BEf-scaling approach for those same electronic states are confirmed from 300 down to 60 eV in the intermediate-energy range. For more details, see Limão-Vieira *et al.* (2015).

6. H_2O

Given that the approximate chemical composition (by weight) of a biological cell is 70% water, 24% macromolecules (proteins, nucleic acids, polysaccharides), and 4% inorganic ions, sugars, and amino acids, it is not surprising that in order to quantitatively assess a radiation dose and any radiation induced damage in biological matter water (H_2O) is a pivotal compound. Indeed, water is often used as the default molecule to represent living tissue in Monte Carlo simulations (Agostinelli *et al.*, 2003; Allison *et al.*, 2006; Muñoz *et al.*, 2007; Salvat, Fernández-Varea, and Sempau, 2011; Champion, Le Loirec, and Stosic, 2012) for describing charged-particle interactions within living tissue. EELS spectra were measured at various incident energies in the range 20 to 200 eV, for scattered electron angles from 3.5° to 130°. A typical energy-loss spectrum from Thorn *et al.* (2007b) is plotted for the relevant excitation states in Fig. 24(a), over the energy-loss range from 6 to 11 eV and at the kinematical conditions of $E_0 = 200$ eV and $\theta = 3°$. The A^1B_1 excitation, in particular, is an important channel for the production of the OH radical. However, even for this important molecule, there are currently only scanty experimental and theoretical results for its electronic excitations (Thorn *et al.*, 2007b, 2007a; Brunger, Thorn, Campbell, Diakomichalis *et al.*, 2008; Ralphs *et al.*, 2013; Rescigno and Orel, 2013; White *et al.*, 2014b; de Urquijo *et al.*, 2014).

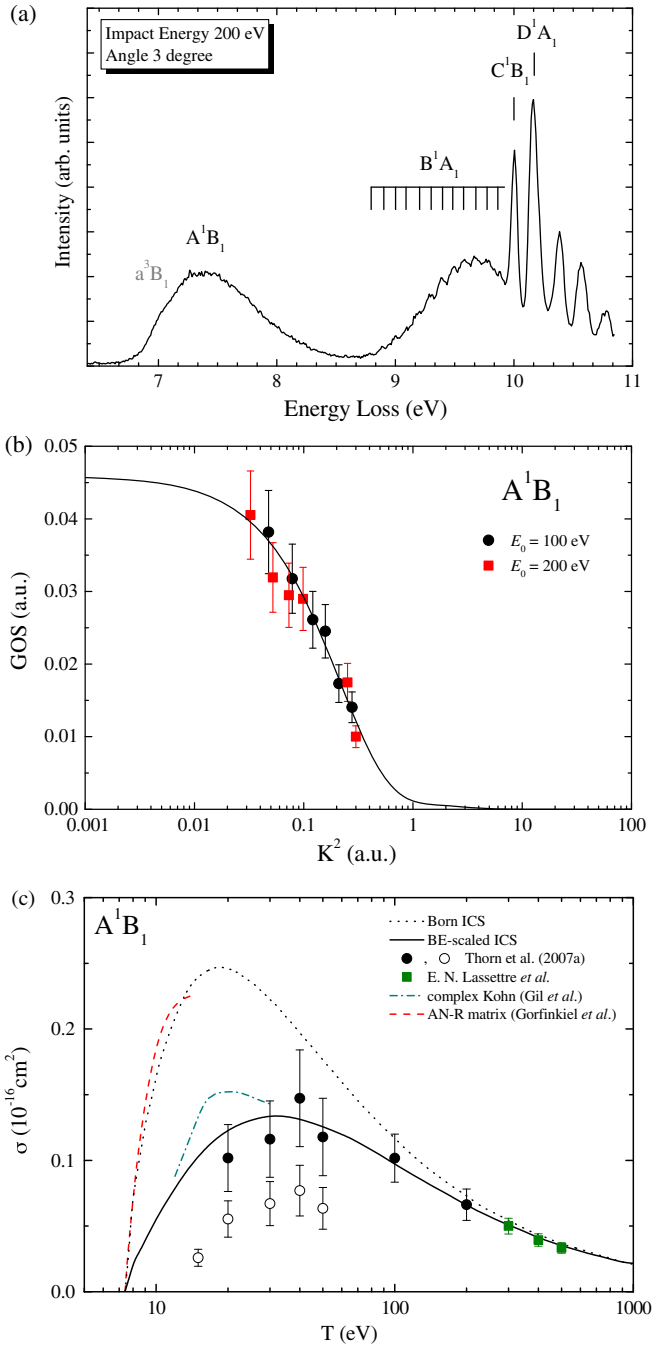

FIG. 24. Electron impact on H_2O. (a) Typical electron energy-loss spectrum $\Delta E \sim 6$–11 eV for electronic-state excitation. The incident electron energy is 200 eV and the scattered electron angle is 3°. (b) GOS vs K^2 for the A^1B_1 electronic state. A Vriens-type fit (Vriens, 1967) to the 100 and 200 eV data (Thorn *et al.*, 2007b) is also shown. (c) ICSs for excitation of the A^1B_1 electronic state. (b), (c) See the legends and the text for further details.

The main dipole-allowed transition in water corresponds to the $\tilde{X}\,^1A_1 \rightarrow \tilde{A}\,^1B_1$ transition and was the focus of the work of Thorn *et al.* (2007b). Extensions of that original study were later provided by Thorn *et al.* (2007a), Brunger, Thorn, Campbell, Diakomichalis *et al.* (2008), and Thorn, Campbell, and Brunger (2009), with that last work providing an

extensive set of ICSs for discrete inelastic processes in H_2O that were incorporated in the database for electron swarm studies in H_2O (Ness *et al.*, 2012) and H_2O and He mixtures (de Urquijo *et al.*, 2014). Work on a subset of the electronic states of water was given by Ralphs *et al.* (2013) and Rescigno and Orel (2013).

Concentrating on excitation of the $\tilde{A}^1B_1$ electronic state, in Fig. 24(b) we show the results of the GOS vs K^2 and Vriens-type fit (Vriens, 1967) from Thorn *et al.* (2007b). In this case, data at both 100 and 200 eV are shown, with the limit theory ($K^2 \to 0$) OOS from that analysis being listed in Table 7 in the Supplemental Material [370]. Independent experimental determinations for this OOS from Laufer and McNesby (1965), Lassettre and White (1974), Lee and Suto (1986), Chan, Cooper, and Brion (1993d), and Yoshino *et al.* (1996, 1997) are also shown in Table 7, as are theoretical results from Buenker and Peyerimhoff (1974), Wood (1974), Williams and Langhoff (1979), Diercksen *et al.* (1982), Theodorakopoulos *et al.* (1985), Phillips and Buenker (1987), Bhanuprakash *et al.* (1989), and Durante *et al.* (1995). The OOS from Thorn *et al.* (2007b) for the A^1B_1 state is in excellent agreement with many of the other experimental results (Lee and Suto, 1986; Chan, Cooper, and Brion, 1993d; Yoshino *et al.*, 1996, 1997) and some of the theory (Phillips and Buenker, 1987; Durante *et al.*, 1995) as well as with the recommended value of Berkowitz (1979).

Following procedures very similar to those outlined in Secs. III and IV, Thorn *et al.* (2007b) derived ICS as a function of energy between 20 and 200 eV. Those data are plotted in Fig. 24(c), along with an adiabatic-nuclei-R-matrix result from Gorfinkiel, Morgan, and Tennyson (2002), a close-coupling complex Kohn calculation from Gil *et al.* (1994), and higher energy ICSs as measured by Lassettre and White (1974). Unscaled Born cross sections were generated from the work of Durante *et al.* (1995), while the BEf-scaling ICS was achieved with the recommended OOS from Berkowitz (1979) with those results also being plotted in Fig. 24(c). Finally, a set of ICS from Flinders University (circles) can be found in Fig. 24(c). Those data were determined by a molecular phase-shift analysis (MPSA) procedure (Campbell *et al.*, 2001) that did not include a Born-dipole term. As the dipole moment of water has a large effect on the very forward angle DCS, the MPSA results failed to provide a physical extrapolation to $\theta = 0°$ and, in spite of the $\sin\theta$ weighting term in the calculation of an ICS from a DCS, gave ICS that were too low in magnitude.

This illustrates the importance of allowing for the molecular dipole in polar species in trying to derive accurate ICS from DCSs that have been measured only over a finite scattered electron angular range. In general, Fig. 24(c) indicates that for the $\tilde{A}^1B_1$ electronic state the BEf-scaling ICS does a good job in reproducing the experimental data over the common (extended) energy range. However, before proceeding, we note the following. For the energies between 20 and 50 eV most of the DCSs were measured at Flinders University, with a couple of crosscheck DCSs, at one or two θ, also being determined at Sophia University. While all those data from both the laboratories overlapped to within their error bars, the Sophia University results were typically a little larger in magnitude. As a consequence, on the basis of obtaining a better quality GOS fit, the Flinders University data were scaled by Kim to the Sophia University data. This we believe was a reasonable approach given the scaling was typically modest and the error bars overlapped.

Since the Flinders and Sophia University investigation, two more studies of note by Ralphs *et al.* (2013) and Rescigno and Orel (2013) have become available for a subset of the electronic states in water and including the $\tilde{A}^1B_1$ state. The first of these studies was an experimental investigation (Ralphs *et al.*, 2013), while the latter was theoretical (Rescigno and Orel, 2013). If we concentrate on the $\tilde{A}^1B_1$ state, then at 15 and 20 eV there is quite good agreement between Ralphs *et al.* and Rescigno and Orel, with both being larger in magnitude than the experimental and BEf-scaled results in Thorn *et al.* (2007b). For energies less than 15 eV, however, there is now a significant disagreement between Ralphs *et al.* (2013) and the theory (Rescigno and Orel, 2013), with the measured ICS being much larger in magnitude than the Kohn calculation. Thus the picture for the A^1B_1 state no longer appears to be as clear cut as indicated in Fig. 24(c). There are, however, two pieces of further information we need to consider before any final judgment can be made.

The first is that in their electron-transport studies in pure H_2O and H_2O/He mixtures, White and colleagues (Ness *et al.*, 2012; de Urquijo *et al.*, 2014) essentially used the BEf-scaling result for the A^1B_1 state in their H_2O cross-section database when solving the Boltzmann equation. As the simulated transport coefficients were in excellent agreement with the measured transport coefficients, this provides some independent evidence in support of the BEf-scaling result. Second, Lima and colleagues recently established the important role of multichannel-coupling effects in electron-molecule scattering (da Costa *et al.*, 2014, 2015; Neves *et al.*, 2015a). In essence, if an *ab initio* calculation is performed with a limited target basis, namely, if the incident electron energy is high enough to access physical channels that are not included in the basis description, the calculated cross sections will always be higher, sometimes significantly higher (by orders of magnitude) than the "correct" result. In their calculation, Rescigno and Orel (2013) included eight states in their basis, whereas in fact at 15 eV there are 25 electronic states that are accessible. Assuming multichannel-coupling effects are important in water, as they are likely to be, we can expect the $\tilde{A}^1B_1$ integral cross section of Rescigno and Orel (2013) to drop in energy and in doing so move toward the BEf-scaling result. This is also precisely what we saw earlier for neon (Hoshino, Murai, Kato, Itikawa *et al.*, 2013; Hoshino, Murai, Kato, Brunger *et al.*, 2013). Nonetheless, electronic-state excitation in water remains something of an open question.

If we followed our recent practice, we would now update the recommended cross-section database of Itikawa and Mason (2005) to incorporate the result from Thorn *et al.* (2007b). However, it is now generally accepted in the community, and demonstrated quite transparently from the work of White and colleagues (Ness *et al.*, 2012; de Urquijo *et al.*, 2014), that this database (Itikawa and Mason, 2005) is inadequate and in need of revision and expansion. Therefore, unlike with Fig. 21(g) for O_2, Fig. 22(e) for CO_2 and so on, we do not provide an updated figure here.

7. BF_3

Boron trifluoride (BF_3), a highly symmetric (D_{3h}) and planar molecule, has been extensively studied by photoabsorption (Hagenow *et al.*, 1989; Suto, Ye, and Lee, 1990) and photoelectron spectroscopies (Boyd and Frost, 1968; Bassett and Lloyd, 1971; Åsbrink *et al.*, 1981; Shpinkova, Holland, and Shaw, 1999; Yencha, Lopes, and King, 2002; Mackie *et al.*, 2003). BF_3 has also attracted interest with regard to its quite broad range of technological applications as a sensitive neutron detector (Chen and Chung, 1997), as an alternative agent for plasma doping (Kruzelecky *et al.*, 1986), and for metal surface treatment (Gutiérrez, Cárabe, and Gandía, 1992; Hunger and Löbig, 1997; Zhang and Matsumoto, 2000; Yamamoto *et al.*, 2006). Because of a need for understanding its molecular properties in terms of modeling phenomena in electron-assisted processes containing BF_3, the first complete EELS of BF_3 was provided by Duflot *et al.* (2014) for energy loss ranging from 10 to 20 eV and at impact energies of 40 to 300 eV.

In addition, they provided calculations showing a more reliable assignment in the spectra (Duflot *et al.*, 2014). The major energy-loss bands, centered at 13.13, 13.98, 14.70, 15.56, and 16.10 eV, can be classified mainly as a mixture of Rydberg-valence transitions due to the promotion of an electron from the occupied to unoccupied molecular orbitals. The lowest lying singlet excited state was previously reported by Hagenow *et al.* (1989) and Suto, Ye, and Lee (1990), with a maximum at 13.13 and 13.19 eV, respectively, which agrees well with the value of 13.13 eV by electron-impact spectroscopy (Duflot *et al.*, 2014). This feature is assigned to the transition $[{}^1A_1' \rightarrow {}^1E',\ \pi(1e'') \rightarrow \pi^*(2a_2'')]$ with the highest calculated oscillator strength (~0.4), and the others of $(n_F \rightarrow \sigma^*)$ and $(\pi \rightarrow \sigma^*)$ character are members of a Rydberg series converging to the lowest ionization energies.

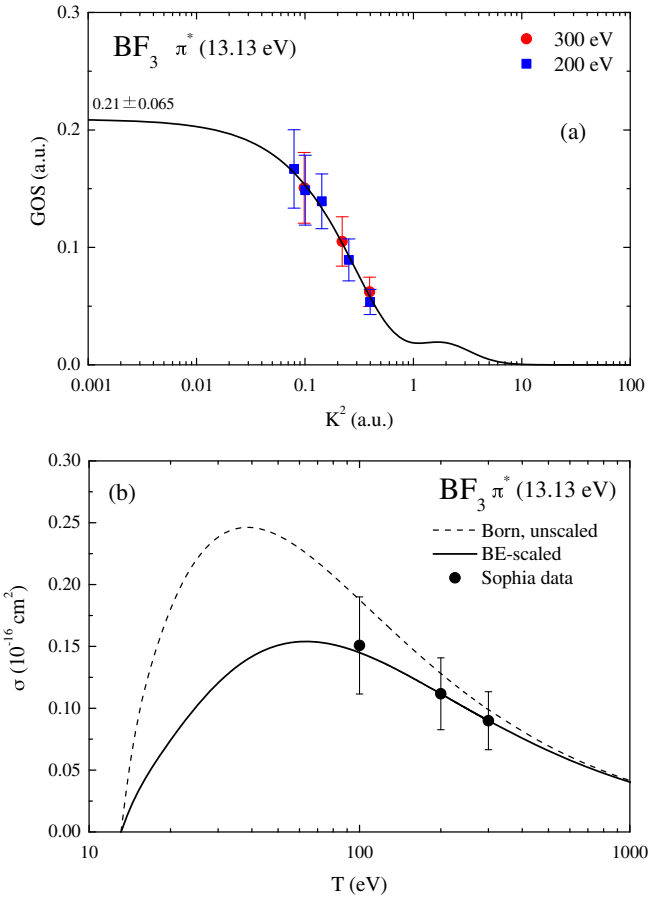

FIG. 25. Electron impact on BF_3. (a) GOS vs K^2 for excitation of the $1e''(\pi) \rightarrow 2a_2''(\pi^*)$ transition from Duflot *et al.* (2014). See the legend and the text for further details. (b) Integral cross sections (10^{-16} cm^2) for excitation of the π^* transition. Measured data (•) and the unscaled Born (dashed curve) and BEf-scaling results (solid curve) are all from Duflot *et al.* (2014).

A generalized oscillator strength analysis was employed by Duflot *et al.* (2014) to derive ICSs from the corresponding DCSs for the strong optically allowed $(\pi, 1e'') \rightarrow (2a_2'', \pi^*)$ transition. This work was restricted to 100, 200, and 300 eV incident electron energies. While a comparison of their f_0 value [0.210 ± 0.065, Fig. 25(a)] with the photoabsorption data shows another assessment for verification and validation of the electron measurement, the OOS value of Duflot *et al.* (2014) is around 30% lower than the oscillator strength (0.26) reported from Hagenow *et al.* (1989). Nonetheless it falls within the experimental uncertainty and thus is not an impediment when computing the corresponding ICS (Duflot *et al.*, 2014). In Fig. 25(b), the BEf-scaling curve of Duflot *et al.* (2014) is depicted, although unfortunately we are not aware of any other data in the literature to compare this result with. However, as the BEf-scaling results are consistent with their measured ICS, they will be appropriate for use for the transition in question in any modeling studies in which BF_3 is an important constituent. We note, however, that significantly more work into BF_3 is still required before any meaningful attempt to construct a recommended database for such modeling studies could be contemplated.

8. C_6H_6

Benzene (C_6H_6), the simplest aromatic hydrocarbon, is a very useful compound as a precursor in many organic synthesis techniques in the petrochemical and pharmaceutical industries. From a more fundamental perspective, it possesses a large dipole polarizability (~70 a.u.) and even though it is nonpolar we might anticipate that its low-energy scattering dynamics is dominated by its dipole polarizability. Additionally, while benzene is a relatively large molecule having 42 electrons, its high symmetry suggests that *ab initio* electron-polyatomic molecule scattering calculations will in principle be more tractable than would otherwise be the case. Finally, benzene plays an important role in the chemistry of some planetary atmospheres including haze formation on Titan (Wilson, Atreya, and Coustenis, 2003) and in the atmosphere of the protoplanetary nebula CRL618 (Cernicharo *et al.*, 2001).

A typical energy-loss spectrum, for an incident electron energy of 100 eV and a scattered electron angle of 5°, for benzene from Kato *et al.* (2011) is shown in Fig. 26(a). The two main dipole-allowed transitions are excitations of the ${}^1B_{1u}$ and ${}^1E_{1u}$ electronic states, although we note that a ${}^3E_{2g}$ state overlaps significantly with the ${}^1B_{1u}$ state and at lower energies would therefore be expected to contribute to the observed

spectral intensity. Following the practices outlined earlier in Secs. III and IV, Kato *et al.* (2011), at $E_0 = 100$ and 200 eV, derived apparent GOS vs K^2 for both the $^1B_{1u}$ and $^1E_{1u}$ states and then applied the limit theorem in each case to determine, respectively, their OOS. An example for the $^1E_{1u}$ electronic state of this process can be found in Fig. 26(b), while the OOS of Kato *et al.* (2011) are compared to the results from other measurements in Table 8 in the Supplemental Material [370]. Note that in Fig. 26(b) individual Vriens-type fits (Vriens, 1967) to the 100 and 200 eV data are shown. In Table 8 in the Supplemental Material [370] the independent experimental results are from Hammond and Price (1955), Pantos, Philis, and Bolovinos (1978), Philis *et al.* (1981), Suto *et al.* (1992), Feng, Cooper, and Brion (2002), and Boechat-Roberty *et al.* (2004). Agreement is probably best between the determination of Kato *et al.* (2011) and those from Hammond and Price (1955), Pantos, Philis, and Bolovinos (1978), and Boechat-Roberty *et al.* (2004).

Employing the derived apparent GOS for each state and at each energy in Eq. (20) and using Eqs. (38), Kato *et al.* (2011) determined relevant ICSs with those results for the $^1B_{1u}$ state being plotted in Fig. 26(c) and for the $^1E_{1u}$ state in Fig. 26(d). Also plotted are results for unscaled Born cross sections, using Read and Whiterod (1965) with the BEf scaling being performed using the OOS of Pantos, Philis, and Bolovinos (1978) [as recommended by Berkowitz (1979)]. Considering Fig. 26(c) first, we find that at the higher energies good agreement between the measured ICS for the $^1B_{1u}$ electronic state and the BEf-scaling result is found. At energies <100 eV, however, the magnitude of the measured ICS for the $^1B_{1u}$ state is larger than that from the BEf-scaling result. As we alluded to earlier, there is a strong overlap between the $^1B_{1u}$ and $^3E_{2g}$ electronic states, so that the behavior we observed in Fig. 26(c) might be ascribed to a strong triplet contribution to the $^1B_{1u}$ intensity. In our discussion in Sec. V.B.5 we noted that when such an overlap between a singlet and a triplet state occurs, the BEf-scaling ICS might be subtracted from the measured ICS in order to derive a cross section for the optically forbidden triplet state. This is precisely what Kato *et al.* (2011) did, with an estimate for the $^3E_{2g}$ cross section also being plotted in Fig. 26(c). While there are no independent calculations or experimental results available for the cross sections of the $^3E_{2g}$ electronic state, the data determined by Kato *et al.* (2011) are consistent with what we might anticipate for electron-impact excitation of an optically forbidden state.

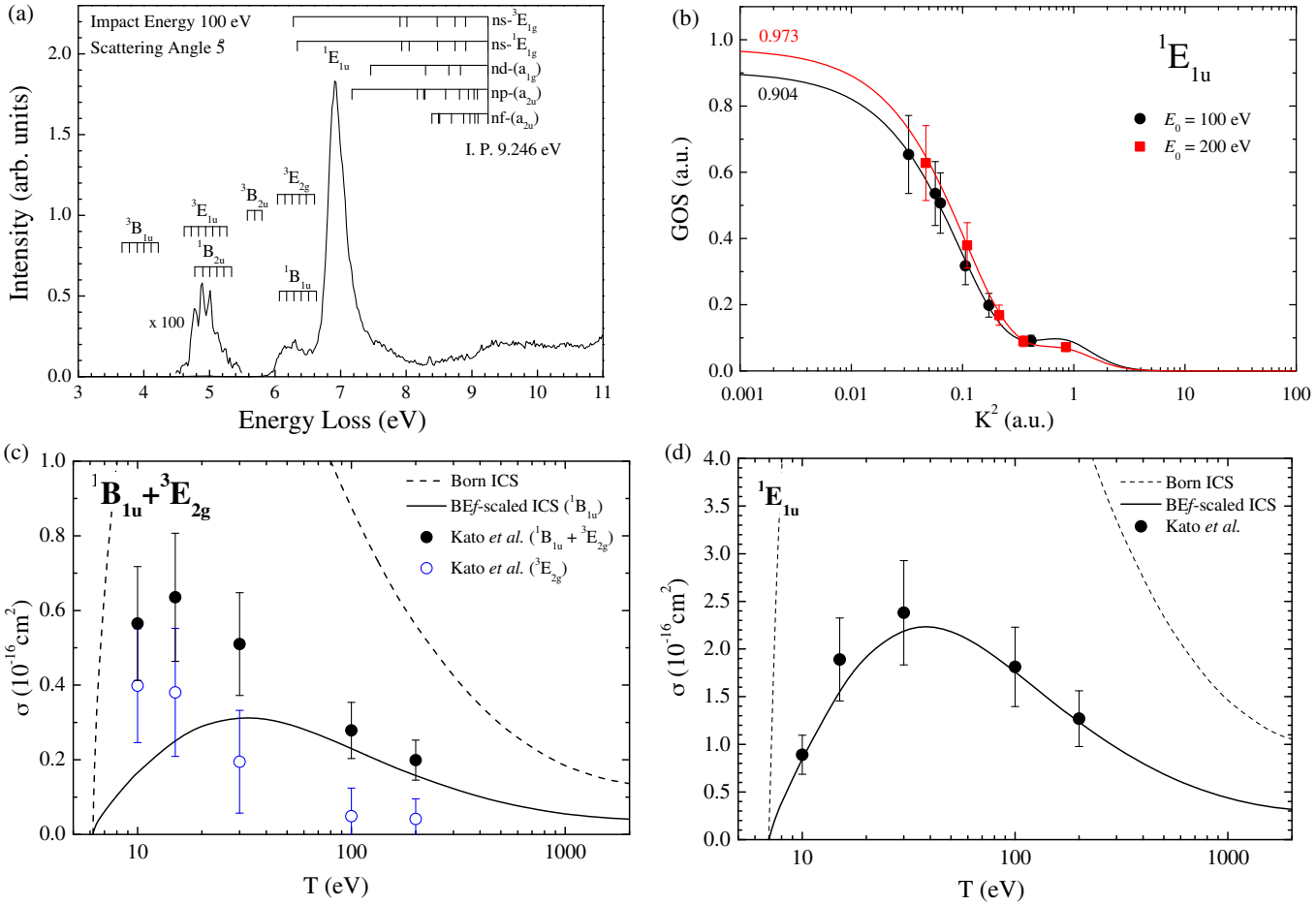

FIG. 26. Electron impact on C_6H_6. (a) Typical electron energy-loss spectrum at an impact energy of 100 eV and scattering angle of 5°. The energy-loss range is $\Delta E \sim 4.5$–14 eV. From Kato *et al.*, 2011. (b) GOS vs K^2 for the $^1E_{1u}$ electronic state. A Vriens-type fit (Vriens, 1967) to the available experimental data (Kato *et al.*, 2011) is also shown. (c) ICSs for excitation of the $^1B_{1u} + {}^3E_{2g}$ electronic states. See the legend and the text for details. (d) Similar to (c) but for the $^1E_{1u}$ electronic state.

Finally, in Fig. 26(d) we considered the ICS for the $^1E_{1u}$ electronic state. This is a very strong dipole-allowed transition so that it is probably by now not too surprising that excellent agreement is found between the measured ICS and their BEf-scaling result for this state.

Recently, an extensive study on another ring compound (phenol) was also reported (Jones *et al.*, 2014; Neves *et al.*, 2015a, 2015b; da Costa *et al.*, 2015). In that work they noted a qualitative similarity between the energy-loss spectra of benzene and phenol [see Fig. 26(a) and Jones *et al.* (2014)], although with eight more electrons to accommodate in phenol their electronic structures are in fact quite different. In addition, with the lifting of the high symmetry in benzene there are many more nondegenerate singlet and triplet states in phenol than benzene. However, those states are very closely spaced so the work in phenol was restricted to reporting OOS, DCS, GOS, and ICS for bands of electronic states (Jones *et al.*, 2014; Neves *et al.*, 2015b). In the case of bands 2–4, BEf-scaling ICS were also reported (Neves *et al.*, 2015b) and given the scope in phenol for low-energy triplet contamination and the high level of interchannel coupling (da Costa *et al.*, 2015) the actual level of accord between the BEf-scaling ICS and the measured ICS was surprisingly good.

VI. CONCLUDING REMARKS

The understanding of radiation action on matter requires a vast range of knowledge of atomic and molecular collision cross sections. In particular, elementary interactions of electrons with atoms and molecules are indispensable for modeling studies of radiation effects (Fuss *et al.*, 2015). Inokuti (1987) noted: "The cross section data are demanded to fulfill the trinity of requirements: *correct*, *absolute*, and *comprehensive*." Here the term comprehensive should be interpreted to mean that the data pertain to a wide range of variables such as the incident electron energy, the energy transfer to the target, and the scattering angle. He also said, "Sometimes, it is said that cross section data obtained from the measurements in the gas phase are irrelevant to the condensed-phase and soft matter problems." This is clearly a wrong view, as explicitly shown by McEachran *et al.* (2012) and White *et al.* (2014b) in their recent work on charged-particle transport in liquids and soft matter. Indeed, those parts of the cross-section data which are governed by the motion of energetic electrons are certainly always relevant to condensed phases. The term energetic electrons means those electrons having kinetic energies far exceeding the potential in the condensed phase. By contrast, electrons of lower energies are in general subject to condensed-phase or coherent scattering effects.

Along with this strategy for the determination of reliable cross sections as originally advised by Platzman, and as summarized by Fano (1975), the Born-Bethe theory has been best applied for testing the consistency of the cross sections as long as the incident particle energy is much higher than the interaction energy, that is, within the framework of perturbation theory. This review emphasized the usefulness of the Born-Bethe approximation along with the scalings discussed for ionization and discrete electronic-state excitation. Its relation to optical transition probabilities—generalized oscillator strengths—and to the plane-wave cross section lies in it being the first term in the expansion in powers of the interaction between an electron and a target atom or molecule. Since the 1970s, the excellent success of the Born-Bethe theory in representing the ionization process is seen in the work of Kim (1975a, 1975b, 1975c), Miller and Manson (1984), Rudd (1989), and Inokuti *et al.* (1994) on the energy distribution of secondary electrons from electron impact.

This review also emphasized the following three aspects: (1) a simple universal improvement introduced in the BEB scaling model, that is, the plane-wave Born cross section scaled by the "Burgess denominator," extends the potential of the Born-Bethe approximation into the intermediate energy region, thereby bridging the gap between the two regions categorized conventionally as "slow" and "fast" collisions. This entire energy range is of great importance in many areas of radiation science, plasma physics, atmospheric science, and other phenomena where electron-driven processes play a role (Duque *et al.*, 2015). In addition, (2) the BEB scaling model can serve to represent integral cross sections in an analytical expression and distinguish it from the data fitting often used instead. In the absence of analytical expressions, integral cross-section values must be prepared in the form of a table, which are often available only at intermittent energy values or over a limited energy range so that reliable data interpolation and extrapolation is required. This point is equally valid for differential cross sections, in terms of finite values of the scattered electron angle only being available and that they are not available for all angles between 0° and 180°. Furthermore, (3) this scaling paradigm includes two approaches, computational and experimental; when it is experimentally difficult to obtain cross sections, the computational approach may be applied to estimate the cross section from simple wave functions, or vice versa. The scaling model is clearly at an advantage, both as being easier to implement and economical in terms of computational cost, compared to fully *ab initio* methods.

Additionally, we presented some of the problems in performing accurate measurements of these targets that were encountered at Sophia University, although they are in fact general to all crossed-beam spectrometers. We have also carefully selected the data that can provide valuable benchmarks for checking the range of validity of the BEf-scaling model and for comparing with different theoretical models and with the normalization of measurements of cross sections from other groups. Although the data presented here are now well established, there is always a need for periodic reappraisal to identify the most accurate cross sections available. The new data are the result of continued improvements in experimental techniques and/or theoretical computations. Electron-impact ionization cross sections successfully calculated for many atoms and molecules by the BEB theory have been compiled, as a general database accessible from the NIST website (http://www.nist.gov/pml/data/ionization). This review, which may also be viewed as that database's extension, provides the current database for optically allowed discrete transition cross sections of neutral atoms and molecules by electron impact and points to the need for a web-based database that focuses on discrete electronic excitation that is similar to that of NIST for ionization.

LIST OF SYMBOLS AND ABBREVIATIONS

BB	Bethe-Born theory. Bethe's pioneering treatment of charged-particle interactions with atoms and molecules, using the Born approximation.
BDA	Born-dipole approximation. A method to calculate rotational excitation cross sections, which might then be summed to vibrationally determine elastic or vibration excitation data.
BE	Binary-encounter models. Each atomic electron viewed as in a binary encounter with the projectile electron and thus acquiring the full momentum transferred.
BE scaling	Adding the binding energy B to the incident electron kinetic energy T, and to the ejected electron energy W in ionization cross sections or to the excitation energy in excitation cross sections.
BV scaling	Burgess-Vriens scaling. Use of the orbital kinetic energy in place of the energy transfer in ionization cross sections.
BEB	Binary-encounter Bethe. A simplification of the BED model with a simpler form of the dipole oscillator strength.
BED	Binary-encounter dipole. Binary-encounter cross sections corrected to reflect the asymptotic behavior given by the dipole contribution that dominates in this limit.
BEf scaling	A combination of BE and f scaling, in which ionization and excitation energies and dipole oscillator strengths are used to scale cross sections.
BEQ	Q-parametrized binary encounter, a more general case of the simplification of the BED model, in which setting $Q = 1$ gives the BEB.
Bethe sum rule	Closely related to the Thomas-Reiche-Kuhn sum rule for the optical limit, it states that the total oscillator strength of an atomic system must sum to the number of oscillators, that is, the total number of electrons in the system.
BO	Born-Oppenheimer approximation in which the large mass difference between an electron and the nuclei, and consequent difference in their velocities, is used to separate adiabatically the two motions.
CC	Close-coupling method. An expansion of the $(N + 1)$-electron wave function in terms of a complete set of N-electron basis functions.
CCC	Convergent close-coupling method. A close-coupling expansion in a very large basis set that yields well-converged results.
DCS	Differential cross section.
DM	Deutsch-Märk method. A semiclassical formalism to calculate electron-impact ionization cross sections.
Dipole oscillator strength f	A measure of the response of an atomic system to electromagnetic radiation. It provides the strength of the coupling of the electrons over spectral frequency intervals, whether in the discrete or the continuum.
EELS	Electron energy-loss spectroscopy.
f scaling	Scaling the Born cross section by the ratio of the accurate to the Born values of the optical oscillator strength.
FC	Franck-Condon principle and factor. An electronic transition in a molecule takes place so rapidly on the time scale of motion of the nuclei that they may be assumed to be frozen, resulting in a "vertical" transition at fixed internuclear radius R. Thereby, that contribution reduces to a simple factor, the squared overlap of the corresponding vibrational wave functions at that R.
FOMBT	First-order many-body theory.
Form factor	Widely used in physics to describe the response of a system to an external disturbance, it is a matrix element of an operator between states of the system independent of details of the disturber. In scattering, it depends only on the target, not the projectile.
GOS	Generalized oscillator strength. Introduced by Bethe, and closely related to the atomic form factor, it is the Fourier component of the electronic charge distribution associated with the transition. Its square gives the scattering cross section, whereas for small momentum transfer it reduces to the optical or dipole oscillator strength.
ICS	Integral cross section.
MTCS	Momentum transfer cross section.
OOS	Optical oscillator strength, the same as the dipole oscillator strength f.
PWB	Plane-wave Born: first Born approximation, with the incident charged-particle considered undeflected and described by a plane wave.
R matrix	A method that connects solutions at small radius to those in the outer region through the logarithmic derivative at the boundary between the regions.
Scattering amplitude	With dimensions of length, it is the matrix element whose squared modulus gives the scattering cross section.
siBED	The BED model with a shielded long-range dipole potential.
TCS	Total cross section.

ACKNOWLEDGMENTS

This work was partially supported through the Japan Society for the Promotion of Science (Grants No. 23540468 and No. 24740274) under agreement with the Japanese Ministry of Education, Sport, Culture and Technology. We express our gratitude to our many co-workers, many of whom have allowed their work to be quoted in this review. H. T. is also indebted to Dr. Irikura (NIST) for his early encouragement to write this review. Recent discussions with Y. Itikawa, I. Shimamura, and P. Limão-Vieira were particularly helpful. H. T. also thanks all the graduate students and postdoctoral research associates with whom he has carried out experiments over the years before his retirement. M. J. B. acknowledges both the Australian Research Council (Grants No. DP160102787 and No. CE0561389) and Flinders University for their support over many years. Additionally, A. R. P. R thanks H. T. and Sophia University for their hospitality during a visit. Finally, four theoretical physicists, the late Professor Fano and Professor Platzman, as well as the late Dr. Inokuti and Dr. Kim, made sustained and decisive contributions over fifty years to radiation science, and we owe much to them.

REFERENCES

Adamson, S., V. Astapenko, M. Deminskii, A. Eletskii, B. Potapkin, L. Sukhanov, and A. Zaitsevskii, 2007, Chem. Phys. Lett. **436**, 308.
Agostinelli, S., *et al.*, 2003, Nucl. Instrum. Methods Phys. Res., Sect. A **506**, 250.
Ajello, J. M., D. Shemansky, T. L. Kwok, and Y. L. Yung, 1984, Phys. Rev. A **29**, 636.
Albat, R., and N. Gruen, 1974, J. Phys. B **7**. L9.
Aleksandrov, Y. M., P. F. Gruzdev, M. G. Kozlov, A. V. Loginov, V. N. Makhov, R. V. Fedorchuk, and M. N. Yakimenko, 1983, Opt. Spektrosk. **54**, 7.
Allan, M., 1995, J. Phys. B **28**, 4329.
Allan, M., 2005, J. Phys. B **38**, 3655.
Allan, M., K. Franz, H. Hotop, O. Zatsarinny, and K. Bartschat, 2009, J. Phys. B **42**, 044009.
Allan, M., O. Zatsarinny, and K. Bartschat, 2006, Phys. Rev. A **74**, 030701(R).
Allison, A. C., and A. Dalgarno, 1970, Mol. Phys. **19**, 567.
Allison, J., *et al.*, 2006, IEEE Trans. Nucl. Sci. **53**, 270.
Anzai, K., *et al.*, 2012, Eur. Phys. J. D **66**, 36.
Arrighini, G. P., F. Biondi, and C. Guidotti, 1980, Mol. Phys. **41**, 1501.
Åsbrink, L., A. Svensson, W. von Niessen, and G. Bieri, 1981, J. Electron Spectrosc. Relat. Phenom. **24**, 293.
Avgoustoglou, E. N., and D. R. Beck, 1998, Phys. Rev. A **57**, 4286.
Baccarelli, I., I. Bald, F. A. Gianturco, E. Illenberger, and J. Kopyra, 2011, Phys. Rep. **508**, 1.
Ballance, C. P., and D. C. Griffin, 2004, J. Phys. B **37**, 2943.
Bassett, P. J., and D. R. Lloyd, 1971, J. Chem. Soc. A **10**, 1551.
Becker, K., H. Deutsch, and M. Inokuti, 2000, Adv. At. Mol. Opt. Phys. **43**, 399.
Beran, J. A., and L. Kevan, 1969, J. Phys. Chem. **73**, 3866.
Berkowitz, J., 1979, *Photoabsorption, Photoionization, and Photoelectron Spectroscopy* (Academic Press, New York).
Berkowitz, J., 2002, *Atomic and Molecular Photoabsorption: Absolute Total Cross Sections* (Academic, San Diego).
Bethe, H. A., 1930, Ann. Phys. (Berlin) **397**, 325.
Bethe, H. A., and E. E. Salpeter, 1977, *Quantum Mechanics of One- and Two-Electron Atoms* (Plenum, New York), p. 256.
Bhanuprakash, K., P. Chandra, C. Chabalowski, and R. J. Buenker, 1989, Chem. Phys. **138**, 215.
Boechat-Roberty, H. M., M. L. M. Rocco, C. A. Lucas, and G. G. B. de Souza, 2000, J. Phys. B **33**, 4525.
Boechat-Roberty, H. M., M. L. M. Rocco, C. A. Lucas, and G. G. B. de Souza, 2004, J. Phys. B **37**, 1467.
Boesten, L., and H. Tanaka, 1992, At. Data Nucl. Data Tables **52**, 25.
Bohr, N., 1913a, Philos. Mag. Ser. 6 **25**, 10.
Bohr, N., 1913b, Philos. Mag. Ser. 6 **26**, 1.
Bohr, N., 1915, Philos. Mag. **30**, 581.
Borges, Jr., I., and C. E. Bielschowsky, 1999, Phys. Rev. A **60**, 1226.
Born, M., 1926, Z. Phys. **38**, 803.
Boyd, R. J., and D. C. Frost, 1968, Chem. Phys. Lett. **1**, 649.
Branchett, S. E., J. Tennyson, and L. A. Morgan, 1990, J. Phys. B **23**, 4625.
Bray, I., D. V. Fursa, A. S. Kadyrov, A. T. Stelbovics, A. S. Kheifets, and A. M. Mukhamedzhanov, 2012, Phys. Rep. **520**, 135.
Bray, I., D. V. Fursa, A. S. Kheifets, and A. T. Stelbovics, 2002, J. Phys. B **35**, R117.
Bray, I., and A. T. Stelbovics, 1992, Phys. Rev. A **46**, 6995.
Brion, C. E., 1975, Radiat. Res. **64**, 37.
Brook, E., M. F. A. Harrison, and A. C. H. Smith, 1978, J. Phys. B **11**, 3115.
Bruce, M. R., and R. A. Bonham, 1993, Int. J. Mass Spectrom. Ion Process. **123**, 97.
Brunger, M. J., and S. J. Buckman, 2002, Phys. Rep. **357**, 215.
Brunger, M. J., S. J. Buckman, and M. T. Elford, 2003, in *Photon and Electron Interactions with Atoms, Molecules and Ions* edited by Y. Itikawa (Springer, Berlin), pp. 6-125, 6-128.
Brunger, M. J., S. J. Buckman, and D. S. Newman, 1990, Aust. J. Phys. **43**, 665.
Brunger, M. J., S. J. Buckman, D. S. Newman, and D. T. Alle, 1991, J. Phys. B **24**, 1435.
Brunger, M. J., and P. J. O. Teubner, 1990, Phys. Rev. A **41**, 1413.
Brunger, M. J., P. A. Thorn, L. Campbell, N. Diakomichalis, H. Kato, H. Kawahara, M. Hoshino, H. Tanaka, and Y.-K. Kim, 2008, Int. J. Mass Spectrom. **271**, 80.
Brunger, M. J., P. A. Thorn, L. Campbell, H. Kato, H. Kawahara, M. Hoshino, H. Tanaka, and Y.-K. Kim, 2008, J. Phys. Conf. Ser. **115**, 012004.
Brunger, M. J., *et al.*, 2014, AIP Conf. Proc. **1588**, 71.
Brunt, J. N. H., G. C. King, and F. H. Read, 1977, J. Phys. B **10**, 1289.
Buckman, S. J., M. J. Brunger, and K. Ratnavelu, 2013, Fusion Sci. Technol. **63**, 385.
Buenker, R. J., M. Honigmann, H.-P. Liebermann, and M. Kimura, 2000, J. Chem. Phys. **113**, 1046.
Buenker, R. J., and S. D. Peyerimhoff, 1974, Chem. Phys. Lett. **29**, 253.
Bultel, A., J. Annaloro, and V. Morel, 2012, J. Phys. Conf. Ser. **399**, 012014.
Burgess, A., 1964, in *Proceedings of the Third International Conference on Electronic and Atomic Collisions*, edited by M. R. C. McDowell (North-Holland, Amsterdam), p. 237.
Campbell, L., and M. J. Brunger, 2009, Geophys. Res. Lett. **36**, L03101.
Campbell, L., and M. J. Brunger, 2013, Plasma Sources Sci. Technol. **22**, 013002.
Campbell, L., M. J. Brunger, A. M. Nolan, L. J. Kelly, A. B. Wedding, J. Harrison, P. J. O. Teubner, D. C. Cartwright, and B. McLaughlin, 2001, J. Phys. B **34**, 1185.

Campbell, L., M. J. Brunger, P. J. O. Teubner, B. Mojarrabi, and D. C. Cartwright, 1997, Aust. J. Phys. **50**, 525.
Campbell, L., H. Tanaka, H. Kato, S. Jayaraman, and M. J. Brunger, 2012, Eur. Phys. J. D **66**, 26.
Cartwright, D. C., 2005 (private communication).
Cartwright, D. C., G. Csanak, S. Trajmar, and D. F. Register, 1992, Phys. Rev. A **45**, 1602.
Celotta, R. J., and R. H. Huebner, 1979, in *Electron Spectroscopy: Theory, Techniques and Applications*, edited by C. R. Brundle and A. D. Baker (Academic Press Inc., London), Vol. 3, p. 41.
Cernicharo, J., A. M. Heras, A. G. G. M. Tielens, J. R. Pardo, F. Herpin, M. Guélin, and L. B. F. M. Waters, 2001, Astrophys. J. **546**, L123.
Champion, C., C. Le Loirec, and B. Stosic, 2012, Int. J. Radiat. Biol. **88**, 54.
Chan, W. F., G. Cooper, and C. E. Brion, 1992, Chem. Phys. **168**, 375.
Chan, W. F., G. Cooper, and C. E. Brion, 1993a, Chem. Phys. **170**, 123.
Chan, W. F., G. Cooper, and C. E. Brion, 1993b, Chem. Phys. **170**, 99.
Chan, W. F., G. Cooper, and C. E. Brion, 1993c, Chem. Phys. **178**, 401.
Chan, W. F., G. Cooper, and C. E. Brion, 1993d, Chem. Phys. **178**, 387.
Chan, W. F., G. Cooper, and C. E. Brion, 1994, Chem. Phys. **180**, 77.
Chan, W. F., G. Cooper, X. Guo, and C. E. Brion, 1992, Phys. Rev. A **45**, 1420.
Chantranupong, L., G. Hirsch, K. Bhanuprakash, R. J. Buenker, M. Kimura, and M. A. Dillon, 1992, Chem. Phys. **164**, 183.
Chen, C.-Y., and C. Chung, 1997, Nucl. Instrum. Methods Phys. Res., Sect. A **395**, 195.
Chen, S. T., and A. Gallagher, 1976, Phys. Rev. A **14**, 593.
Chen, S. T., D. Leep, and A. Gallagher, 1976, Phys. Rev. A **13**, 947.
Cheng, H.-D., L.-F. Zhu, Z.-S. Yuan, X.-J. Lin, J.-M. Sun, W.-C. Jiang, and K.-Z. Xu, 2005, Phys. Rev. A **72**, 012715.
Christophorou, L. G., and J. K. Olthoff, 2001, in *Electron Collisions with Molecules in Gases: Applications to Plasma Diagnostics and Modeling*, edited by M. Kimura and Y. Itikawa, Adv. At. Mol. Opt. Phys. Vol. 44 (Academic Press, San Diego), pp. 59, 155.
Christophorou, L. G., J. K. Olthoff, and M. V. V. S. Rao, 1996, J. Phys. Chem. Ref. Data **25**, 1341.
Chung, S., and C. C. Lin, 1974, Phys. Rev. A **9**, 1954.
Chung, S., and C. C. Lin, 1980, Phys. Rev. A **21**, 1075.
Chutjian, A., and G. A. Segal, 1972, J. Chem. Phys. **57**, 3069.
Csanak, G., D. C. Cartwright, S. K. Srivastava, and S. Trajmar, 1984, in *Electron-Molecule Interactions and Their Applications*, edited by L. G. Christophorou (Academic Press Inc., Orlando), Vol. 1, p. 1.
Cubric, D., D. J. L. Mercer, J. M. Channing, G. C. King, and F. H. Read, 1999, J. Phys. B **32**, L45.
Curtis, L. J., *et al.*, 1995, Phys. Rev. A **51**, 4575.
da Costa, R. F., M. H. F. Bettega, M. T. do. N. Varella, E. M. de Oliveira, and M. A. P. Lima, 2014, Phys. Rev. A **90**, 052707.
da Costa, R. F., *et al.*, 2015, J. Chem. Phys. **142**, 104304.
de Urquijo, J., E. Basurto, A. M. Juárez, K. F. Ness, R. E. Robson, M. J. Brunger, and R. D. White, 2014, J. Chem. Phys. **141**, 014308.
Deutsch, H., K. Becker, and T. D. Märk, 1995, Int. J. Mass Spectrom. Ion Process. **151**, 207.
Deutsch, H., K. Becker, S. Matt, and T. D. Märk, 2000, Int. J. Mass Spectrom. **197**, 37.
Deutsch, H., C. Cornelissen, L. Cespiva, V. Bonacic-Koutecky, and T. D. Märk, 1993, Int. J. Mass Spectrom. Ion Process. **129**, 43.
Deutsch, H., and T. D. Märk, 1987, Int. J. Mass Spectrom. Ion Process. **79**, R1.
Deutsch, H., T. D. Märk, V. Tarnovsky, K. Becker, C. Cornelissen, L. Cespiva, and V. Bonacic-Koutecky, 1994, Int. J. Mass Spectrom. Ion Process. **137**, 77.
Diercksen, G. H. F., W. P. Kraemer, T. N. Rescigno, C. F. Bender, B. V. McKoy, S. R. Langhoff, and P. W. Langhoff, 1982, J. Chem. Phys. **76**, 1043.
Dillon, M. A., and M. Inokuti, 1981, J. Chem. Phys. **74**, 6271.
Dillon, M. A., and M. Inokuti, 1985, J. Chem. Phys. **82**, 4415.
Dodt, D., A. Dinklage, K. Bartschat, and O. Zatsarinny, 2010, New J. Phys. **12**, 073018.
Duflot, D., M. Hoshino, P. Limão-Vieira, A. Suga, H. Kato, and H. Tanaka, 2014, J. Phys. Chem. A **118**, 10955.
Duque, H. V., T. P. T. Do, M. C. A. Lopes, D. A. Konovalov, R. D. White, M. J. Brunger, and D. B. Jones, 2015, J. Chem. Phys. **142**, 124307.
Durante, N., U. T. Lamanna, G. P. Arrighini, and C. Guidotti, 1995, Theor. Chim. Acta **90**, 115.
Ehlers, V. J., and A. Gallagher, 1973, Phys. Rev. A **7**, 1573.
Eidelsberg, M., A. Jolly, J. L. Lemaire, W.-ÜL. Tchang-Brillet, J. Breton, and F. Rostas, 1999, Astron. Astrophys. **346**, 705.
Engmann, S., M. Stano, P. Papp, M. J. Brunger, Š. Matejčík, and O. Ingólfsson, 2013, J. Chem. Phys. **138**, 044305.
Erwin, D. A., and J. A. Kunc, 2008, J. Appl. Phys. **103**, 064906.
Fabian, W., and B. R. Lewis, 1974, J. Quant. Spectrosc. Radiat. Transfer **14**, 523.
Fano, U., 1954, Phys. Rev. **95**, 1198.
Fano, U., 1975, Radiat. Res. **64**, 217.
Fano, U., and J. W. Cooper, 1968, Rev. Mod. Phys. **40**, 441.
Fano, U., and A. R. P. Rau, 1986, *Atomic Collisions and Spectra* (Academic Press Inc., Orlando).
Feng, R., G. Cooper, and C. E. Brion, 2002, J. Electron Spectrosc. Relat. Phenom. **123**, 199.
Fliflet, A. W., and V. McKoy, 1980, Phys. Rev. A **21**, 1863.
Flosadóttir, H. D., B. Ómarsson, I. Bald, and O. Ingólfsson, 2012, Eur. Phys. J. D **66**, 13.
Francis-Staite, J. R., T. M. Maddern, M. J. Brunger, S. J. Buckman, C. Winstead, V. McKoy, M. A. Bolorizadeh, and H. Cho, 2009, Phys. Rev. A **79**, 052705.
Franck, J., and G. Hertz, 1914, Verh. Dtsch. Phys. Ges. (Berlin) **16**, 457.
Frisch, M. J., *et al.*, 2010, Gaussian09, Revision B.01, Gaussian Inc., Wallington, CT, www.gaussian.com.
Fursa, D. V., and I. Bray, 1997, J. Phys. B **30**, 5895.
Fuss, M. C., L. Ellis-Gibbings, D. B. Jones, M. J. Brunger, F. Blanco, A. Muñoz, P. Limão-Vieira, and G. García, 2015, J. Appl. Phys. **117**, 214701.
Fuss, M. C., A. G. Sanz, F. Blanco, J. C. Oller, P. Limão-Vieira, M. J. Brunger, and G. García, 2013, Phys. Rev. A **88**, 042702.
Gallagher, J. W., C. E. Brion, J. A. R. Samson, and F. W. Langhoff, 1988, J. Phys. Chem. Ref. Data **17**, 9, and references therein.
Garrett, B. C., L. T. Redmon, C. W. McCurdy, and M. J. Redman, 1985, Phys. Rev. A **32**, 3366.
Geiger, J., and H. Schmoranzer, 1969, J. Mol. Spectrosc. **32**, 39.
Gibson, N. D., and J. S. Risley, 1995, Phys. Rev. A **52**, 4451.
Gil, T. J., T. N. Rescigno, C. W. McCurdy, and B. H. Lengsfield, III, 1994, Phys. Rev. A **49**, 2642.
Gorfinkiel, J. D., L. A. Morgan, and J. Tennyson, 2002, J. Phys. B **35**, 543.
Gote, M., and H. Ehrhardt, 1995, J. Phys. B **28**, 3957.

Graves, D. B., M. J. Kushner, J. W. Gallagher, A. Garscadden, G. S. Oehrlein, and A. V. Phelps, 1996, *Database Needs for Modeling and Simulation of Plasma Processing* (National Academy Press, Washington, DC).
Gray, B. S., I. D. Latimer, and S. P. Spoor, 1996, J. Phys. D **29**, 50.
Green, A. E. S., and S. K. Dutta, 1967, J. Geophys. Res. **72**, 3933.
Gruzdev, P. F., and A. V. Loginov, 1973, Opt. Spectrosc. (USSR) **35**, 1.
Gryziński, M., 1965a, Phys. Rev. **138**, A305.
Gryziński, M., 1965b, Phys. Rev. **138**, A322.
Gryziński, M., 1965c, Phys. Rev. **138**, A336.
Gutiérrez, M. T., J. Cárabe, and J. J. Gandía, 1992, J. Appl. Phys. **71**, 6140.
Hagenow, G., K. Hottmann, H. W. Jochims, and H. Baumgärtel, 1989, Chem. Phys. **137**, 287.
Hake, Jr., R. D., and A. V. Phelps, 1967, Phys. Rev. **158**, 70.
Hall, R. I., G. Joyez, J. Mazeau, J. Reinhardt, and C. Schermann, 1973, J. Phys. (Les Ulis, Fr.) **34**, 827.
Hall, R. I., and F. H. Read, 1984, in *Electron-Molecule Collisions*, edited by I. Shimamura and K. Takayanagi (Plenum Press, New York), p. 351.
Hammond, V. J., and W. C. Price, 1955, Trans. Faraday Soc. **51**, 605.
Hargreaves, L. R., J. R. Francis-Staite, T. M. Maddern, M. J. Brunger, and S. J. Buckman, 2007, Meas. Sci. Technol. **18**, 2783.
Harting, E., and F. H. Read, 1976, *Electrostatic Lenses* (Elsevier, Amsterdam).
Hauschildt, P. H., S. Starrfield, S. N. Shore, F. Allard, and E. Baron, 1995, Astrophys. J. **447**, 829.
Hayashi, H., and Y. Udagawa, 2011, in *Charged Particle and Photon Interactions with Matter*, edited by Y. Hatano, Y. Katsumura, and A. Mozumder (CRC Press, Taylor & Francis Group, Boca Raton), p. 87.
Hibbert, A., M. Ledourneuf, and M. Mohan, 1993, At. Data Nucl. Data Tables **53**, 23.
Hoshino, M., H. Kato, D. Suzuki, H. Tanaka, I. Bray, D. V. Fursa, S. J. Buckman, O. Ingólfsson, and M. J. Brunger, 2010, Plasma Sci. Technol. **12**, 348.
Hoshino, M., H. Kato, H. Tanaka, I. Bray, D. V. Fursa, S. J. Buckman, O. Ingólfsson, and M. J. Brunger, 2009, J. Phys. B **42**, 145202.
Hoshino, M., H. Murai, H. Kato, M. J. Brunger, Y. Itikawa, and H. Tanaka, 2013, J. Chem. Phys. **139**, 184301.
Hoshino, M., H. Murai, H. Kato, M. J. Brunger, Y. Itikawa, and H. Tanaka, 2015, J. Chem. Phys. **142**, 129903.
Hoshino, M., H. Murai, H. Kato, Y. Itikawa, M. J. Brunger, and H. Tanaka, 2013, Chem. Phys. Lett. **585**, 33.
Hoshino, M., H. Murai, H. Kato, Y. Itikawa, M. J. Brunger, and H. Tanaka, 2015, Chem. Phys. Lett. **626**, 111.
Hudson, J. E., C. Vallance, M. Bart, and P. W. Harland, 2001, J. Phys. B **34**, 3025.
Huebner, R. H., R. J. Celotta, S. R. Mielczarek, and C. E. Kuyatt, 1975, J. Chem. Phys. **63**, 4490.
Hunger, H.-J., and G. Löbig, 1997, Thin Solid Films **310**, 244.
Huo, W. M., and F. A. Gianturco, 1995, *Computational Methods for Electron-Molecule Collisions* (Plenum Press, New York).
Huo, W. M., V. Tarnovsky, and K. H. Becker, 2002, Chem. Phys. Lett. **358**, 328.
Imhof, R. E., and F. H. Read, 1977, Rep. Prog. Phys. **40**, 1.
Inn, E. C. Y., K. Watanabe, and M. Zelikoff, 1953, J. Chem. Phys. **21**, 1648.
Inokuti, M., 1971, Rev. Mod. Phys. **43**, 297.
Inokuti, M., 1981, Comments At. Mol. Phys. **10**, 99.
Inokuti, M., 1987, in *Nuclear and Atomic Data for Radiotherapy and Related Radiobiology: Proceedings of an Advisory Group Meeting on Nuclear and Atomic Data for Radiotherapy and Related Radiobiology* (International Atomic Energy Agency, Vienna), pp. 357–365.
Inokuti, M., M. Kimura, M. A. Dillon, and I. Shimamura, 1994, *Cross Section Data*, edited by M. Inokuti, Adv. At. Mol. Opt. Phys. 33 (Academic Press, San Diego), p. 215.
Itikawa, Y., 2002, J. Phys. Chem. Ref. Data **31**, 749.
Itikawa, Y., 2003, in *Photon and Electron Interactions with Atoms, Molecules, and Ions*, Landolt-Börnstein Vol. I/17, Subvolume C (Springer, Berlin, Germany).
Itikawa, Y., 2007, *Molecular Processes in Plasmas* (Springer-Verlag, Berlin).
Itikawa, Y., 2009, J. Phys. Chem. Ref. Data **38**, 1.
Itikawa, Y., 2015, J. Phys. Chem. Ref. Data **44**, 013105.
Itikawa, Y., and N. Mason, 2005, J. Phys. Chem. Ref. Data **34**, 1.
Jalink, H., D. H. Parker, and S. Stolte, 1987, J. Mol. Spectrosc. **121**, 236.
Jones, D. B., *et al.*, 2014, J. Chem. Phys. **141**, 074314.
Kanik, I., J. M. Ajello, and G. K. James, 1996, J. Phys. B **29**, 2355.
Kanik, I., J. C. Nickel, and S. Trajmar, 1992, J. Phys. B **25**, 2189.
Karwasz, G. P., R. S. Brusa, and A. Zecca, 2001, La Rivista del Nuovo Cimento **24**, 1.
Kato, H., M. Hoshino, H. Tanaka, P. Limão-Vieira, O. Ingólfsson, L. Campbell, and M. J. Brunger, 2011, J. Chem. Phys. **134**, 134308.
Kato, H., H. Kawahara, M. Hoshino, H. Tanaka, M. J. Brunger, and Y.-K. Kim, 2007, J. Chem. Phys. **126**, 064307.
Kato, H., H. Kawahara, M. Hoshino, H. Tanaka, L. Campbell, and M. J. Brunger, 2008, Phys. Rev. A **77**, 062708.
Kato, H., *et al.*, 2009, Research Report NIST-DATA Series No. NIFS-DATA-108, Toki, Japan.
Kawahara, H., H. Kato, M. Hoshino, H. Tanaka, and M. J. Brunger, 2008a, Phys. Rev. A **77**, 012713.
Kawahara, H., H. Kato, M. Hoshino, H. Tanaka, L. Campbell, and M. J. Brunger, 2008b, J. Phys. B **41**, 085203.
Kawahara, H., D. Suzuki, H. Kato, M. Hoshino, H. Tanaka, O. Ingólfsson, L. Campbell, and M. J. Brunger, 2009, J. Chem. Phys. **131**, 114307.
Khakoo, M. A., J. Muse, K. Ralphs, R. F. da Costa, M. H. F. Bettega, and M. A. P. Lima, 2010, Phys. Rev. A **81**, 062716.
Khakoo, M. A., and J. Segura, 1994, J. Phys. B **27**, 2355.
Khakoo, M. A., H. Silva, J. Muse, M. C. A. Lopes, C. Winstead, and V. McKoy, 2008, Phys. Rev. A **78**, 052710.
Khakoo, M. A., and S. Trajmar, 1986, Phys. Rev. A **34**, 146.
Khakoo, M. A., *et al.*, 2002, Phys. Rev. A **65**, 062711.
Kim, Y.-K., 1975a, Radiat. Res. **61**, 21.
Kim, Y.-K., 1975b, Radiat. Res. **64**, 96.
Kim, Y.-K., 1975c, Radiat. Res. **64**, 205.
Kim, Y.-K., 2001, Phys. Rev. A **64**, 032713.
Kim, Y.-K., 2007, J. Chem. Phys. **126**, 064305.
Kim, Y.-K., and J.-P. Desclaux, 2002, Phys. Rev. A **66**, 012708.
Kim, Y.-K., and M. E. Rudd, 1994, Phys. Rev. A **50**, 3954.
Kim, Y.-K., J. P. Santos, and F. Parente, 2000, Phys. Rev. A **62**, 052710.
Kirby, K., and D. L. Cooper, 1989, J. Chem. Phys. **90**, 4895.
Klump, K. N., and E. N. Lassettre, 1978, J. Electron Spectrosc. Relat. Phenom. **14**, 215.
Kruzelecky, R. V., D. Racansky, S. Zukotynski, J. M. Perz, D. Polk, and W. M. Lau, 1986, J. Non-Cryst. Solids **79**, 19.
Kuyatt, C. E., S. R. Mielczarek, and M. J. Weiss, 1976, J. Chem. Phys. **65**, 3481.
Lane, N. F., 1980, Rev. Mod. Phys. **52**, 29.

Laricchiuta, A., R. Celiberto, and M. Capitelli, 2000, Chem. Phys. Lett. **329**, 526.
Lassettre, E. N., 1965, J. Chem. Phys. **43**, 4479.
Lassettre, E. N., 1969, Can. J. Chem. **47**, 1733.
Lassettre, E. N., S. M. Silverman, and M. E. Krasnow, 1964, J. Chem. Phys. **40**, 1261.
Lassettre, E. N., and A. Skerbele, 1971, J. Chem. Phys. **54**, 1597.
Lassettre, E. N., and A. Skerbele, 1974, *Methods of Experimental Physics*, edited by D. Williams (Academic Press, New York), Vol. 3, p. 868.
Lassettre, E. N., A. Skerbele, and M. A. Dillon, 1969, J. Chem. Phys. **50**, 1829.
Lassettre, E. N., A. Skerbele, M. A. Dillon, and K. J. Ross, 1968, J. Chem. Phys. **48**, 5066.
Lassettre, E. N., and E. R. White, 1974, J. Chem. Phys. **60**, 2460.
Laufer, A. H., and J. R. McNesby, 1965, Can. J. Chem. **43**, 3487.
Lavvas, P., M. Galand, R. V. Yelle, A. N. Heays, B. R. Lewis, G. R. Lewis, and A. J. Coates, 2011, Icarus **213**, 233.
Lavvas, P., R. V. Yelle, A. N. Heays, L. Campbell, M. J. Brunger, M. Galand, and V. Vuitton, 2015, Icarus **260**, 29.
Lee, L. C., and M. Suto, 1984, J. Chem. Phys. **80**, 4718.
Lee, L. C., and M. Suto, 1986, Chem. Phys. **110**, 161.
Leep, D., and A. Gallagher, 1976, Phys. Rev. A **13**, 148.
Lefebvre-Brion, H., and R. W. Field, 1986, *Perturbations in the Spectra of Diatomic Molecules* (Academic, Orlando).
Lenard, P., 1902, Ann. Phys. (Berlin) **313**, 149.
Lewis, B. R., J. P. England, S. T. Gibson, M. J. Brunger, and M. Allan, 2001, Phys. Rev. A **63**, 022707.
Lewis, B. R., S. T. Gibson, M. Emami, and J. H. Carver, 1988, J. Quant. Spectrosc. Radiat. Transfer **40**, 469.
Li, Y., M. Honigmann, K. Bhanuprakash, G. Hirsch, R. J. Buenker, M. A. Dillon, and M. Kimura, 1992, J. Chem. Phys. **96**, 8314.
Lide, D. R., 2007, Ed., *CRC Handbook of Chemistry and Physics* (Boca Raton, FL), 88th ed.
Ligtenberg, R. C. G., P. J. M. van der Burgt, S. P. Renwick, W. B. Westerveld, and J. S. Risley, 1994, Phys. Rev. A **49**, 2363.
Limão-Vieira, P., *et al.*, 2015, J. Chem. Phys. **142**, 064303.
Lindsay, B. G., K. F. McDonald, W. S. Yu, and R. F. Stebbings, 2004, J. Chem. Phys. **121**, 1350.
Liu, J. W., and S. Hagstrom, 1993, Phys. Rev. A **48**, 166.
Lotz, W., 1968, Z. Phys. **216**, 241.
Lurio, A., 1965, Phys. Rev. **140**, A1505.
Machado, L. E., E. P. Leal, and G. Csanak, 1982, J. Phys. B **15**, 1773.
Mackie, R. A., L. G. Shpinkova, D. M. P. Holland, and D. A. Shaw, 2003, Chem. Phys. **288**, 211.
Maddern, T. M., L. R. Hargreaves, M. Bolorizadeh, M. J. Brunger, and S. J. Buckman, 2008, Meas. Sci. Technol. **19**, 085801.
Maddern, T. M., L. R. Hargreaves, J. R. Francis-Staite, M. J. Brunger, S. J. Buckman, C. Winstead, and V. McKoy, 2008, Phys. Rev. Lett. **100**, 063202.
Makabe, T., and Z. Lj. Petrovic, 2015, *Plasma Electronics: Applications in Microelectronic Device Fabrication* (CRC Press, Taylor & Francis Group, Boca Raton), 2nd ed.
Malyshev, M. V., V. M. Donnelly, and S. Samukawa, 1998, J. Appl. Phys. **84**, 1222.
Märk, T. D., 1984, in *Electron-Molecule Interactions and Their Applications*, edited by L. G. Christophorou (Academic Press Inc., Orlando), Vol. 1, p. 251.
Märk, T. D., 1992, Plasma Phys. Controlled Fusion **34**, 2083.
Martinez, R., B. Sierra, C. Redondo, M. N. Sánchez Rayo, and F. Castaño, 2004, J. Chem. Phys. **121**, 11653.
Massey, H. S. W., 1976, *Negative Ions* (Cambridge University Press, London).
Massey, H. S. W., E. H. S. Burhop, and H. B. Gilbody, 1969, *Electronic and Ionic Impact Phenomena,* (Clarendon Press, Oxford), Vols. I and II, 2nd ed.
Massey, H. S. W., and C. B. O. Mohr, 1931, Proc. R. Soc. A **132**, 605.
McCurdy, Jr., C. W., and V. McKoy, 1974, J. Chem. Phys. **61**, 2820.
McEachran, R. P., *et al.*, 2012, J. Phys. B **45**, 045207.
Merabet, H., M. Bailey, R. Bruch, J. Hanni, S. Bliman, D. V. Fursa, I. Bray, K. Bartschat, H. C. Tseng, and C. D. Lin, 2001, Phys. Rev. A **64**, 012712.
Miller, J. H., and S. T. Manson, 1984, Phys. Rev. A **29**, 2435.
Miller, W. F., and R. L. Platzman, 1957, Proc. Phys. Soc. London Sect. A **70**, 299.
Montague, R. G., M. F. A. Harrison, and A. C. H. Smith, 1984, J. Phys. B **17**, 3295.
Morrison, M. A., and A. E. Greene, 1978, J. Geophys. Res. **83**, 1172.
Moshkalyov, S. A., P. G. Steen, S. Gomez, and W. G. Graham, 1999, Appl. Phys. Lett. **75**, 328.
Mott, N. F., 1930, Proc. R. Soc. A **126**, 259.
Mott, N. F., and H. S. W. Massey, 1965, *The Theory of Atomic Collisions* (Clarendon Press, Oxford), 3rd ed.
Muñoz, A., F. Blanco, J. C. Oller, J. M. Peréz, and G. García, 2007, in *Advances in Quantum Chemistry*, edited by J. R. Sabin and E. Brändas (Academic Press, New York), Vol. 52, p. 21.
Natali, S., C. E. Kuyatt, and S. R. Mielczarek, 1973, as quoted in J. Berkowitz, *Photoabsorption, Photoionization and Photoelectron Spectroscopy* (Academic Press, New York), p. 80.
Ness, K. F., R. E. Robson, M. J. Brunger, and R. D. White, 2012, J. Chem. Phys. **136**, 024318.
Neves, R. F. C., *et al.*, 2015a, J. Chem. Phys. **142**, 104305.
Neves, R. F. C., D. B. Jones, M. C. A. Lopes, F. Blanco, G. García, K. Ratnavelu, and M. J. Brunger, 2015b, J. Chem. Phys. **142**, 194305.
Newell, W. R., M. A. Khakoo, and A. C. H. Smith, 1980, J. Phys. B **13**, 4877.
Nickel, J. C., P. W. Zetner, G. Shen, and S. Trajmar, 1989, J. Phys. E **22**, 730.
Nikitović, Ž. D., V. D. Stojanović, J. P. Booth, and Z. Lj. Petrović, 2009, Plasma Sources Sci. Technol. **18**, 035008.
Nishimura, H., W. M. Huo, M. A. Ali, and Y.-K. Kim, 1999, J. Chem. Phys. **110**, 3811.
Noble, C. J., K. Higgins, G. Wöste, P. Duddy, P. G. Burke, P. J. O. Teubner, A. G. Middleton, and M. J. Brunger, 1996, Phys. Rev. Lett. **76**, 3534.
Ogawa, S., and M. Ogawa, 1975, Can. J. Phys. **53**, 1845.
Padial, N., G. Csanak, B. V. McKoy, and P. W. Langhoff, 1981, Phys. Rev. A **23**, 218.
Panajotović, R., V. Pejčev, M. Konstantinović, D. Filipović, V. Bočvarski, and B. Marinković, 1993, J. Phys. B **26**, 1005.
Pantos, E., J. Philis, and A. Bolovinos, 1978, J. Mol. Spectrosc. **72**, 36.
Peitzmann, F. J., and J. Kessler, 1990, J. Phys. B **23**, 2629.
Petrović, Z. Lj., S. Marjanović, S. Dujko, A. Banković, G. Malović, S. Buckman, G. Garcia, R. White, and M. Brunger, 2014, Appl. Radiat. Isot. **83**, 148.
Peyerimhoff, S. D., and R. J. Buenker, 1968, J. Chem. Phys. **49**, 2473.
Pflüger, T., O. Zatsarinny, K. Bartschat, A. Senftleben, X. Ren, J. Ullrich, and A. Dorn, 2013, Phys. Rev. Lett. **110**, 153202.
Philis, J., A. Bolovinos, G. Andritsopoulos, E. Pantos, and P. Tsekeris, 1981, J. Phys. B **14**, 3621.
Phillips, M. H., L. W. Anderson, and C. C. Lin, 1985, Phys. Rev. A **32**, 2117.
Phillips, R. A., and R. J. Buenker, 1987, Chem. Phys. Lett. **137**, 157.

Poll, H. U., C. Winkler, D. Margreiter, V. Grill, and T. D. Märk, 1992, Int. J. Mass Spectrom. Ion Process. **112**, 1.
Puech, V., and S. Mizzi, 1991, J. Phys. D **24**, 1974.
Rabalais, J. W., J. M. McDonald, V. Scherr, and S. P. McGlynn, 1971, Chem. Rev. **71**, 73.
Ralphs, K., G. Serna, L. R. Hargreaves, M. A. Khakoo, C. Winstead, and V. McKoy, 2013, J. Phys. B **46**, 125201.
Rao, M. V. V. S., and S. K. Srivastava, 1997, *Abstracts of the XXth ICPEAC, Abstract Mo150*, edited by F. Aumayr, G. Betz, and H. P. Winter (Vienna, Austria).
Rau, A. R. P., 1971, Phys. Rev. A **4**, 207.
Rau, A. R. P., and U. Fano, 1967, Phys. Rev. **162**, 68.
Read, F. H., and G. L. Whiterod, 1965, Proc. Phys. Soc. London **85**, 71.
Register, D. F., S. Trajmar, G. Steffensen, and D. C. Cartwright, 1984, Phys. Rev. A **29**, 1793.
Rescigno, T. N., and A. E. Orel, 2013, Phys. Rev. A **88**, 012703.
Robson, R. E., R. D. White, and M. Hildebrandt, 2014, Eur. Phys. J. D **68**, 188.
Rohr, K., and F. Linder, 1976, J. Phys. B **9**, 2521.
Rost, J. M., and T. Pattard, 1997, Phys. Rev. A **55**, R5.
Rudd, M. E., 1989, Int. J. Rad. Appl. Instrum. Part D Nucl. Tracks. Radiat. Meas. **16**, 213.
Rudge, M. R. H., 1968, Rev. Mod. Phys. **40**, 564.
Salvat, F., J. M. Fernández-Varea, and J. Sempau, 2011, *PENELOPE 2011, A Code System for Monte Carlo Simulation of Electron and Photon Transport* (OECD—Nuclear Energy Agency).
Sanz, A. G., M. C. Fuss, A. Muñoz, F. Blanco, P. Limão-Vieira, M. J. Brunger, S. J. Buckman, and G. García, 2012, Int. J. Radiat. Biol. **88**, 71.
Savin, D. W., *et al.*, 2012 Rep. Prog. Phys. **75**, 036901.
Schweinzer, J., R. Brandenburg, I. Bray, R. Hoekstra, F. Aumayr, R. K. Janev, and H. P. Winter, 1999, At. Data Nucl. Data Tables **72**, 239.
Scott, G. E., and K. K. Irikura, 2005, J. Chem. Theory Comput. **1**, 1153.
Shah, M. B., D. S. Elliott, and H. B. Gilbody, 1987, J. Phys. B **20**, 3501.
Shah, M. B., D. S. Elliot, P. McCallion, and H. B. Gilbody, 1988, J. Phys. B **21**, 2751.
Shemansky, D. E., J. M. Ajello, D. T. Hall, and B. Franklin, 1985, Astrophys. J. **296**, 774.
Shimamura, I., and K. Takayanagi, 1984, in *Electron-Molecule Collisions*, edited by I. Shimamura and K. Takayanagi (Plenum Press, New York).
Shpinkova, L. G., D. M. P. Holland, and D. A. Shaw, 1999, Mol. Phys. **96**, 323.
Shyn, T. W., C. J. Sweeney, and A. Grafe, 1994, Phys. Rev. A **49**, 3680.
Shyn, T. W., C. J. Sweeney, A. Grafe, and W. E. Sharp, 1994, Phys. Rev. A **50**, 4794.
Sohn, W., K.-H. Kochem, K. Jung, H. Ehrhardt, and E. S. Chang, 1985, J. Phys. B **18**, 2049.
Spence, D., R. H. Huebner, H. Tanaka, M. A. Dillon, and R.-G. Wang, 1984, J. Chem. Phys. **80**, 2989.
Srivastava, R., T. Zuo, R. P. McEachran, and A. D. Stauffer, 1993, J. Phys. B **26**, 1025.
Srivastava, S. K., A. Chutjian, and S. Trajmar, 1975, J. Chem. Phys. **63**, 2659.
Srivastava, S. K., and S. Jensen, 1977, J. Phys. B **10**, 3341.
Suto, M., X. Wang, J. Shan, and L. C. Lee, 1992, J. Quant. Spectrosc. Radiat. Transfer **48**, 79.
Suto, M., C. Ye, and L. C. Lee, 1990, Phys. Rev. A **42**, 424.
Suzuki, D., H. Kato, M. Ohkawa, K. Anzai, H. Tanaka, P. Limão-Vieira, L. Campbell, and M. J. Brunger, 2011, J. Chem. Phys. **134**, 064311.
Suzuki, T. Y., H. Suzuki, S. Ohtani, B. S. Min, T. Takayanagi, and K. Wakiya, 1994, Phys. Rev. A **49**, 4578.
Takatsuka, K., and V. McKoy, 1981, Phys. Rev. A **24**, 2473.
Takayanagi, K., and Y. Itikawa, 1970, Adv. At. Mol. Phys. **6**, 105.
Tan, K. H., C. E. Brion, Ph. E. Van der Leeuw, and M. J. van der Wiel, 1978, Chem. Phys. **29**, 299.
Tanaka, H., L. Boesten, D. Matsunaga, and T. Kudo, 1988, J. Phys. B **21**, 1255.
Tanaka, H., and R. H. Heubner, 1976, Argonne National Laboratory, Radiological and Environmental Research Division ANL-76-65 (Argonne National Laboratory, USA), p. 14.
Tanaka, H., T. Ishikawa, T. Masai, T. Sagara, L. Boesten, M. Takekawa, Y. Itikawa, and M. Kimura, 1998, Phys. Rev. A **57**, 1798.
Tanaka, H., and Y. Itikawa, 2011, in *Charged Particle and Photon Interactions with Matter*, edited by Y. Hatano, Y. Katsumura, and A. Mozumder (CRC Press, Taylor & Francis Group, Boca Raton, FL), p. 27.
Tanaka, H., T. Okada, L. Boesten, T. Suzuki, T. Yamamoto, and M. Kubo, 1982, J. Phys. B **15**, 3305.
Tanaka, H., and O. Sueoka, 2001, in *Electron Collisions with Molecules in Gases: Applications to Plasma Diagnostics and Modeling*, Adv. At. Mol. Opt. Phys. Vol. 44 (Academic Press, San Diego), p. 1.
Tennyson, J., 1996, J. Phys. B **29**, 6185.
Teulet, P., J. P. Sarrette, and A. M. Gomes, 1999, J. Quant. Spectrosc. Radiat. Transfer **62**, 549.
Theodorakopoulos, G., I. D. Petsalakis, C. A. Nicolaides, and R. J. Buenker, 1985, J. Chem. Phys. **82**, 912.
Thompson, W. R., M. B. Shah, and H. B. Gilbody, 1995, J. Phys. B **28**, 1321.
Thomson, J. J., 1897, Philos. Mag. Ser. 5 **44**, 293.
Thorn, P., L. Campbell, and M. Brunger, 2009, PMC Phys. B **2**, 1.
Thorn, P. A., M. J. Brunger, H. Kato, M. Hoshino, and H. Tanaka, 2007a, J. Phys. B **40**, 697.
Thorn, P. A., *et al.*, 2007b, J. Chem. Phys. **126**, 064306.
Trajmar, S., 1973, Phys. Rev. A **8**, 191.
Trajmar, S., and D. C. Cartwright, 1984, in *Electron—Molecule Interactions and Their Applications*, edited by L. G. Christophorou (Academic Press Inc., Orlando), Vol. 1, p. 156.
Trajmar, S., and J. W. McConkey, 1994, in *Cross Section Data*, edited by M. Inokuti, Adv. At. Mol. Opt. Phys. Vol. 33 (Academic Press, San Diego), p. 63.
Trajmar, S., J. M. Ratliff, G. Csanak, and D. C. Cartwright, 1992, Z. Phys. D **22**, 457.
Trajmar, S., and D. F. Register, 1984, in *Electron-Molecule Collisions*, edited by I. Shimamura and K. Takayanagi (Plenum Press, New York), p. 427.
Trajmar, S., W. Williams, and D. C. Cartwright, 1971, in *Proceedings VII ICPEAC*, edited by T. R. Groves and F. J. de Heer (North-Holland, Amsterdam), p. 1066.
Trajmar, S., W. Williams, and A. Kuppermann, 1972, J. Chem. Phys. **56**, 3759.
Tsurubuchi, S., K. Watanabe, and T. Arikawa, 1990, J. Phys. Soc. Jpn. **59**, 497.
Vos, M., R. P. McEachran, G. Cooper, and A. P. Hitchcock, 2011, Phys. Rev. A **83**, 022707.
Vriens, L., 1966, Proc. Phys. Soc. London **89**, 13.
Vriens, L., 1967, Phys. Rev. **160**, 100.

Vriens, L., 1969, in *Case Studies in Atomic Physics*, edited by E. W. McDaniel and M. R. C. McDowell (North-Holland, Amsterdam), Vol. 1, p. 335.
Vriens, L., J. A. Simpson, and S. R. Mielczarek, 1968, Phys. Rev. **165**, 7.
Wakiya, K., 1978, J. Phys. B **11**, 3913.
Wannier, G. H., 1953, Phys. Rev. **90**, 817.
Westerveld, W. B., H. G. M. Heideman, and J. van Eck, 1979, J. Phys. B **12**, 115.
White, R. D., M. J. Brunger, N. A. Garland, R. E. Robson, K. F. Ness, G. Garcia, J. de Urquijo, S. Dujko, and Z. Lj. Petrović, 2014a, Eur. Phys. J. D **68**, 125.
White, R. D., *et al.*, 2014b, Appl. Radiat. Isot. **83**, 77.
Wiese, W. L., M. W. Smith, and B. M. Glennon, 1966, Natl. Stand. Ref. Data Ser. No. NSRDS-NBS-4, "Atomic Transition Probabilities, Vol. **I**, Hydrogen Through Neon," p. 126.
Williams, G. R. J., and P. W. Langhoff, 1979, Chem. Phys. Lett. **60**, 201.
Williams, J. F., 1981, J. Phys. B **14**, 1197.
Wilson, E. H., S. K. Atreya, and A. Coustenis, 2003, J. Geophys. Res. (Planets) **108**, issue (E2), 5014.
Wood, M. H., 1974, Chem. Phys. Lett. **28**, 477.
Wrkich, J., D. Mathews, I. Kanik, S. Trajmar, and M. A. Khakoo, 2002, J. Phys. B **35**, 4695.
Xu, W.-Q., J.-M. Sun, Y.-Y. Wang, and L.-F. Zhu, 2010, Phys. Rev. A **82**, 042716.
Yamamoto, H., S. Matsumoto, K. Okada, J. Yu, and K. Hirakuri, 2006, Diamond Relat. Mater. **15**, 1357.
Yencha, A. J., M. C. A. Lopes, and G. C. King, 2002, Chem. Phys. **279**, 55.
Yoon, J.-S., M.-Y. Song, J.-M. Han, S. H. Hwang, W.-S. Chang, B. J. Lee, and Y. Itikawa, 2008, J. Phys. Chem. Ref. Data **37**, 913.
Yoon, J.-S., M.-Y. Song, H. Kato, M. Hoshino, H. Tanaka, M. J. Brunger, S. J. Buckman, and H. Cho, 2010, J. Phys. Chem. Ref. Data **39**, 033106.
Yoshino, K., J. R. Esmond, W. H. Parkinson, K. Ito, and T. Matsui, 1996, Chem. Phys. **211**, 387.
Yoshino, K., J. R. Esmond, W. H. Parkinson, K. Ito, and T. Matsui, 1997, Chem. Phys. **215**, 429.
Younger, S. M., 1981, J. Quant. Spectrosc. Radiat. Transfer **26**, 329.
Zatsarinny, O., and K. Bartschat, 2004, J. Phys. B **37**, 2173.
Zatsarinny, O., and K. Bartschat, 2012a, Phys. Rev. A **86**, 022717.
Zatsarinny, O., and K. Bartschat, 2012b, Phys. Rev. A **85**, 062710.
Zatsarinny, O., and K. Bartschat, 2013, J. Phys. B **46**, 112001.
Zecca, A., G. P. Karwasz, and R. S. Brusa, 1996, Riv. Nuovo Cimento **19**, 1.
Zelikoff, M., K. Watanabe, and E. C. Y. Inn, 1953, J. Chem. Phys. **21**, 1643.
Zeman, V., K. Bartschat, T. J. Gay, and K. W. Trantham, 1997, Phys. Rev. Lett. **79**, 1825.
Zetner, P. W., I. Kanik, and S. Trajmar, 1998, J. Phys. B **31**, 2395.
Zhang, W. J., and S. Matsumoto, 2000, Chem. Phys. Lett. **330**, 243.
Zhong, Z. P., R. F. Feng, K. Z. Xu, S. L. Wu, L. F. Zhu, X. J. Zhang, Q. Ji, and Q. C. Shi, 1997, Phys. Rev. A **55**, 1799.
Zhong, Z. P., K. Z. Xu, R. F. Feng, X. J. Zhang, L. F. Zhu, and X. J. Liu, 1998, J. Electron Spectrosc. Relat. Phenom. **94**, 127.
Zhu, L.-F., J.-M. Sun, and K.-Z. Xu, 2007, *Book of Abstracts, XXV ICPEAC*, edited by J. Anton, R. Moshamner, C.-D. Schröter, and J. Ullrich (University of Freiburg Press, Freiburg, Germany).
Zipf, E. C., 1985, Planet. Space Sci. **33**, 1303.
Zobel, J., U. Mayer, K. Jung, and H. Ehrhardt, 1996, J. Phys. B **29**, 813.
See Supplemental Material at [http://link.aps.org/supplemental/10.1103/RevModPhys.88.025004] for Tables 1–8, containing important physical and chemical constants and OOS values.